Three-Dimensional Bio-Printed Tubular Tissue Using Dermal Fibroblast Cells as a New Tissue-Engineered Vascular Graft for Venous Replacement

MAKOTO HAYASAKA,* TAKASHI KOKUDO,* JUNICHI KANEKO,* TAKEHIRO CHIYODA,* ANNA NAKAMURA,† MANABU ITOH,‡ KAZUHIRO ENDO,§ KOICHI NAKAYAMA,† AND KIYOSHI HASEGAWA*

The current study was a preliminary evaluation of the feasibility and biologic features of three-dimensionally bio-printed tissue-engineered (3D bio-printed) vascular grafts comprising dermal fibroblast spheroids for venous replacement in rats and swine. The scaffold-free tubular tissue was made by the 3D bio-printer with normal human dermal fibroblasts. The tubular tissues were implanted into the infrarenal inferior vena cava of 4 male F344-rnu/rnu athymic nude rats and the short-term patency and histologic features were analyzed. A larger 3D bio-printed swine dermal fibroblast-derived prototype of tubular tissue was implanted into the right jugular vein of a swine and patency was evaluated at 4 weeks. The short-term patency rate was 100%. Immunohistochemistry analysis showed von Willebrand factor positivity on day 2, with more limited positivity observed on the luminal surface on day 5. Although the cross-sectional area of the wall differed significantly between preimplantation and days 2 and 5, suggesting swelling of the tubular tissue wall (both $p < 0.01$), the luminal diameter of the tubular tissues was not significantly altered during this period. The 3D bio-printed scaffold-free tubular tissues using human dermal or swine fibroblast spheroids may produce better tissue-engineered vascular grafts for venous replacement in rats or swine. ***ASAIO Journal*** **2024; 70:1008–1015**

Key Words: 3D bio-printer, dermal fibroblast, synthetic vascular prosthesis, tissue-engineered, venous replacement

From the *Hepato-Biliary-Pancreatic Surgery Division, Department of Surgery, Graduate School of Medicine, The University of Tokyo, Tokyo, Japan; †Center for Regenerative Medicine Research, Faculty of Medicine, SAGA University, Saga, Japan; ‡Faculty of Medicine, Department of Thoracic and Cardiovascular Surgery, Saga University, Saga, Japan; and §Department of Surgery, Division of Gastroenterological, General and Transplant Surgery Jichi Medical University, Tochigi, Japan.

Submitted for consideration January 2024; accepted for publication in revised from April 2024.

Disclosure: The authors have no conflicts of interest to report.

This study was funded by Grants in Aid for Scientific Research, Tokyo, Japan, and the work was supported by grant nos. 18K16252 (Kokudo) and 19K09191 (Kaneko) from the Ministry of Education, Culture, Sports, Science, and Technology of Japan.

Correspondence: Kiyoshi Hasegawa, Hepato-Biliary-Pancreatic Surgery Division, Department of Surgery, Graduate School of Medicine, The University of Tokyo, 7-3-1 Hongo, Bunkyo-ku, Tokyo, 113-8655, Japan. Emails: jkaneko-gi@umin.ac.jp, kihase-tky@umin.ac.jp.

Copyright © ASAIO 2024

DOI: 10.1097/MAT.0000000000002224

Background

Complete excision of malignant tumors invading the inferior vena cava (IVC), hepatic vein, portal vein, or superior mesenteric vein is currently the only curative surgical option, especially in hepato-biliary-pancreatic surgery or urologic surgery. Replacement of these veins with an autologous vein graft is ideal, but size mismatch is a challenging obstacle.[1] Although cryopreserved homologous veins are sometimes used, the supply is insufficient in Japan due to the donor shortage, and the availability is limited to only a few institutions.[2,3]

Synthetic vascular prostheses developed for arterial replacement are another option. Novel synthetic vascular prostheses for veins have not yet been developed because of their tendency toward thrombogenicity due to low flow and pressure, less biocompatibility, and vulnerability to infection.[4,5] The migration of synthetic vascular prostheses into adjacent organs also causes injuries and is another concern over the long term.[6] New bio- or tissue-engineered vascular grafts are expected to provide more safety and greater versatility for venous replacement. New bio-printing technologies allow for the assembly of predesigned three-dimensional (3D) structures synthesized using cellular spheroids from human dermal fibroblasts without the need for scaffold materials.[7,8] The successful development of tubular structures using only fibroblast- or mixed-cell spheroids and their implantation in rat aorta has been reported,[9,10] but the use of these bio-printed structures for venous replacement has not yet been reported.

The technical feasibility of obtaining a single-cell source, fibroblasts, from superficial tissues such as human skin to construct tubular tissue allows for less invasive procedures than those needed to obtain cells from other, deeper organs.[11] The current study was a preliminary evaluation of the feasibility and biologic features of new 3D-printed tissue-engineered vascular grafts comprising human dermal or swine fibroblast spheroids for venous replacement in rats and swine.

Materials and Methods

Cell Culture

Primary normal human dermal fibroblasts (CC-2509; Lonza, Basel, Switzerland) or porcine allogeneic primary dermal fibroblasts from Cell Biologics (Chicago, IL) were cultured in fibroblast growth medium (Dulbecco's modified Eagle's medium [DMEM; Wako Pure Chemical Industries, Osaka, Japan] supplemented with 10% fetal bovine serum [FBS; Hyclone, Logan, UT] and 100 U/ml penicillin/streptomycin [Invitrogen, Carlsbad, CA]) in an incubator at 37°C under a humidifie

atmosphere with 5% CO_2. The culture medium was replaced every 2–3 days. Upon reaching 90% confluence, fibroblasts were detached using 0.25% trypsin-ethylenediaminetetraacetic acid (Life Technology Corporation, Grand Island, NY) and passaged every 5 days. For this study, cells up to the fifth passage were used.

To form spheroids, fibroblast suspensions were adjusted to a concentration of 7.5×10^5 cells/ml. Subsequently, 100 µl aliquots were plated into each well of ultra-low-attachment, round-bottom 96-well plates (Sumilon PrimeSurface; Sumitomo Bakelite, Tokyo, Japan) in the 3D culture medium consisting of DMEM supplemented with 2% FBS (Hyclone), insulin (Wako), 5 µg/ml epidermal growth factor (R&D Systems, Minneapolis, MN), 5 µg/ml fibroblast growth factor (FGF; Wako), 25 µg/ml ascorbic acid (Wako), and 100 U/ml penicillin/streptomycin (Invitrogen), and incubated at 37°C under a humidified atmosphere with 5% CO_2. After 72 h, the fibroblasts aggregated to form spheroids with a median diameter of 449 µm (range = 265–486 µm).

Creation of Tubular Tissue From Multicellular Spheroids Using a Bio-Three-Dimensional Printer

The Regenova Bio-3D printer (Cyfuse Biomedical KK, Tokyo, Japan) was used to assemble the scaffold-free construct, as previously reported.[12,13] To assemble the construct using the Bio-3D printer, the spheroids were individually picked up and placed into a 7 mm Kenzan needle array (Figure 1A). The 7 mm round Kenzan comprises a single row of 36 needles arranged in a 7 mm diameter circle (Figures 1C, 2B). Approximately 1 week after 3D bio-printing, the spheroids fused to form a single tubular construct (Figures 1, A and B, 2B). The needle array was then removed, and the fibroblast tubular construct was transferred onto a 5 mm polydimethylsiloxane tube. Additional incubation of over 90 days was necessary for the fibroblasts within the tube to reorganize and strengthen the construct (Figures 1C, 2C). Incubation was carried out in DMEM (Fujifilm Wako Pure Chemical Corporation, Osaka, Japan) supplemented with 2% FBS (Hyclone), FGF, epidermal growth factor, hydrocortisone, insulin, L (+)-ascorbic acid (Fujifilm Wako Pure Chemical Corporation), and 40 µg/ml gentamicin (Lonza) in a bioreactor equipped with a flow system. The medium in the reactor was changed twice a week. All cultures were incubated at 37°C in a humidified atmosphere of 5% CO_2 and 95% air. At this stage, the fibroblast tube measured 0.5 mm in width and approximately 10 mm in length (Figure 2C).

Implantation of the Tubular Tissue Into the Inferior Vena Cava in Rat

The study protocols (P16-119) were approved by the University of Tokyo animal ethics committee according to the Animal Research: Reporting of In Vivo Experiments (ARRIVE) guidelines (Japanese version). Male F344-rnu/rnu athymic nude rats (n = 4, 12–15 weeks old, CLEA Japan Inc., Tokyo, Japan) were used. These rats lack T-cell function and are thus immunotolerant to xenografts. The length, and inner and outer diameters of the tubular tissue were 8, 2, and 4 mm, respectively (Figure 3A). The tubular tissue (n = 4) was implanted into each infrarenal IVC under general anesthesia with 2–3% isoflurane. The IVC was exposed as much as possible, clamped at the cranial and caudal sides with vascular clamps, and then cut between the vascular clamps without excising. An end-to-end anastomosis was performed with a 10–0 polypropylene interrupted suture under a 10× stereo microscope (S9E; Leica Microsystems, Tokyo, Japan) (Figure 3B). No anticoagulation or antiplatelet medications were administered during or after the operation. On postoperative day 5, a laparotomy was performed, and the patency of the IVC was directly assessed by Doppler ultrasonography. The implanted tubular tissue was then removed for further pathologic examination, and the rats were euthanized by an overdose of pentobarbital sodium (Somnopentyl; Kyoritsuseiyaku Corp. Tokyo, Japan).

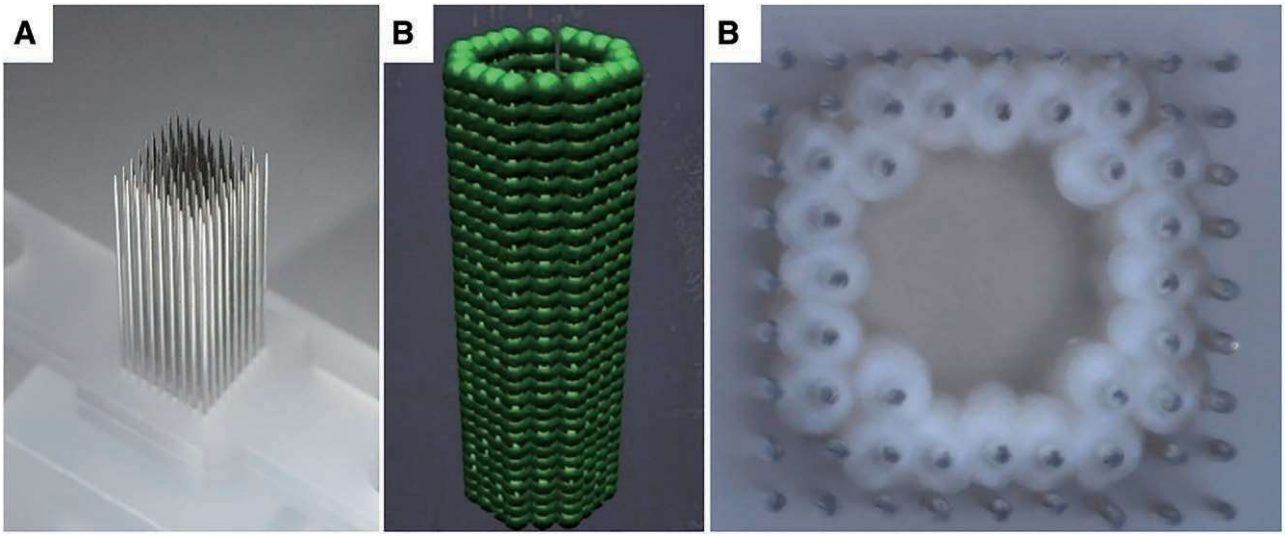

Figure 1. The Bio-3D printer has a needle array (Kenzan) comprising 160 μm diameter stainless-steel microneedles arranged at 400 μm intervals (**A**). Tubular tissue was designed using the computer software Bio-3D Designer (**B**). Spheroids were automatically placed in a controlled position using the microneedles (**C**). 3D, three-dimensional.

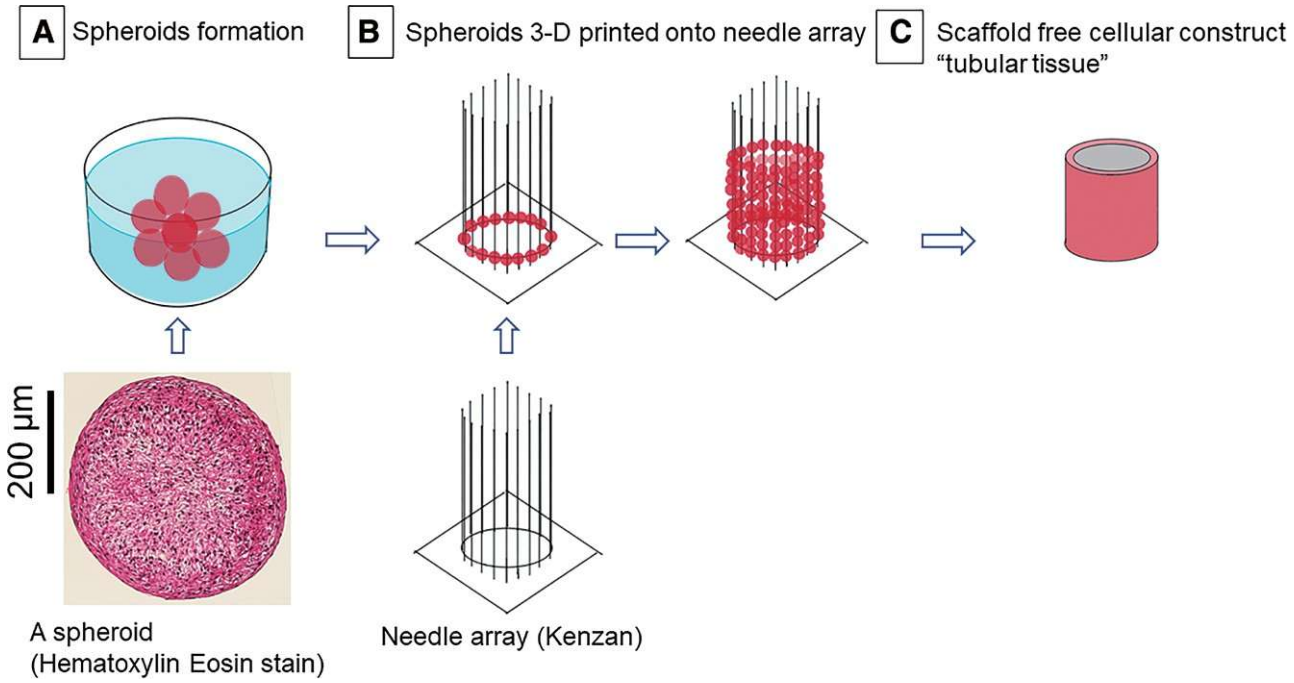

Figure 2. Schematic diagram showing the 3D bio-printing process. Hematoxylin-eosin staining showing an example of a spheroid with cultured human dermal cells (below **A**). Spheroid aggregation (**A**). The nozzle picks up spheroids one by one and places them onto the microneedles of the Kenzan (below **B** and **B**). Completion of scaffold-free tubular tissue comprising only live cells as a tissue-engineered vascular graft (**C**). 3D, three-dimensional. full color online

Figure 3. Tissue-engineered vascular grafts (length 8 mm, inner and outer diameters, 2 and 4 mm, respectively (**A**). Implanted tissue-engineered vascular graft (**B**) with good patency on Doppler ultrasonography (**C**) and a steady flow (**D**). Median venous flow speed was 6.1 cm/s (range = 3.9–8.2) on postoperative day 2 and 5.2 cm/s (range = 5.1–5.2) on postoperative day 5, with no significant difference between them (p = 0.72). full color online

Histologic and Immunohistochemical Examination

Histologic analyses were performed on postoperative day 2 (n = 2) and postoperative day 5 (n = 2) after implantation in rats using a polarizing microscope (BX51; Olympus Corp, Tokyo, Japan) with imaging software (cellSens Standard; Olympus Corp.). The tissue morphology was examined following hematoxylin-eosin (HE) staining. For immunohistochemical analysis, tissues were fixed in neutral buf- fer formalin. The tissue was sectioned to 4 µm thickness using a microtome and labeled using the immunoenzyme (peroxidase-antiperoxidase) method. Immunohistochemical analysis was performed to evaluate the expression of von Willebrand factor (vWF) and cluster of differentiation 31 (CD31) as endothelial cell markers, and erythroblast transformation-specific-related gene (ERG)[14] as an endothelial differentiation and angiogenesis marker (Abcam plc. Tokyo, Japan).

The inner and outer diameter and length of the tubu- lar tissue structures were observed and directly measured under a digital stereo zoom microscope (Leica S6 D; Leica Microsystems, Wetzlar, Germany). The wall and luminal area of cross-sections of each tubular tissue structure, and the ratio of the areas with and without vWF expression in the cross-section of the wall were measured preimplantation, and on days 2 and 5 to evaluate the remodeling process using

Image J software (version 1.44; National Institute of Health, Bethesda, MD).[15]

Preliminary Implantation of Tubular Tissue Into the Swine Jugular Vein

A Göttingen mini-pig (female, 8 months old, 16.6 kg; Kitayama Labs and Oriental Yeast Co., Ltd., Ina, Japan) was anesthetized with 2–4% isoflurane inhalation. A larger 3D bioprinted swine dermal fibroblast-derived prototype of tubular tissue (n = 1) with length, and inner and outer diameters of 14, 5, and 8 mm, respectively (Figure 4A), was implanted in the right jugular vein under 3× surgical loupes (SurgiTel; Oral Care, Inc, Tokyo, Japan). Oral ampicillin (125 mg/body) and an intramuscular injection of buprenorphine hydrochloride (0.2 mg/body) were administered daily for 7 days after implantation. Neither immunosuppressants nor steroids were administered. Patency was examined by Doppler ultrasound (Arietta Prologue; Hitachi Co. Ltd, Tokyo, Japan) every week. Computed tomography (SOMATOM Definition AS+, Siemens, Germany) was performed to assess the blood flow and luminal diameter of the implanted tubular tissue using intravenous (*via* contralateral internal jugular vein) contrast medium (Omnipaque; GE Health Care, Tokyo, Japan) at 4 weeks after implantation.

Number of Spheroids

The trial data indicated that of the 288 spheroids set up (number of spheroids detected) for printing, 286 spheroids were successfully used (number of empty wells after spheroid pick up), resulting in a 99.3% accuracy rate for spheroids picked up by the printer. In the current study, we fabricated four tubular tissues for rats (22 spheroids × 40 layers = 880 spheroids/each) and one tubular tissue for swine (36 spheroids × 80 layers = 2880 spheroids).

Statistical Analysis

Data were compared using the Wilcoxon signed-rank test and are expressed as median and range. A p value <0.05 was considered statistically significant. JMP Pro statistical software (SAS Institute, Cary, NC, Version 17.0.0) was used for the analysis.

Results

Rat Venous Experiment Model

Actual median length, and inner and outer diameters of the tubular tissue were 9.4 mm (range = 8.3–14.0), 2.1 mm (range = 1.8–2.8), and 3.9 mm (range = 3.8–5.6), respectively. In all four rats, implanted tubular tissues were patent on days 2–5 (Figure 3C) with no mural thrombus detected (Figure 5). Median venous flow speed was 6.1 cm/s (range = 3.9–8.2) on postoperative day 2 and 5.2 cm/s (range = 5.1–5.2) on postoperative day 5, with no significant difference between them (p = 0.72; Figure 3D). Although the cross-sectional area of the wall differed significantly between preimplantation and days 2 and 5, suggesting swelling of the tubular tissue wall (both p < 0.01; Figure 6B), the luminal diameter of the tubular tissues did not differ significantly between preimplantation and days 2 and 5 after implantation (p = 0.32 and p = 0.26; Figure 6A). Acute inflammatory cell infiltration into the circumference of the implanted tubular tissues was not observed (Figure 5, HE).

An optical microscopy image of a low-power field view of a rat showed no inflammatory cell infiltration, indicat- ing no acute rejection or infection of the tubular tissue in HE-stained sections (Figure 5, HE). No mural thrombus was found among all cross sections. Immunohistochemistry analysis showed vWF positivity on almost 67% of the luminal side of the cross-sectional area of the wall on day 2, with more limited positivity observed on the luminal surface on day 5 (Figure 5, vWF), which was expected to form an endothelial cell layer on the luminal surface. CD31 and ERG endothelial cell markers, however, remained negative on days 2 and 5 (Figure 7, CD31, ERG). In the high-power view, vWF positivity was more evident on the surface of the luminal area, potentially indicating endothelial cell colonization. Flat cells on those surfaces indicative of endothelial cell colonization, however, were not apparent in HE-stained sections (Figure 7, HE, vWF).

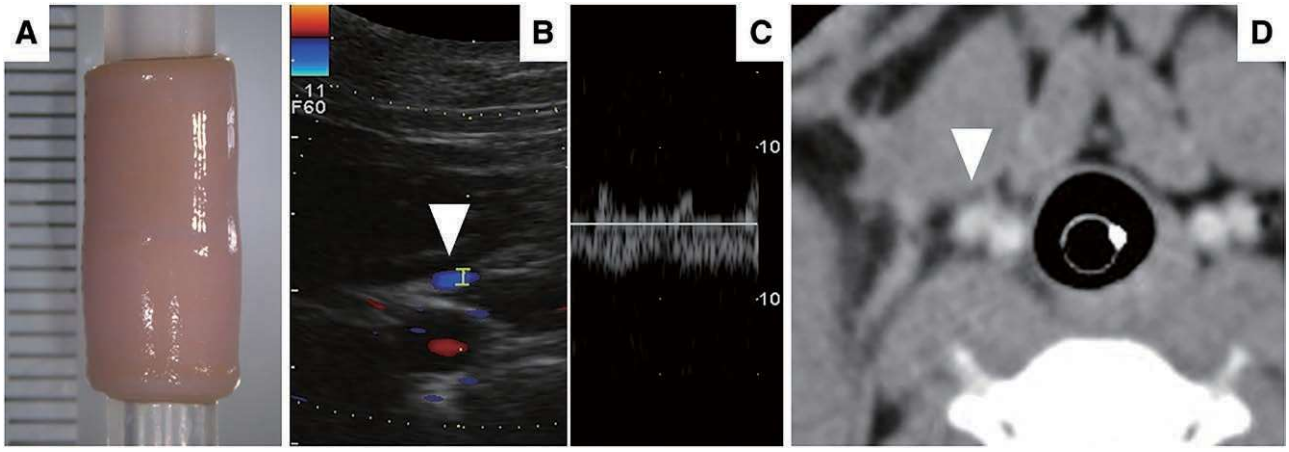

Figure 4. For the swine jugular vein (**A**), Doppler ultrasonography showed good patency (**B**) with a steady flow rate of 7.8 cm/s (**C**). Contrast-enhanced computed tomography also showed favorable patency without stenosis or mural thrombus at 28 days after implantation (**D**). full color online

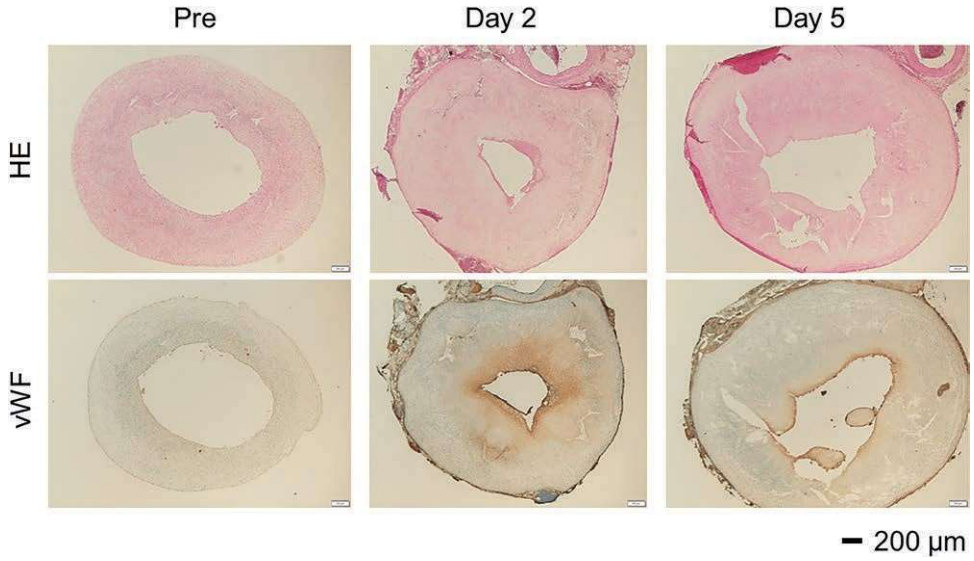

Figure 5. Optical microscope image with low-power field view of a rat graft showing no inflammatory cell infiltration, indicating no acute rejection or infection in hematoxylin and eosin-stained tubular tissue (HE). No mural thrombus was observed in any of the cross sections. Immunohistochemical analysis showed vWF positivity on almost 67% of the luminal side of the cross-sectional area of the wall on postoperative day 2, with more limited positivity on the luminal surface on postoperative day 5 (vWF), which was expected to subsequently form an endothelial cell layer on the luminal surface. HE, hematoxylin eosin; vWF, von Willebrand factor. full color online

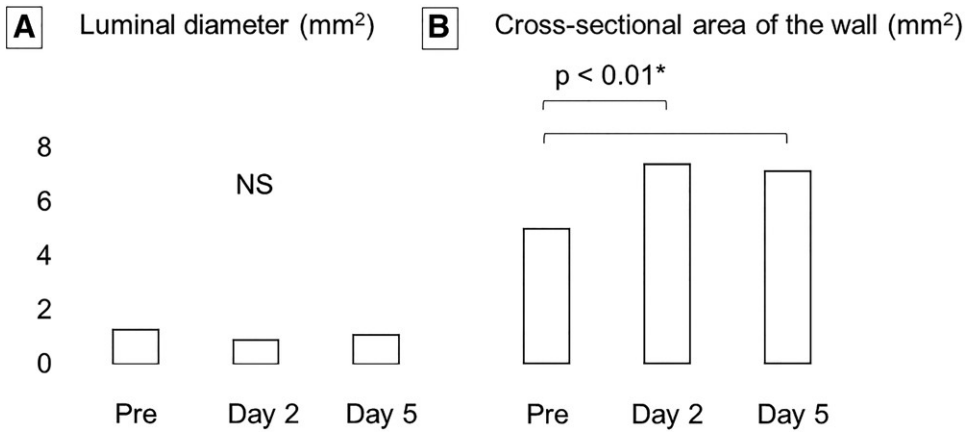

Figure 6. Although there was no significant difference in the luminal diameter of the tubular tissues between preimplantation and postoperative days 2 and 5 after implantation ($p = 0.32$ and $p = 0.26$, respectively) (**A**), the cross-sectional area of the wall showed a significant difference between preimplantation and postoperative days 2 and 5 (both $p < 0.01$) (**B**). All patency rates were 100% in the short term.

Swine Venous Experiment Model

The actual length, and inner and outer diameters of the tubular tissue were 15.1, 4.9, and 7.0 mm, respectively. Doppler ultrasonography showed patency with a steady flow, 6.8 cm/s (Figure 4, B and C). Contrast-enhanced computed tomography also showed favorable patency with no stenosis or mural thrombus at 28 days after implantation (Figure 4D). The patency rate was 100% over the short term. A swine was kept alive for collection of additional data after the 4 week timepoint.

Discussion

This is the first report of synthetic vascular prostheses, or tissue-engineeredvasculargrafts,producedusing3Dbio-printing to fabricate tubular tissues from human or swine dermal fibroblast spheroids for venous implantation in rats and swine, respectively. The new bio-printed synthetic vascular prostheses exhibited better short-term patency rates without mural thrombus and histologic reaction in rats and 28 day patency in swine.

In contrast to the numerous reports on arterial synthetic vascular prostheses, the development of a prosthesis for veins has long been overlooked. Recent advancements in hepatobiliary-pancreatic surgical procedures have increased the need for a new venous synthetic vascular prosthesis to replace major abdominal veins.[16] In the clinical setting, studies reporting the patency rates of venous replacements using synthetic vascular prostheses are limited. For example, in hepatic venous reconstruction, although the 4 week patency rate of expanded polytetrafluoroethylene grafts is 81%, the 4 month patency rate is only 39%.[17] Synthetic vascular prostheses are often

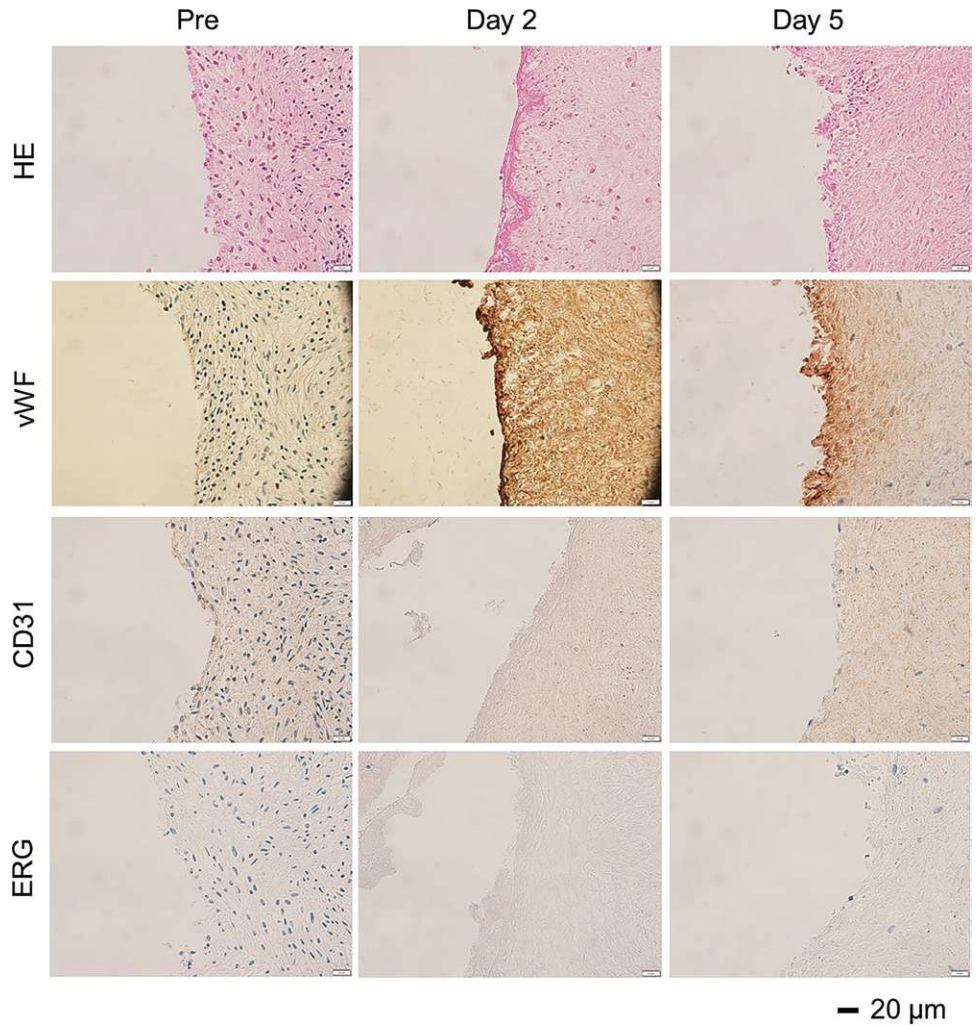

Figure 7. High-power view showing more vWF positivity on the surface of the luminal area, which may indicate endothelial cell colonization. Flat cells were not apparent on those surfaces in HE staining (HE, vWF). CD31 and ERG staining were negative on postoperative days 2 and 5 (CD31, ERG). CD31, cluster of differentiation 31; ERG, erythroblast transformation-specific-related gene; HE, hematoxylin-eosin; vWF, von Willebrand factor. full color online

obstructed by platelet activation, leukocyte adhesion, thrombosis, and intimal hyperplasia.[18] Thus, a higher patency rate is necessary for newer tissue-engineered vascular grafts aimed at venous replacement.

Fibroblasts may be the most suitable cell source for regenerative medicine.[11] Fibroblasts are already used to develop tubular structures that are dehydrated and decellularized for arterial implantation.[19] Our eventual goal is to use a patient's own dermal fibroblasts in the clinical setting. Isolation and culture of human dermal fibroblasts is an established procedure. Therefore, in the current study, we used human dermal fibroblasts in immunodeficiency rat models. A recent study[20] showed that dry-preserved multilayered fibroblast cell sheets promote angiogenesis and wound healing in a mouse ulcer model by releasing high levels of intracellular FGF2, hepatocyte growth factor, and vascular endothelial growth factor (VEGF), which is the most important factor for better and faster endothelial remodeling. A study of rabbit external iliac arteries showed that endothelialization was nearly complete (92%) at 7 days with local VEGF delivery compared with less than 40% endothelialization at 7 days without VEGF delivery.[21] In the current study, we successfully developed a tubular tissue structure consisting of live fibroblast cells using 3D bioprinting technology. Although the present experimental model achieved 100% short-term patency, significant potential swelling of the tubular tissue wall at day 2 may be problematic. No difference in the venous flow speed was observed on ultrasonography, however, between postoperative days 2 and 5, indicating that the inner diameter did not become stenotic because a narrow inner diameter generally leads to an increased flow speed. Further studies are needed to evaluate the remodeling processes of fibroblast spheroids, as well as the mechanism of wall swelling and its long-term impact on the graft.

Although the remodeling process is key to developing new synthetic vascular prostheses, endothelialization of conventional synthetic vascular prostheses does not generally occur.[22] Endothelialization in remodeling processes contributes to antithrombogenic and antiatherogenic properties for better patency and protects the graft from infection.[23] In experimental models, there are few reports of synthetic vascular prostheses for veins in animals. On the other hand, in a recent report, endothelialization occurred in a silk fibroin

vascular graft, which is a model of venous replacement with high biocompatibility.[16] Kiritani *et al.*[16] described that CD31- positive endothelial cells covered the whole luminal surface of silk fibroin vascular grafts at 4 weeks in a rat IVC replace- ment model, which had a high patency rate. In the current study, we achieved a 100% short-term patency rate in rats (5 days, n = 4), but found no CD31-positive endothelial cells. In rabbits and rats, completion of endothelialization must occur within 28 days.[16,21] The current study was a 5 day pre- liminary evaluation of 3D-printed tissue-engineered vascular grafts for venous replacement. Longer observation periods are necessary for future experiments, however, because CD31 was expected to be positive in the vWF-positive cells and result in faster endothelialization in this experimental model.

In a previous study of tissue-engineered vascular grafts for arteries, a similar protocol was reported except the spheroids came from a mixed-cell source comprising human umbilical vein endothelial cells (40%), human aortic smooth muscle cells (10%), and normal human dermal fibroblasts (50%).[9] Here, based on another report of artery grafts,[10] we only used dermal fibroblast cells to make the spheroids. As mentioned in the introduction, this approach may have considerable advantages. Through this process, blood vessels can be made using cells obtained from the patient's own skin and require no immunosuppressants. In a previous report on artery replace- ment using 3D bio-printed tubular tissue derived from human dermal fibroblasts,[10] postimplantation histopathologic exami- nation revealed host-derived cells, including vascular endo- thelial cells, vascular smooth muscle cells, and elastic fibers. Those findings indicate that the new tissue-engineered vascu- lar grafts can undergo ideal remodeling processes for venous replacement.

Limitations

This preliminary study has some limitations, including a short observation period. The present experimental model could not show whether an endothelial cell layer would form on the luminal surface even though the surface was positive for vWF. The role of living dermal fibroblasts is still not clear. As a negative control, inactivated dermal fibroblasts would be use- ful to compare endothelization. Highly biocompatible cryo- preserved homologous vein or silk fibroin synthetic grafts may be useful as a positive control. In addition, the sample size in current study was small. Further research is needed to address these limitations.

Conclusions

Three-dimensional bio-printed scaffold-free tubular tis- sues using human dermal or swine fibroblast spheroids may produce better tissue-engineered vascular grafts for venous replacement in rats or swine.

References

1. Zwart ES, Yilmaz BS, Halimi A, et al: Venous resection for pancre- atic cancer, a safe and feasible option? A systematic review and meta-analysis. *Pancreatology* 22: 803–809, 2022.
2. Yamamoto M, Akamatsu N, Aoki T, et al: Safety and efficacy of cryopreserved homologous veins for venous reconstruction in pancreatoduodenectomy. *Surgery* 161: 385–393, 2017.
3. Yamamoto M, Akamatsu N, Hayashi A, et al: Safety and efficacy of venous reconstruction in liver resection using cryopreserved homologous veins. *J Hepatobiliary Pancreat Sci* 24: 511–519, 2017.
4. Zilla P, Bezuidenhout D, Human P: Prosthetic vascular grafts: Wrong models, wrong questions and no healing. *Biomaterials* 28: 5009–5027, 2007.
5. Teebken OE, Haverich A: Tissue engineering of small diameter vascular grafts. *Eur J Vasc Endovasc Surg* 23: 475–485, 2002.
6. Chung Y-K, Park C-S: Migration of synthetic vascular graft used for middle hepatic vein reconstruction during living donor liver transplantation using a modified right liver graft: A collective review of worldwide cases. *Ann Liver Transplant* 2: 127–131, 2022.
7. Plikus MV, Wang X, Sinha S, et al: Fibroblasts: Origins, definitions, and functions in health and disease. *Cell* 184: 3852–3872, 2021.
8. Moldovan NI, Hibino N, Nakayama K: Principles of the Kenzan method for robotic cell spheroid-based three-dimensional bio- printing. *Tissue Eng Part B Rev* 23: 237–244, 2017.
9. Itoh M, Nakayama K, Noguchi R, et al: Scaffold-free tubular tis- sues created by a bio-3D printer undergo remodeling and endothelialization when implanted in rat aortae. *PLoS One* 10: e0136681, 2015.
10. Itoh M, Mukae Y, Kitsuka T, et al: Development of an immunodefi- cient pig model allowing long-term accommodation of artificial human vascular tubes. *Nat Commun* 10: 2019, 2244.
11. Yanagihara M, Matsuno Y, Ueno K, et al: Fibroblasts are the most suitable cell source for regenerative medicine due to their high intracellular fibroblast growth factor 2 content. *Biochem Biophys Rep* 35: 101510, 2023.
12. Murata D, Arai K, Nakayama K: Scaffold-free bio-3D printing using spheroids as "bio-inks" for tissue (Re-)construction and drug response tests. *Adv Healthc Mater* 9: e1901831, 2020.
13. Nakayama K: *Kenzan Method for Scaffold-Free Biofabrication - Development of Scaffold-Free*

3D Biofabrication System "Kenzan Method". Switzerland, Springer, 2020, pp. 1–15.
14. Han R, Pacifici M, Iwamoto M, Trojanowska M: Endothelial erg expression is required for embryogenesis and vascular integrity. *Organogenesis* 11: 75–86, 2015.
15. Schneider CA, Rasband WS, Eliceiri KW: NIH Image to ImageJ: 25 years of image analysis. *Nat Methods* 9: 671–675, 2012.
16. Kiritani S, Kaneko J, Ito D, et al: Silk fibroin vascular graft: A prom- ising tissue-engineered scaffold material for abdominal venous system replacement. *Sci Rep* 10: 21041, 2020.
17. Yi NJ, Suh KS, Lee HW, et al: An artificial vascular graft is a useful interpositional material for drainage of the right anterior section in living donor liver transplantation. *Liver Transpl* 13: 1159– 1167, 2007.
18. Haruguchi H, Teraoka S: Intimal hyperplasia and hemodynamic factors in arterial bypass and arteriovenous grafts: A review. *J Artif Organs* 6: 227–235, 2003.
19. Syedain Z, Reimer J, Lahti M, Berry J, Johnson S, Tranquillo RT: Tissue engineering of acellular vascular grafts capable of somatic growth in young lambs. *Nat Commun* 7: 12951, 2016.
20. Matsuno Y, Yanagihara M, Ueno K, et al: Dry preserved multi- layered fibroblast cell sheets are a new manageable tool for regenerative medicine to promote wound healing. *Sci Rep* 12: 12519, 2022.
21. Van Belle E, Tio FO, Couffinhal T, Maillard L, Passeri J, Isner JM: Stent endothelialization. Time course, impact of local catheter delivery, feasibility of recombinant protein administration, and response to cytokine expedition. *Circulation* 95: 438–448, 1997.
22. Chlupac J, Filova E, Bacakova L: Blood vessel replacement: 50 years of development and tissue engineering paradigms in vas- cular surgery. *Physiol Res* 58(suppl 2): S119–S140, 2009.
23. Seligsohn U, Lubetsky A: Genetic susceptibility to venous throm- bosis. *N Engl J Med* 344: 1

Original research article

IJAO The International Journal of Artificial Organs

Thick silk fibroin vascular graft: A promising tissue-engineered scaffold material for abdominal vein grafts in middle-sized mammals

The International Journal of Artificial Organs
2024, Vol. 47(3) 190-197
© The Author(s) 2024
Article reuse guidelines:
sagepub.com/journals-permissions
DOI: 10.1177/03913988241234547
journals.sagepub.com/home/jao
Sage

Kaito Fukuda[1], Junichi Kaneko[1], Sho Kiritani[1], Yui Sawa[1], Masaaki Morito[1], Mariko Tanaka[2], Tetsuo Ushiku[2], Chieh-Jen Cheng[3], Takashi Tanaka[3], Ryo Tanaka[3], **Tetsuo Asakura[4], Yoshikuni Kawaguchi[1], Nobuhisa Akamatsu[1] and Kiyoshi Hasegawa**

Abstract

Abdominal vein replacement with synthetic tissue-engineered vascular grafts constructed from silk-based scaffold material has not been reported in middle-sized mammals. Fourteen canines that underwent caudal vena cava replacement with a silk fibroin (SF) vascular graft (15 mm long and 8 mm diameter) prepared with natural silk biocompatible thread were allocated to two groups, thin and thick SF groups, based on the graft wall thickness. The short-term patency rate and histologic reactions were compared. The patency rate at 2 weeks after replacement in the thin and thick SF groups was 50% and 88%, respectively ($p = 0.04$). CD31-positive endothelial cells covered the luminal surface of both groups at 4 weeks. The elastic modulus of the thick SF graft was significantly better than that of the thin SF graft (0.0210 and 0.0007 N/m^2, $p < 0.01$). Roundness of thick SF groups ($o = 0.8$ mm) was better than thin SF ($o = 2.0$ mm). There was significant difference between the groups ($p = 0.01$). SF vascular grafts are a promising tissue-engineered scaffold material for abdominal venous system replacement in middle-sized mammals, with thick-walled grafts being superior to thin- walled grafts.

Keywords

Hepatobiliary pancreatic surgery, venous replacement, silk fibroin, synthetic vascular graft

Date received: 30 October 2023; accepted: 7 February 2024

[1]Hepato-Biliary-Pancreatic Surgery Division, Department of Surgery, Graduate School of Medicine, The University of Tokyo, Bunkyo-ku, Tokyo, Japan
[2]Department of Pathology, Graduate School of Medicine, The University of Tokyo, Bunkyo-ku, Tokyo, Japan
[3]Department of Veterinary Surgery, Tokyo University of Agriculture and Technology, Fuchu, Tokyo, Japan
[4]Department of Biotechnology, Tokyo University of Agriculture and Technology, Koganei, Fuchu, Tokyo, Japan

Corresponding authors:
Junichi Kaneko, Hepato-Biliary-Pancreatic Surgery Division, Department of Surgery, Graduate School of Medicine, The University of Tokyo, 7-3-1 Hongo, Bunkyo-ku, Tokyo 113-8655, Japan.
Email: jkaneko-gi@umin.ac.jp

Kiyoshi Hasegawa, Hepato-Biliary-Pancreatic Surgery Division, Department of Surgery, Graduate School of Medicine, The University of Tokyo, 7-3-1 Hongo, Bunkyo-ku, Tokyo 113-8655, Japan.
Email: kihase-tky@umin.ac.jp

Introduction

Complete excision is currently the only curative treatment option for hepatobiliary pancreatic cancer. Although this cancer often invades major abdominal venous systems, such as the hepatic veins, inferior vena cava, portal vein, and superior mesenteric vein,[1-3] there was no better synthetic vascular grafts than expanded polytetrafluoroethylene as a material for those venous replacement.

For artery replacement, fully synthesized vascular grafts constructed from expanded polytetrafluoroethylene are fre- quently used. Although expanded polytetrafluoroethylene vascular grafts have been applied for vein replacement in hepato-biliary-pancreatic surgery,[4] their use is limited due to low-flow thrombogenicity without endothelialization and higher graft infection rates in contaminated tissue beds under digestive fluids.[5] Additionally, fully synthetic vascu- lar grafts remain in the human body permanently and the long-term effects are unclear. To date, no alternative tissue- engineered venous grafts or scaffolds have been reported.

Silk fibroin (SF) is a promising tissue-engineered scaffold material derived from silk fiber with good biocompatibility, high affinity for cells, and susceptibility to proteolytic degradation in vivo without antigenicity.[6] Artery replacement in a rat model using double-raschel knitted SF vascular grafts coated with an SF sponge has been reported.[6,7] A recent study reported that SF application for rat vein replace- ment produced a better short-term outcome than expanded polytetrafluoroethylene, with acceptable patency and vascu- lar remodeling.[8] The potential for extrapolation of these findings of better patency from our previous study in rats to a larger animal such as humans, however, is unknown. Veins comprise a low-pressure system, which, in humans, gener- ally ranges from 8 to 10 mmHg with the central venous pres- sure ranging from 0 to 6 mmHg.[9] The intra-abdominal pressure of middle- and large-sized mammals is higher than that of small mammals. For example, the intra-abdominal pressure of a rat is 2.2 mmHg,[10] whereas it is 7.4 mmHg in canines and ranges from 5 to 15 mmHg in humans.[11,12] A higher intra-abdominal pressure than venous pressure can cause veins to collapse. A highly elastic synthetic vascular graft, therefore, could potentially collapse and obstruct sooner.

To explore the application of SF grafts in clinical practice, it is important to evaluate wider and longer synthetic SF vascular grafts in middle-sized mammals. The present study examined the patency rate and histologic reaction of thick and thin SF vascular grafts, thick and thin SF films with different wall strengths, as replacements for the caudal vena cava in a middle-sized mammal (canine).

Materials and methods

SF vascular grafts coated with an SF sponge

The vascular SF grafts were prepared as follows. SF double-raschel knit tubes with SF threads from *Bombyx mori* were prepared by two-needle stitch knitting on a computer-controlled double-raschel knit machine (Fukui Warp Knitting Co Ltd, Fukui City, Japan).[13] In detail, fertilized eggs of *Bombyx mori* were supplied by Gunma Sericultural Technology Center, and the larvae were reared in Asakura laboratory by feeding them an artificial diet (Silk Mata 2M, Nippon Nosan Kogyo Corp., Tokyo, Japan). *B. mori* cocoons were obtained. Marseille soap and sodium carbonate were purchased from Miyoshi soap Corp., Japan and Tokyo chemical industry Co., Ltd., Tokyo, Japan. A silk fiber was of 42 Deniers. For use in canines, the inner diameter was 8 mm. The SF fibers contained a small amount of silk sericin to maintain thread strength and avoid SF thread breakage in the knitting process. Therefore, the knit SF tube had to be degummed in a mixture of sodium carbonate (0.08% w/v) and Marseille soap (0.12% w/v) solution at 95°C for 2 h to remove the remaining silk sericin. Removal of silk sericin was confirmed by scanning electron microscope (Real surface view microscope VE-7800, Keyence, Tokyo, Japan).[14]

Thin coating (thin SF group). An expanded polytetrafluoroethylene rod was inserted into the knit SF tube. The rod covered with the SF tube was immersed into a pipe filled with a mixed aqueous solution of SF and glycerin (as a porogen) at a 1:1 (w/w) ratio for coating. Preparation of the SF aqueous solution was described previously.[15] The pipe was placed in a desiccator under a reduced pressure of 100 hPa until no air bubbles were observed on the coated surface of the SF tube.

Thick coating (thick SF group). A SF tube was set in a coax- ial pipe and a mixed aqueous solution of SF and glycerin was poured into the gap between the pipe and SF tube. In details, the difference between the fabrication method of thin and thick coating was as follows: for thin coatings, the SF tube was removed from the pipe before freezing at −20°C, and then only the SF tube was freeze-dried later. On the other hand, for thick coatings, the SF tube was freeze-dried with the pipe at the same time, while still immersed in the solution.

The SF tubes of both groups were frozen at −20°C overnight before immersing in distilled water. Both SF grafts were freeze-dried and kept in a refrigerator until implantation into an animal.

Scanning SF grafts and measurement of physical properties

The knitted pattern of the SF fibers from the outside surface and a cross-section of 8-mm diameter SF grafts were observed by scanning electron microscopy (JSM-6360LA, Japan Electron Optics Laboratory Ltd., Tokyo, Japan).

Sample size was 10 mm long, 8 mm in diameter and total six SF grafts were used (three thick SF and three thin SF, respectively). The breaking strengths of the SF graft were measured using a tabletop material tester (EZ-graph,

SIMAZU Coup., Kyoto, Japan)[16]. Each sample SF vascu- lar graft was placed in the testing machine and slowly extending it until they broke (Supplemental Figure 1A). The load cell was 100 N, and the stretching rate was 2 mm/ min.

The compressive elastic modulus of the knitted grafts (10 mm long, 8 mm in diameter) was also determined using the same tabletop material tester. The load cell was 5 N, and the compression rate was 2 mm/min. The elastic modulus (N/mm^2), when compressed to 25% of the diameter, was calculated with the following formula: Elastic Modulus (Young's modulus), $E = \sigma$ (compressive stress)/ε (Δdiameter / diameter, strain) using analysis software (TRAPEZIUM, SIMAZU Coup., Kyoto, Japan; Supplemental Figure 1B, C).

Animal model

The study protocols (I-P16-034) and (R03-32) were approved by the University of Tokyo and the Tokyo University of Agriculture and Technology Animal Ethics Committee in accordance with the Japanese and ARRIVE (Animal Research: Reporting of In Vivo Experiments) guidelines. We used female beagles (Kitayama Labes Co.,Ltd., Nagano, Japan) weighing 8–17 kg. All canines were kept in cages for 2–4 weeks with a 12-h light/dark cycle. The canines were fasted overnight before undergo- ing the surgical procedure.

Surgical procedure

All surgical procedures were performed by hepato-biliary-pancreatic surgeons (KF, SK, and JK). The canines under- went general anesthesia using midazolam (0.2 mg/kg: Sandoz K.K, Tokyo, Japan) and buprenorphine (0.02 mg/ kg; Nissin Co, Kanagawa, Japan) as premedication fol- lowed by intravenous injection of propofol (3 mg/kg body weight, titrated to effect; JMS Co., Ltd, Hiroshima, Japan) for induction and isoflurane (1.3%–1.6%; Pfizer, New York, NY, USA) for maintenance anesthesia by a veterinar- ian (C.C.). Cefazolin (20 mg/kg; Nichi-Iko Pharmaceutical Co, Ltd, Toyama, Japan) was given intravenously at the time of induction. No postoperative antibiotics were administered.

The caudal vena cava was exposed from the bifurcation of the renal veins to the bifurcation of the iliac veins, and all branches of the caudal vena cava were ligated and divided with 3-0 silk (Alfresa Pharma CO., Osaka, Japan) knotted sutures using an electric scalpel. After intravenous injection of unfractionated heparin (100 IU/kg; AY Pharmaceuticals Co., Ltd, Tokyo, Japan), the proximal and distal portions of the caudal vena cava were clamped with vascular clips. Approximately 15 mm of the caudal vena cava was removed and replaced with the SF vascular graft (15 mm long, 8 mm in diameter) by continuous sutures using 6-0 Prolene (Johnson & Johnson med Co., Raritan, NJ, USA), starting with two stay sutures 180° apart at both the cranial and cau- dal sides, then suturing the back wall, followed by the front wall. The cranial and caudal sides of the vascular graft were de-clamped (Figure 2). Anticoagulants, Dalteparin (100 U/ kg three-times-daily, Nichi-Iko Pharmaceutical Co, Ltd, Toyama, Japan) was given subcutaneously for 7 days.. Clopidogrel (Sawai Pharmaceutical Co, Ltd, Osaka, Japan) was given orally at day 0 with a loading dose of 4 mg/kg followed by 2 mg/kg once daily on days 1, 2, 3, 5, and 7.

Patency assessment

The patency of the SF graft vascular grafts was monitored extracorporeally by Doppler ultrasonography (EnVisor M25040A; Phillips, Tokyo, Japan) on postoperative days 1, 3, 5, and 7, and then every week for 4 weeks, and then every month. Graft occlusion was defined as the absence of a color Doppler signal. In the absence of a color Doppler signal, the canine was anesthetized as mentioned above, and the graft was grossly and pathologically evaluated.

Histologic analysis

At 4 weeks after surgery or at the time of confirming an occlusion, the canines underwent general anesthesia as described above. The grafts were carefully removed with the surrounding tissue. Cross-sections of the middle of the SF grafts were fixed in 20% formalin, embedded in paraf- fin, and sectioned (4-μm thick, Tissue-Tek Auto Section, Sakura Finetek Japan Co., Ltd.) for hematoxylin and eosin staining. Elastica van Gieson staining was applied to detect elastic and collagen fibers. Immunohistochemical staining was performed as previously reported.[17] The sections were incubated with primary antibodies, including alkaline phosphatase-conjugated anti-alpha smooth muscle actin (anti-αSMA; clone 1A4, MilliporeSigma, St. Louis, MO, USA), anti-rat CD 31 antibody (clone TLD-3A12, BD Biosciences, San Jose, CA, USA), and anti-podoplanin antibody (ab11936, Abcam, Cambridge, MA, USA) fol- lowed by incubation with biotinylated anti-mouse immu- noglobulin (Ig) G secondary antibody (DAKO, Glostrup, Denmark).

Roundness was measured on each cross-section of thin and thick SF grafts in hematoxylin and eosin staining, was calculated with the following formula: roundness (mm, diameter measurement method) = difference between cir- cumscribed and inscribed circle in diameter / 2. The analy- sis was performed using Image J software (version 1.44; National Institute of Mental Health Bethesda, MD, USA).[18] To know thickness of normal native caudal vena cava of canine, hematoxylin and eosin, and EVG staining were performed.

Rats were also anesthetized and grossly and pathologi- cally evaluated at 1 month and 12 months after surgery. To

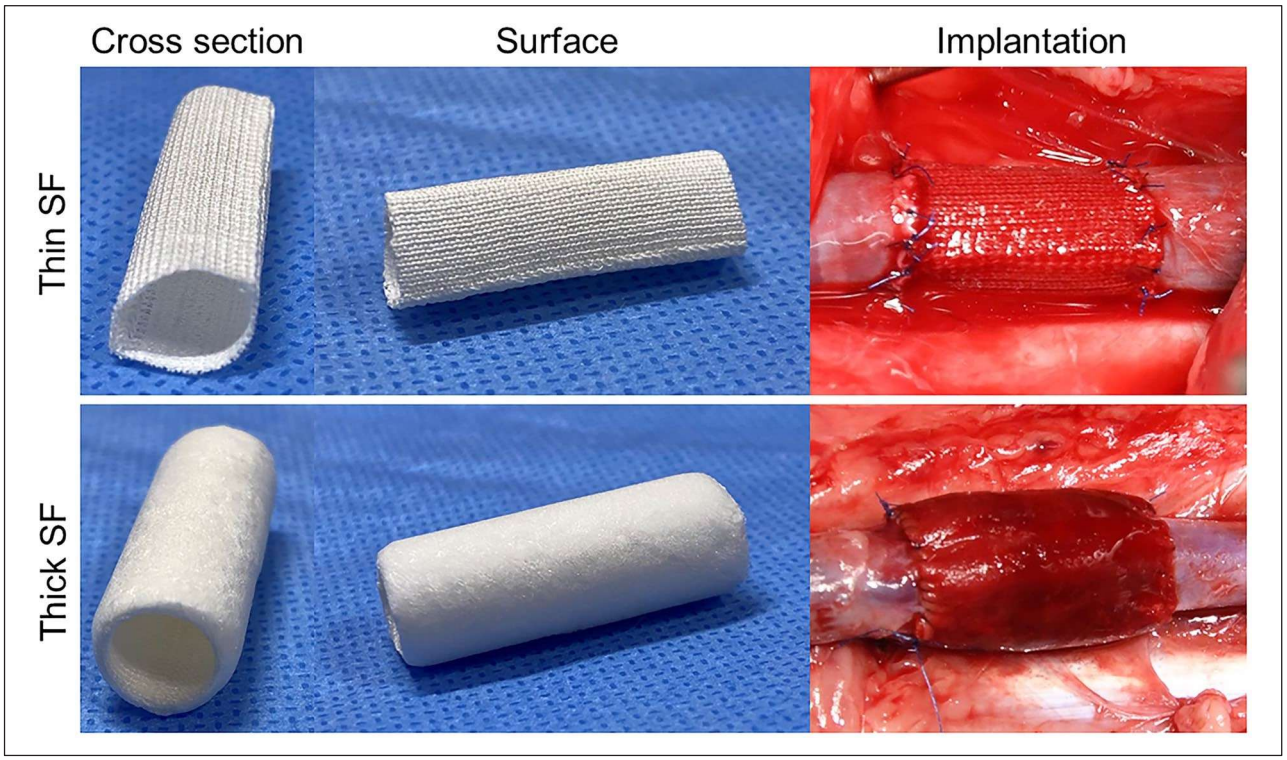

Figure 1. Thin SF had a reticulate appearance on gross examination, whereas the thick SF had a sponge-like appearance with a soft texture. In both SF groups, the graft turned red after implantation in canine (8.0 mm in diameter, 15 mm length) because the blood cells infiltrated the interfiber space, but did not leak out of the graft.

determine the degree of degradation, semi-quantitative analysis was used to evaluate the ratio of SF fibers and infiltrated tissue area of a representative cross-section of the SF graft wall. SF fibers, observed as aggregations of transparent dots on a representative cut surface, were encircled by yellow lines on a histologic image by three surgeons (KF, JK, and YS). The area of infiltrated autologous cells—the other area of the whole SF graft wall—was encircled with a blue line. The ratio of the remaining SF fiber area (yellow) to autologous cells (blue) was determined to calculate the area of 1 cut surface of the SF graft that was replaced by autologous cells at 1 and 12 months. The analysis was performed using Image J software (version 1.44; National Institute of Mental Health Bethesda, MD, USA).[18]

Statistical analysis

Continuous variables are expressed as the median and range. The backgrounds of each group were compared using the Mann–Whitney *U* test or Student *t* test. The log-rank test was used to compare the patency rate. A *p*-value less than 0.05 was considered statistically significant. Statistical analysis was conducted using software (JMP Pro version 16.0.0; SAS Institute, Cary, NC, USA).

Results

Appearance, scanning electron microscopy of SF grafts, and measurement of its physical properties

Thin SF grafts had a reticulate appearance on gross examination, whereas the thick SF grafts had a sponge-like appearance with a soft texture (Figure 1). After implantation, the color of grafts in both SF groups changed to red because blood cells infiltrated the interfiber space, but did not leak out of the graft. Scanning electron microscopy images, including the surfaces and cross-sections of SF grafts coated with SF sponges, are shown in Figure 2. The images revealed a reticulate and sponge-like appearance of both the thin and thick SF surfaces. In the cross-section, the thickness of the thin SF was 500 μm, whereas the thick SF graft thickness was 1500 μm. The cross-section view revealed that two-thirds of the external side of the thick SF grafts was coated with SF sponge.

Breaking strength was not significantly different between the thin and thick SF groups (35.5 and 42.2, $p = 0.29$), whereas the elastic modulus differed significantly (0.0210 and 0.0007 N/m^2, $p < 0.01$, Figure 2a, b). Stress-strain curve was shown in Supplemental Figure 2.

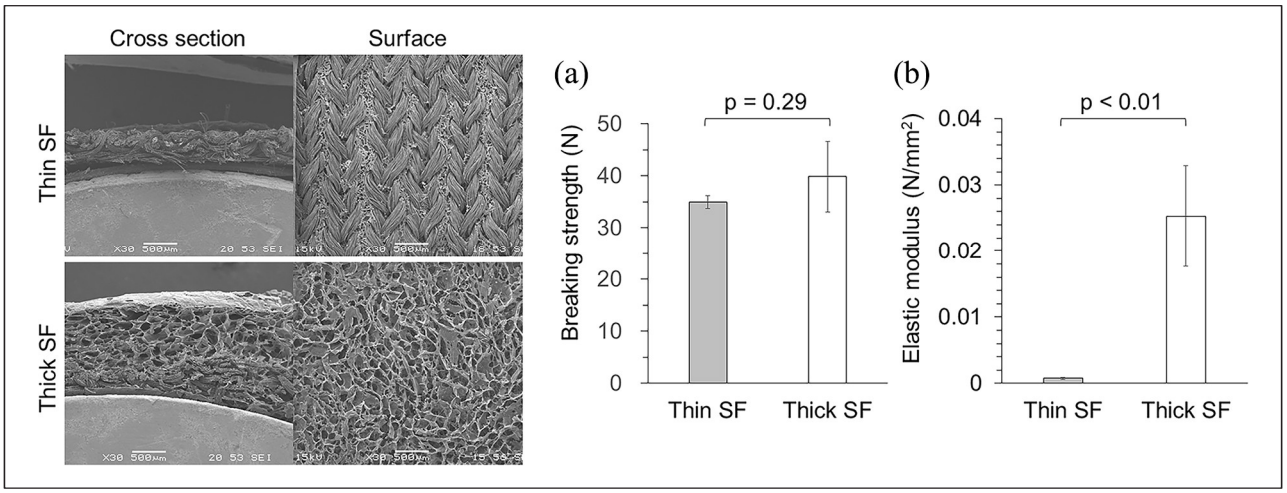

Figure 2. Scanning electron microscopy images including the surfaces and cross-sections of SF grafts coated with SF sponges are shown. Breaking strength did not differ significantly between the thin and thick SF groups (35.5 and 42.2, $p = 0.29$), whereas the elastic modulus was significantly different between groups (0.0210 and 0.0007 N/m^2, $p < 0.01$).

Animal model

We implanted 12 canines, 4 with the thin SF graft (thin SF group) and 8 with the thick SF graft (thick SF group). The median weight of the thin SF group was 8.0 kg (range 7.6–8.8) and that of the thick SF group was 8.2 (range 7.5–9.4), indicating no significant difference between groups (p = 0.864). The median diameter (8.0 mm vs 8.0 mm; p = 1.000) and length (15 mm [range 15–19 mm] vs 15 mm [range 15–15], p = 0.296) of the replaced caudal vena cava were not significantly different between the groups.

The inferior vena cava of two rats (13–14 weeks of age, weighing 400 g) were replaced by thin and small SF grafts (3 mm diameter, 10 mm length).

Graft patency

A representative Doppler ultrasonography result showing the flow inside the SF graft, indicating better venous flow, is shown in Figure 3a, b. Although the thin SF graft seemed to show slight stenosis of the intra-luminal diameter compared with the other parts of the canine caudal vena cava (Figure 3a), the thick SF graft seemed to have the same intra-luminal diameter (Figure 3b).

On postoperative day 1 (24 h later), the intra-luminal diameters differed significantly between the thin and thick SF vascular grafts (2.23 and 4.27 mm, respectively, $p < 0.01$, Figure 3) The patency rate is shown in Figure 4. Although there was no significant difference between the groups (log-rank, p = 0.18), there was a significant difference at day 14 (Student's t test, p = 0.04). At 28 days later, 50% (4/8) of the thick SF grafts were patent.

In the two rats, the grafts were patent at both 1 and 12 months, with no complications.

Histologic analysis

Hematoxylin and eosin staining of the thin and thick SF vascular grafts is shown in Figure 5. The graft lumens of both groups remained patent, but the walls of the thin SF grafts were deformed (Figure 5a) compared with those of the thick SF grafts (Figure 5b). In both the thin and thick SF vascular grafts, cellular proliferation was observed around the SF fibers, and the luminal surfaces were covered by flat cells (Figure 5). Elastica van Gieson staining of the SF vascular grafts revealed collagen fibers around the SF fibers, but no elastic fibers, (Figure 5, EVG). CD31 was expressed on the luminal surface of both SF vascular graft types (Figure 5, CD31). Anti-alpha smooth muscle actin antibody staining of the SF vascular grafts was positive (Figure 5, αSMA).

Roundness of thick SF groups (o = 0.8 mm) was better than thin SF (o = 2.0 mm). There was significant difference between the groups (p = 0.01).

Hematoxylin and eosin and EVG staining of normal native caudal vena cava of canine showed that wall thickness was around 1200 μm (Supplemental Figure 3a, b). It was approximately two times thicker than native caudal vena cava of rat, around 600 μm in previ- ous our report [8].

Discussion

This is the first report of SF vascular grafts for abdominal venous replacement in a canine model. We found that SF vascular grafts require a certain modulus of elasticity to have less deformity and better patency in middle-sized mammals. Furthermore, 89.5% of the SF vascular wall at 12 months was substituted by autologous cells, indicating better SF vascular graft degradation ability in rat.

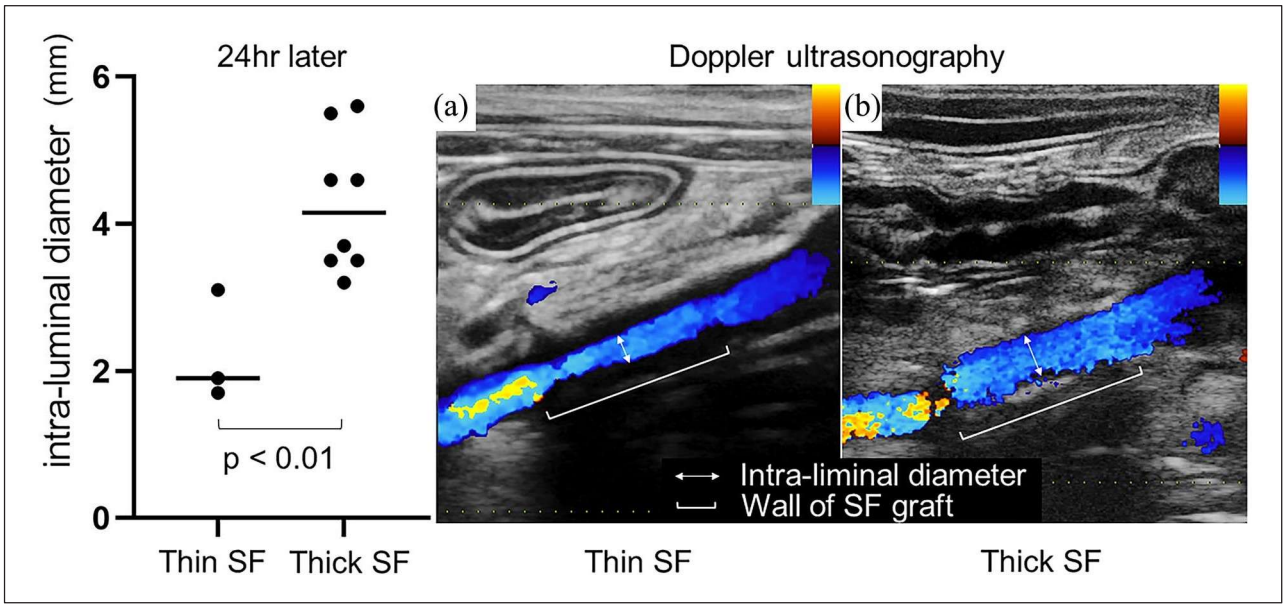

Figure 3. A representative Doppler ultrasonography result showing colored flow inside of the SF graft, indicating better venous flow as shown in (a) and (b). Although the thin SF grafts exhibited slight stenosis of the intra-luminal diameter compared with the other parts of the canine caudal vena cava (a), the thick SF was not stenotic (b). The intra-luminal diameter of the thin and thick SF vascular grafts was significantly different on postoperative day 1 (2.23 mm vs 4.27 mm, respectively, $p < 0.01$). Note, yellow color (a and b) indicated high velocity with disturbed flow, suggesting stenosis of anastomosis.

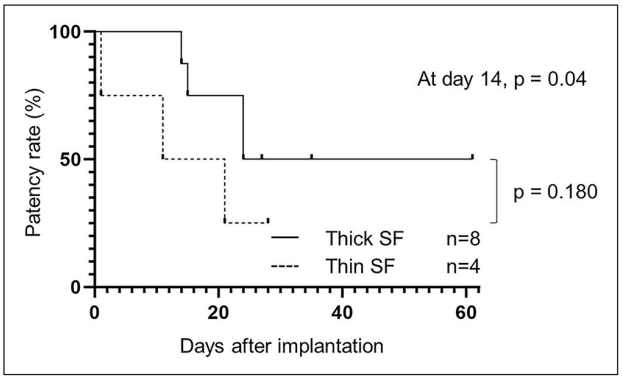

Figure 4. Although there was no overall significant difference in the patency of the grafts between groups (log-rank, $p = 0.18$), a significant difference was detected at day 14 (Student's t test, $p = 0.04$). At 28 days, 50% of the grafts in the thick SF group were patent (4/8).

Unlike the arterial system, vein walls do not have much elasticity due to a lack of, or fewer, elastic fibers in mammals. Contrary to our expectation, the thick SF grafts with a certain modulus of elasticity had better patency. In present study, we concluded that tortuous wall with narrow lumen due to inferior of roundness of thin SF grafts made inside narrower and led to earlier occlusion. As patency rate was shown in Figure 4, initial experiment using thin SF graft resulted in early obstruction, with 75% occlusion within 21 days (at day 14, $p = 0.04$). This led us to decide to increase the elasticity by adding thickness to the SF grafts, creating a new thick SF graft. We found that synthetic SF vascular grafts for the abdominal venous system should have a better modulus of elasticity, at least 40 N/mm^2 in canine caudal vena cava replacement model. The flexibility of the venous wall is another crucial point for maintaining a certain luminal diameter, but the thin SF grafts tended to collapse soon after insertion into the canine abdominal vein. As mentioned in the introduction, the larger the mam- mal's body size, the higher the intra-abdominal pressure.[11] We found that a certain wall strength was required to main- tain the luminal diameter, even for synthetic vein grafts. Further studies are needed to determine the precise corre- lation among venous pressure, intrabdominal pressure, wall strength of the SF vascular graft, and the change in flexibility after replacement.

Matsumura et al.[19] reported graft stenosis that occurred at 1 month after venous replacement using 8-mm diameter biodegradable scaffolds consisting of polyglycolide knit- ted fibers with a 3.6-mm intra-liminal diameter. They sug- gested that stenotic changes may lead to tissue regeneration disorders, blood flow disturbance, and more thrombogen- esis. In the present study, we found that stenosis developed at 24 h after replacement. The intra-liminal diameter of the thick SF vascular graft (4.3 mm) was larger than that of the thin SF graft (2.2 mm). The venous system has low pres- sure, however, and vascular grafts require higher elasticity to avoid stenosis and maintain better patency. Intramural thrombus was another problem and 50% of the thick SF grafts became obstructed within 4 weeks. A previous report

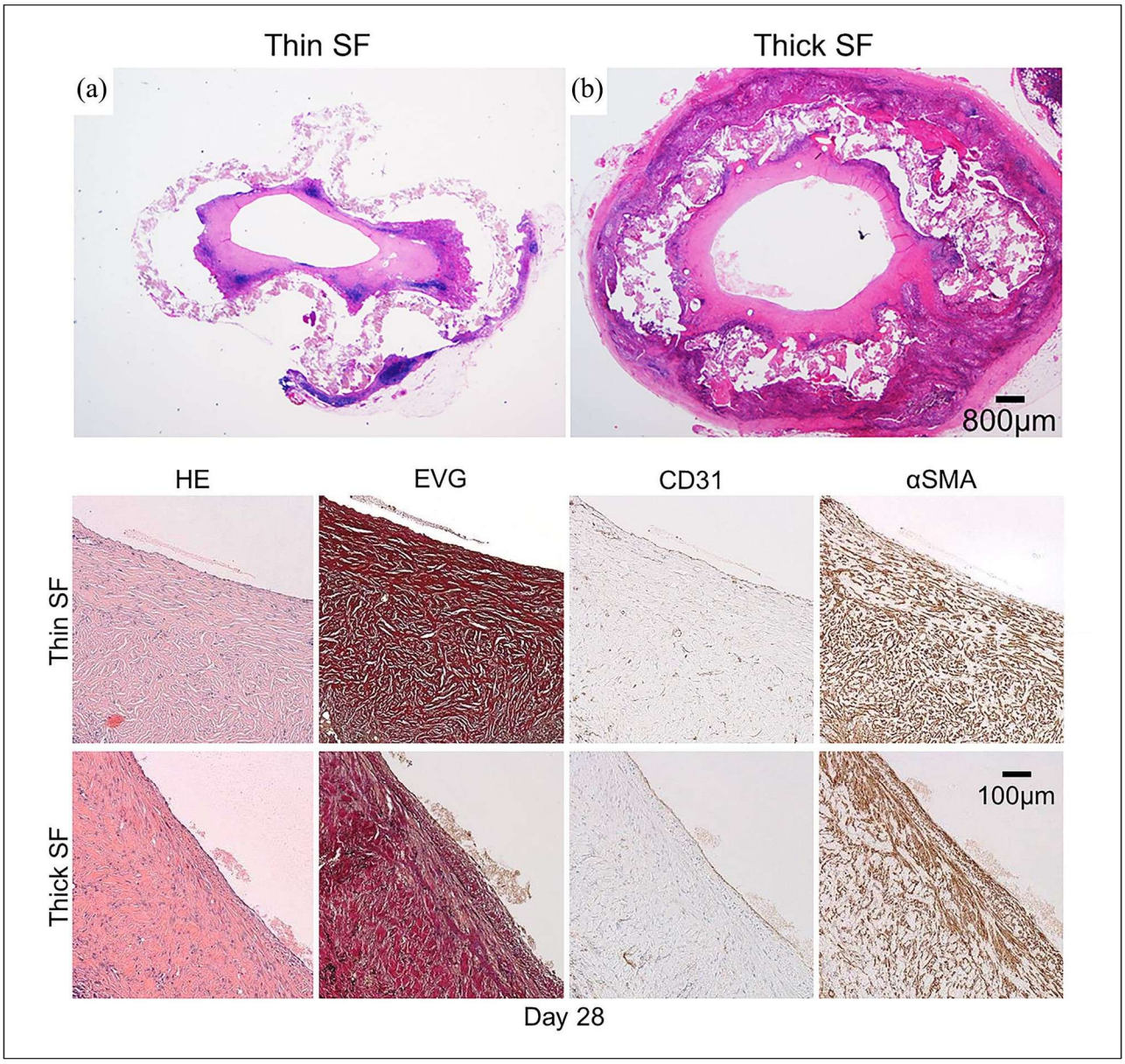

Figure 5. Hematoxylin and eosin staining of thin and thick SF vascular grafts is shown. The lumens of both the thin and thick grafts remained patent, but the wall of the thin SF graft was deformed (a) compared with the thick SF graft (b). In both the thin and thick SF vascular grafts, cellular proliferation was observed around the SF fibers, and the luminal surfaces were covered by flat cells. Elastica van Gieson staining of the SF vascular graft revealed collagen fibers (red) around the SF fibers, but no elastic fibers (EVG). CD31 was expressed on the luminal surface of both SF vascular graft types (CD31). Anti-alpha smooth muscle actin (αSMA) antibody staining of the SF vascular grafts was positive and adjacent to CD31-positive cells.

confirmed that endothelialization occurs within 4 weeks after venous replacement in rat,[8] and the present study is the first to confirm endothelialization in a canine model with a SF vascular graft. Early after placement of the SF vascular graft, however, the graft developed low-flow thrombogenicity without endothelialization. SF vascular grafts may need to be coated with a heparin-like substance coating to avoid early intramural thrombus development, and this requires further study.

Although we did not establish tolerance against bacterial infection in this study, autologous cells were seeded into the SF fibers of present the SF vascular grafts in canine. Outcome might allow SF vascular grafts to tolerate bacterial infection, but further studies are needed.

In conclusion, thick SF vascular grafts were better than thin SF vascular grafts as a promising tissue-engineered scaffold material for abdominal vein replacement in middle-sized mammals

Author contributions

Conceptualization: S.K., J.K., R.T., and T.A. Methodology: J.K., R.T., M.T., T.U., and T.A. Data curation: K.F., S.K., Y.S., M.M., C.C., T.T., and J.K. Formal Analysis: S.K., J.K., M.T., and T.U. Writing—original draft: K.F. and J.K. Writing—review & edit- ing: Y.K., N.A., and K.H. Funding acquisition and Project administration: J.K. and K.H. Supervision: Y.K., N.A., and K.H. All authors read and approved the final version of the manuscript for submission.

Declaration of conflicting interests

The author(s) declared no potential conflicts of interest with respect to the research, authorship, and/or publication of this article.

Funding

The author(s) disclosed receipt of the following financial support for the research, authorship, and/or publication of this article: This study was funded by NIPRO Corp., Tokyo, Japan., and the work was supported by grant no. 19K09191 (Kaneko) from the Ministry of Education, Culture, Sports, Science, and Technology of Japan, as an academic-industrial collaboration.

ORCID iDs

Junichi Kaneko https://orcid.org/0000-0002-1284-5639 Kiyoshi Hasegawa https://orcid.org/0000-0001-8734-740X

Supplemental material

Supplemental material for this article is available online.

References

1. Lynch SM, Vrieling A, Lubin JH, et al. Cigarette smoking and pancreatic cancer: a pooled analysis from the pancre- atic cancer cohort consortium. *Am J Epidemiol* 2009; 170: 403–413.
2. Demir IE, Jäger C, Schlitter AM, et al. R0 versus R1 resec- tion matters after pancreaticoduodenectomy, and less after distal or total pancreatectomy for pancreatic cancer. *Ann Surg* 2018; 268: 1058–1068.
3. Klaiber U, Leonhardt CS, Strobel O, et al. Neoadjuvant and adjuvant chemotherapy in pancreatic cancer. *Langenbecks Arch Surg* 2018; 403: 917–932.
4. Chu CK, Farnell MB, Nguyen JH, et al. Prosthetic graft reconstruction after portal vein resection in pancreaticoduo- denectomy: a multicenter analysis. *J Am Coll Surg* 2010; 211: 316–324.
5. Shell DHt, Croce MA, Cagiannos C, et al. Comparison of small-intestinal submucosa and expanded polytetrafluoroeth- ylene as a vascular conduit in the presence of gram-positive contamination. *Ann Surg* 2005; 241: 995–1001; discussion 1001–1004.
6. Asakura T, Tanaka T and Tanaka R. Advanced silk fibroin biomaterials and application to small-diameter silk vascular grafts. *ACS Biomater Sci Eng* 2019; 5: 5561–5577.
7. Enomoto S, Sumi M, Kajimoto K, et al. Long-term patency of small-diameter vascular graft made from fibroin, a silk- based biodegradable material. *J Vasc Surg* 2010; 51: 155–164.
8. Kiritani S, Kaneko J, Ito D, et al. Silk fibroin vascular graft: a promising tissue-engineered scaffold material for abdomi- nal venous system replacement. *Sci Rep* 2020; 10: 21041.
9. Tansey EA, Montgomery LEA, Quinn JG, et al. Understanding basic vein physiology and venous blood pressure through simple physical assessments. *Adv Physiol Educ* 2019; 43: 423–429.
10. Lee T and Yoon SM. The role of intra-abdominal pressure measurement in Awake rat cystometry. *Int Neurourol J* 2013; 17: 44–47.
11. Smith SE and Sande AA. Measurement of intra-abdominal pressure in dogs and cats. *J Vet Emerg Crit Care* 2012; 22: 530–544.
12. Milanesi R and Caregnato RC. Intra-abdominal pressure: an integrative review. *Einstein* 2016; 14: 423–430.
13. Aytemiz D, Sakiyama W, Suzuki Y, et al. Small-diameter silk vascular grafts (3 mm diameter) with a double-raschel knitted silk tube coated with silk fibroin sponge. *Adv Healthc Mater* 2013; 2: 361–368.
14. Yagi T, Sato M, Nakazawa Y, et al. Preparation of double- raschel knitted silk vascular grafts and evaluation of short- term function in a rat abdominal aorta. *J Artif Organs* 2011; 14: 89–99.
15. Asakura T, Kuzuhara A, Tabeta R and Saito H. Conformational characterization of Bombyx mori silk fibroin in the solid state by high-frequency carbon-13 cross polarization-magic angle spinning NMR, x-ray diffraction, and infrared spectroscopy. *Macromolecules* 1985; 18: 1841–1845.
16. Saotome T, Hayashi H, Tanaka R, et al. Introduction of VEGF or RGD sequences improves revascularization prop- erties of Bombyx mori silk fibroin produced by transgenic silkworm. *J Mater Chem B* 2015; 3: 7109–7116.
17. Sata M, Saiura A, Kunisato A, et al. Hematopoietic stem cells differentiate into vascular cells that participate in the pathogenesis of atherosclerosis. *Nat Med* 2002; 8: 403–409.
18. Schneider CA, Rasband WS and Eliceiri KW.

NIH Image to ImageJ: 25 years of image analysis. *Nat Methods* 2012; 9: 671–675.
19. Matsumura G, Nitta N, Matsuda S, et al. Long-term results of cell-free biodegradable scaffolds for in situ tissue-engi- neering vasculature: in a canine inferior vena cava model. *PLoS ONE* 2012; 7: e35760.

Metallic Stents for Hepatic Venous Outflow Obstruction After Living- Donor Liver Transplantation and their Therapeutic Effects

Rihito Nagata[a], Nobuhisa Akamatsu[a], Eisuke Shibata[b], Hidemasa Takao[b], Akihiko Ichida[a], Yuichiro Mihara[a], Yoshikuni Kawaguchi[a], Takeaki Ishizawa[a], Junichi Kaneko[a], Junichi Arita[a], Sumihito Tamura[a], Osamu Abe[b], and Kiyoshi Hasegawa[a]*

[a]Department of Surgery, Artificial Organ and Transplantation Division, Graduate School of Medicine, The University of Tokyo, Bunkyo-Ku, Tokyo, Japan; and [b]Department of Radiology, Graduate School of Medicine, The University of Tokyo, Bunkyo-Ku, Tokyo, Japan

ABSTRACT

Background. Living-donor liver transplantation (LDLT) is established as a standard therapy for end-stage liver disease; however, vessel reconstruction is more demanding due to the short length and small size of the available structures compared with deceased-donor whole liver trans- plantation. Interventional radiology (IR) has become the first-line treatment for vascular compli- cations after LDLT. Hepatic venous outflow obstruction (HVOO) is a life-threatening complication after LDLT. The aim of this study of 592 adult-to-adult LDLT cases was to investi- gate the safety and efficacy of stent implantation for HVOO after LDLT.

Methods. Records of patients who developed HVOO requiring any treatment were collected with special reference to the metallic stent implantation. There were 232 left-side grafts and 360 right-side grafts. Sixteen cases developed HVOO after LDLT with an incidence rate of 2.7%, 5 with a left liver graft (2%), and 11 with a right-side graft (3%). The IR was attempted for 14 cases; among those, 8 cases were treated by stent implantation.

Results. The technical success rate of the initial stent implantation was 100%. The pressure gradient at the stenotic site significantly improved from 12.2 (range, 10.9-20.4 cm H_2O) to 3.9 cm H_2O (range, 1.4-8.2 cm H_2O; $P = .03$). The volume of the congested graft liver decreased significantly from 1448 (range, 788-2170 mL) to 1265 mL (range, 748-1665 mL; $P = .01$), and the serum albumin level improved significantly from 3.3 (range, 1.7-3.7 g/dL) to 3.7 g/dL (range, 2.9-4.1 g/dL; $P = .02$). No procedure-related complication was noted, and the long-term stent patency was 100%.

Conclusion. Metallic stent implantation for stenotic venous anastomosis after LDLT is a safe and effective treatment.

LIVING-DONOR liver transplantation (LDLT) is an estab- lished treatment for end-stage liver disease, where the number of deceased donors is severely scarce [1]. With continu- ing advancements in both surgical techniques and post-trans- plant management, the short- and long-term outcomes of LDLT are now equivalent to those of deceased-donor liver transplantation (DDLT) [2].

Hepatic venous outflow obstruction (HVOO) is a serious complication that may lead to graft failure and mortality as high as 17% to 24% [3–8]. The discussion about HVOO and its management after LDLT is not sufficient [7–11] despite the numerous technical refinements of venous reconstruction, including our institution [9,12,13]. The surgical procedures for LDLT are technically more demanding than those for DDLT using whole-size grafts, mainly due to its small and short ves- sels being anastomosed. The frequency of HVOO is reported to

*Address correspondence to Kiyoshi Hasegawa MD, PhD, Artificial Organ and Transplantation Division, Department of Surgery, Graduate School of Medicine, The University of Tokyo, 7-3-1 Hongo, Bunkyo-Ku, Tokyo 113-8655, Japan. Telephone: 81-3-3815-5411; Fax: 81-3-5684-3989. E-mail: hasegawa-2su@h.u-tokyo.ac.jp

© 2023 Elsevier Inc. All rights reserved.
230 Park Avenue, New York, NY 10169

0041-1345/20
https://doi.org/10.1016/j.transproceed.2023.11.009

be 2.3% to 11.9% for LDLT [7–11] but only 0.8% to 3.8% for DDLT [3,7,14]. In the early days of LDLT, redo surgeries were often performed as a treatment for HVOO [15]. A direct surgi- cal approach to the stenotic site is usually difficult and danger- ous due to severe adhesions around the anastomotic site, applying inflow occlusion techniques of reconstructed vessels, and the enlarged congested graft.

Consequently, interventional radiology (IR) is currently con- sidered the first choice for the treatment of HVOO. Several inves- tigators have reported their recent experiences of implanting self- expandable metallic stents into the hepatic or portal vein after liver transplantation or other hepatobiliary and pancreatic surger- ies [3,7–11,14,16–20]. The reported clinical success rate of stent implantation in the hepatic vein is 73% to 92% [7,9–11,14]. However, to our knowledge, little information has been reported on how clinical parameters such as graft volume and biochemical findings have changed with stent implantation. In this study, we reviewed cases of HVOO after LDLT with the presentation of our ingenious method for venous reconstruction using cryopre- served venous homografts to prevent HVOO. We also evaluated the therapeutic effects of stent implantation for the treatment of HVOO and validated the safety and efficacy of the procedure.

PATIENTS AND METHODS

Patient Data

This retrospective study of prospectively collected data was conducted in accordance with the ethical guidelines for clinical studies at the Tokyo University Hospital. We retrospectively screened a cohort of 605 adult (>18 years of age) LDLT cases at The University of Tokyo Hospital from January 1996 to December 2020. Among them, 3 retransplantation cases and 10 auxiliary partial orthotopic liver transplantation cases were excluded. Therefore, the total number of the surveyed cases was 592.

The indications for LDLT were hepatitis C virus cirrhosis (n = 154, 26%), primary biliary cholangitis (n = 107, 18%), hepa- titis B virus cirrhosis (n = 75, 13%), acute liver failure (n = 51, 9%), nonalcoholic steatohepatitis or cryptogenic cirrhosis (n = 46, 8%), primary sclerosing cholangitis (n = 38, 6%), alcoholic liver cirrhosis (n = 35, 6%), biliary atresia (n = 31, 5%), autoimmune hepatitis (n = 22, 4%), metabolic diseases (n = 16, 3%), and others (n = 17, 3%). The graft types comprised the right liver graft (RLG; n = 328, 55%), left liver graft (LLG; n = 232, 39%), and right lateral sector graft (RLSG; n = 32, 5%).

Patients who developed HVOO after LDLT were fully picked up by reviewing the medical records. This study was approved by the Institutional Review Board at The University of Tokyo Hospital. Written informed consent was obtained from all patients before LDLT, and at each time, an interven- tional procedure was needed.

Graft Selection, Operative Procedure, and Post-Transplant Management

The following is a brief description of LDLT at our institu- tion. The lower limit of the graft was set at 35% of the estimated volume of the recipient standard liver volume [21]. For donor safety, an LLG procurement is the first choice if it satisfies the lower limit. If LLG is not applicable, an RLG is indicated if the donor's remnant liver is >30% of the donor's total liver volume. Regarding RLG, the tributaries of the mid- dle hepatic vein (MHV) in the right paramedian sector (namely, V5 and V8) are reconstructed with a cryopreserved venous homograft to avoid serious congestion [6]. If the conditions are not met, and the volume of the right lateral sector exceeds 35% of the recipient standard liver volume, then an RLSG is considered.

We use cryopreserved venous homografts to facilitate venous outflow reconstruction and to prevent HVOO after regenerative hypertrophy for all graft types. As shown in Figure 1, either the double inferior vena cava (IVC) method or the anterior patch method is used in RLG depending on the presence or absence of the inferior right hepatic vein (IRHV), and the circular cuff method is used for an LLG. These methods allow the anastomo- sis to be a large orifice and provide a relaxed and expandable space to act as a reservoir [5,6,12,13].

Hepatic arterial reconstruction is routinely performed under a microscope [22], and duct-to-duct biliary recon- struction is our rule except for cases in which the bile duct cannot be used, such as biliary atresia or primary sclerosing cholangitis [23]. Postoperative anticoagulation with continuous injection of low-molecular-weight heparin (LMWH) is indicated for all recipients and maintained for 14 days, and twice-daily Doppler ultrasonogram to confirm blood flow for the same 14 days. Administration of 2 immunosuppressive agents, methylprednisolone and tacrolimus, is standard. Mycophenolate mofetil is used in combination with immu- nosuppressive agents for patients with impaired renal func- tion or ABO-incompatible transplants. We do not routinely use mammalian target of rapamycin (mTOR) inhibitors except in cases where it is necessary to alleviate the side effects of mycophenolate mofetil or tacrolimus or in cases of post-transplant de novo malignancy development. Addi- tionally, desensitization therapy with rituximab is indicated in ABO-incompatible cases or in those with a high titer of preformed donor-specific antibodies [24,25].

Clinical Diagnosis of HVOO

During the early acute period after LDLT, HVOO was usually detected in a daily Doppler ultrasonogram or routine contrast- enhanced computed tomography (CE-CT). Otherwise, HVOO was suspected in patients who exhibited massive ascites or pleural effusion that resists diuretics despite normal graft func- tion or various abnormal laboratory data such as hypoalbumine- mia, hyperbilirubinemia, and elevated liver enzymes if rejection or infectious disease were ruled out. Then, subsequent abdomi- nal ultrasonography and CE-CT were performed. The diagnosis of HVOO is fundamentally based on the morphologic findings of CE-CT, which was finally confirmed via the finding of direct venography, and an indication for stent implantation was decided.

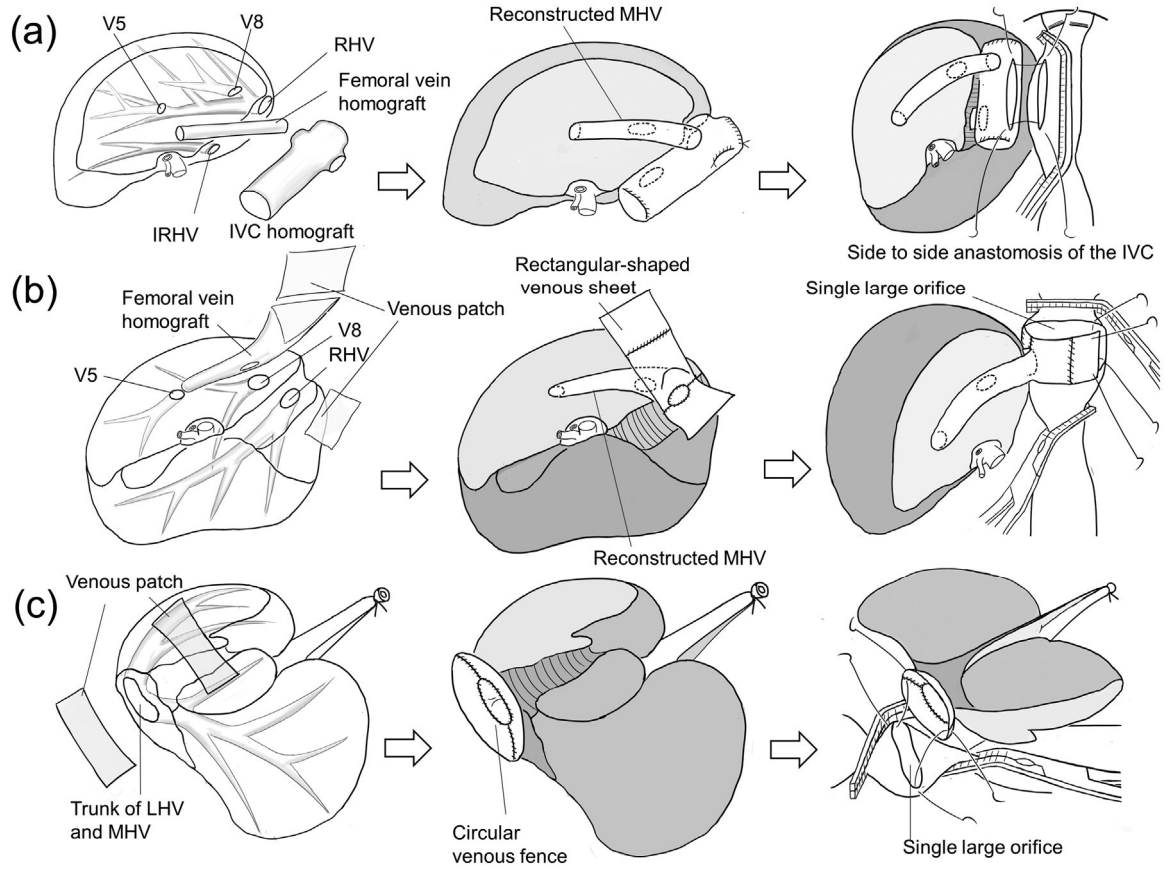

Fig 1. Venous reconstruction using cryopreserved venous homograft. A venous homograft is used to create a wide orifice and a reservoir between the graft hepatic vein and the recipient inferior vena cava (IVC). The actual pattern of reconstruction is modified on a case-by-case basis depending on the location and number of hepatic veins to be reconstructed and the diameter and length of the available cryopreserved venous homograft. (A) The double IVC method is applied for right liver graft or right lateral sector graft with inferior right hepatic vein (IRHV). The RHV, IRHV, and middle hepatic vein (MHV) tributaries are anastomosed to the IVC homograft. (B) The anterior patch method is applied for right liver graft or right lateral sector graft without IRHV. The venous patch is attached to the ventral end of the RHV (reconstructed MHV) to make a large rectangular venous sheet. The recipient IVC is incised to place all the hepatic veins into a large common orifice. After the anastomosis, the venous patch forms the anterior wall of the IVC and expands to function as a reservoir. (C) The circular cuff method is applied for left liver graft. A patch of a venous graft surrounds the orifice of the MHV and LHV, creating a large venous cuff. This cuff is anastomosed with a large opening in the recipient IVC and functions as a reservoir. IRHV, inferior right hepatic vein; IVC, inferior vena cava; LHV, left hepatic vein; MHV, middle hepatic vein; RHV, right hepatic vein.

Interventional Treatment

All IR procedures were performed under the collaboration of transplant surgeons and experienced radiologists. Under local anesthesia, the central venous puncture was performed, and the vascular sheath of 8 Fr in diameter (Supersheath, Medikit, Co, Ltd) was inserted. We prefer the right femoral vein approach to the right internal jugular vein approach because it circumvents the need for catheters and interventional devices to pass through the right atrium and because it eliminates the requirement for manipulation around the patient's head and neck, thereby reduc- ing stress on the patient. The main catheter was inserted into the graft hepatic vein using a 0.035-in guidewire (Radifocus, Terumo, Co.). The stenotic site was then fully dilated using a bal- loon dilation catheter (Admiral Xtreme, Medtronic, Ltd) with a0.035-inch stiff guidewire (Amplatz Super Stiff, Boston Scien- tific). Subsequently, an intravascular metallic stent was implanted. The optimal stent to be implanted was selected from the following 5 types depending on the clinical condition of each case (Wallstent RP, Boston Scientific; C Luminexx, Bard Peripheral Vascular Inc; Niti-S, TaeWoong Medical, Co; Pal- maz, Cardinal Health, Inc; and SMART, Cardinal Health, Inc). The pressure gradients between the proximal and distal sites of the stenosis were measured before and after the procedure. After the procedure, an intravenous infusion of conventional or LMWH was administered, which was thereafter changed to oral anticoagulant and maintained. Warfarin was administered as first-line, or edoxaban was prescribed in cases later than 2020. These anticoagulants were continued permanently.

Change in Laboratory Data and Volume of Graft Liver and Spleen

Serum albumin, platelet counts, aspartate aminotransferase and alanine aminotransferase, and total bilirubin in the peripheral blood were compared before and 1 month after stenting to investigate whether stent implantation improved graft liver function.

Additionally, we compared the volume change of the graft and spleen before and after the IR, as graft congestion and the subsequent portal hypertension due to HVOO increase the vol- ume of both the graft and spleen, which will theoretically be improved after successful resolution of the HVOO after IR. Changes in graft liver and spleen volumes using CE-CT images were obtained before and after the IR. These volumes were measured by 3-dimensional volume analysis software (Synapse Vincent, Fujifilm, Inc.).

Statistical Analysis

Continuous variables were expressed as median with range. Paired continuous data were compared with the Wilcoxon rank- sum test. Statistical significance was defined as $P < .05$. All sta- tistical analyses were performed using SPSS version 25 (IBM SPSS, Inc).

RESULTS

Development of HVOO and Outcomes

The incidence rate of HVOO after LDLT was 2.7% (16 of 592). Stratified by the graft type, the incidence rate of HVOO was 2.2% (5 of 232) in LLG, 2.4% (8 of 328) in RLG, and 9.4% (3 of 32) in RLSG. Table 1 provides the characteristics of all patients, clinical manifestations, treatment details, implanted stent size, implantation sites, and observational periods. Each patient was assigned a case number from 1 to 16. Case 1, who had HVOO due to the recurrence of Budd-Chiari's syndrome, accompanied by graft failure with portal vein obstruction, died before therapeutic intervention because the deterioration of his condition was so rapid. Three patients underwent redo surgery for HVOO: case 2 was treated by redo surgery alone, case 3 by redo surgery followed by an additional 2 sessions of IR, and case 4 underwent redo surgery for refractory HVOO after 4 sessions of IR.

For these 3 cases, the redo surgeries were performed during the early stages of our liver transplant program. The last redo surgery was performed in 2005 on a patient who had undergone a liver transplant in 2003. Of the 3 patients who underwent redo surgery, 2 eventually died. The cause of death was chronic renal failure in one and chronic graft liver failure in the other. They survived 16.7 years and 2.6 years, respectively, after redo sur- gery. Of the 16 cases, there were cases 5 to 8 could be treated with balloon dilation alone. Of these, 3 cases did not experience a recurrence after an initial IR session, and 1 case (case 7) required 2 additional IR sessions. The remaining 8 patients (5 men and 3 women) underwent hepatic vein stent implantation. The type of graft was RLG in 5 cases and RLSG in 3 cases. The indications for LDLT in these patients were as follows: hepatitis C cirrhosis (n = 3), primary sclerosing cholangitis (n = 2), bili- ary atresia (n = 2), and Wilson's disease (n = 1). In the only case where a stent was implanted during the first IR procedure (case 9), the decision to stent implantation was made due to obvious flexion as well as stenosis. In case 16, the degree of ste- nosis was so severe that stent implantation was considered nec- essary from the beginning. However, because of a massive thrombus to implant the stent, the condition of the hepatic vein was too severe. The patient needed to be improved by several sessions of thrombolysis before stent implantation. The remain- ing 6 patients were treated with balloon dilation alone for the first procedure. However, they had inadequate response or recurrence, and stents were implanted in the second or subse- quent IR procedures. Figure 2 shows CE-CT and an angiogram of the actual procedure before and after stent implantation in a representative case.

Changes in the Clinical Variables Before and After Stent Implantation

For clinical reasons, the pressure gradient could not be mea- sured in 2 patients. The pressure gradients in 6 cases showed significant improvement from 12.2 (10.9-20.4 cm H_2O) to 3.9 cm H_2O (1.4-8.2 cm H_2O; $P = .03$; Fig 3). As for the bio- chemical values 1 month after treatment, serum albumin levels improved significantly from 3.3 (1.7-3.7 g/dL) to 3.7g/dL (2.9-4.1 g/dL; $P=.02$). Platelet counts 1 month after the procedure showed a tendency to increase from 16×10^4/mL ($2.6\text{-}56.8 \times 10^4$/mL) to 20.6×10^4/mL ($6.5\text{-}54.9 \times 10^4$/mL); however, the difference did not reach statistical significance ($P= .12$; Fig 4). Other clinical variables did not show statistical significance before and 1 month after the treatment, as shown below.

- Aspartate aminotransferase: from 24 (17-123 IU/L) to 26 IU/L (13-59 IU/L; $P= .94$)
- Alanine aminotransferase; from 25 (8-165 IU/L) to 16 IU/L (13-90 IU/L; $P= .48$)
- Total bilirubin: from 1.3 (0.4-5.0 mg/dL) to 1.2 mg (0.3-4.2 mg/dL; $P= .25$)

Of the 8 patients, 6 had massive pleural effusion or ascites, all of which were finally cured by the stent implantation.

Volumetric Change in the Graft Liver and Spleen

The median range of the pre-procedural volume of the graft liver was 1448 mL (788-2170 mL), and the post-procedural vol- ume was 1265 mL (748-1665 mL). The graft liver volume was significantly decreased after stent implantation ($P= .01$).

As for the splenic volume, 3 patients had already undergone splenectomy before or during the LDLT; therefore, the splenic volume could be measured in 5 recipients. The median with range of the splenic volume before the stent was 447 mL (137- 855 mL), and after the procedure was 411 mL (149-586 mL);

Table 1. Clinical Details of 16 Cases of Hepatic Venous Outflow Obstruction

	Patient profile			Details of LDLT			Clinical problems	Treatment procedure	Interval time (d)			Implanted stent		Observational period (y)			Outcome
Case	Age at LDLT	Sex	Diseases	Year	Graft type	Venous reconstruction			LDLT to onset of problems	Onset to initial intervention	Initial intervention to stent	Location	Size (mm)	Since LDLT	Since onset of problems	Since stent implantation	
1	53	M	Budd-Chiari	2013	LLG	IVC homograft interposition	Gastrointestinal bleeding/Liver failure	Best supportive care	718	NA				2.2	0.2		Death
2	48	F	Crypt.	1998	LLG	Direct anastomosis	Ascites	Surgery	1911	25				22	16.7		Death
3	52	M	B-LC	2001	RLG	Direct anastomosis	Hyperbilirubinemia and graft congestion on CE-CT	Surgery + IRx2	78	5				2.8	2.6		Death
4	21	M	BA	2003	RLG	IVC replacement	Ascites	IRx4 + Surgery	406	16				20.2	19		Alive
5	38	F	PBC	2004	LLG	Direct anastomosis	Ascites	IRx1	34	3				19.1	19		Alive
6	49	F	PBC	2011	RLG	Double IVC	Ascites	IRx1	211	15				12.1	11.6		Alive
7	37	M	PSC	2016	LLG	Circular cuff	Ascites/Pleural effusion	IRx3	627	2				6.8	5.1		Alive
8	63	F	NASH, AIH	2018	LLG	Circular cuff	Ascites/Pleural effusion	IRx1	66	12				4.5	4.3		Alive
9	28	F	PSC	2012	RLG	Anterior patch	Ascites/Pleural effusion	IRx1 + Stent	15	1	0	RHV	10x80	10.4	10.3	10.3	Alive
10	19	F	BA	2015	RLSG	Double IVC	Severe stricture on routine MRI	IRx3 + Stent	718	50	12	RHV	10x69	8.2	6.3	6.1	Alive
11	47	M	C-LC	2012	RLG	Double IVC	Pleural effusion/Edema	IRx5 + Stent	749	9	309	IRHV	10x39	10.4	8.4	7.5	Alive
12	23	M	Wilson	2014	RLG	Anterior patch	Pleural effusion	IRx6 + Stent	51	15	174	RHV	10x49	8.9	8.7	8.2	Alive
13	28	M	C-LC	2021	RLG	Double IVC	Severe hepatic dysfunction/ Pleural effusion	IRx6 + Stent	73	0	104	RHV	12x60	2.3	2.1	1.7	Alive
14	50	M	C-LC	2012	RLG	Double IVC	Hepatic dysfunction/Pleural effusion	IRx3 + Stent + IRx1	1130	76	23	RHV	10x69	10.8	7.5	7.2	Alive
15	39	M	PSC	2020	RLSG	Double IVC	Ascites/Pleural effusion	IRx2 + Stent + IRx1	7	0	112	IRHV	12x40	3	3	2.7	Alive
16	31	F	BA	2015	RLSG	Double IVC	Acute liver failure	IRx5 + Stent + IRx6	305	0	8	RHV	12x60	7.8	7	6.9	Alive

LDLT, living-donor liver transplant; LLG, left liver graft; Crypt., cryptogenic cirrhosis; B-LC, hepatitis B cirrhosis; RLG, right liver graft; CE-CT, contrast-enhanced computed tomography; IR, interventional radiology; BA, biliary atresia; IVC, inferior vena cava; PBC, primary biliary cholangitis; PSC, primary sclerosing cholangitis; NASH, nonalcoholic steatohepatitis; AIH, autoimmune hepatitis; MRI, magnetic resonance imaging; RHV, right hepatic vein; IRHV, inferior right hepatic vein; RLSG, right lateral sector graft; C-LC, hepatitis C cirrhosis; Wilson, Wilson's disease.

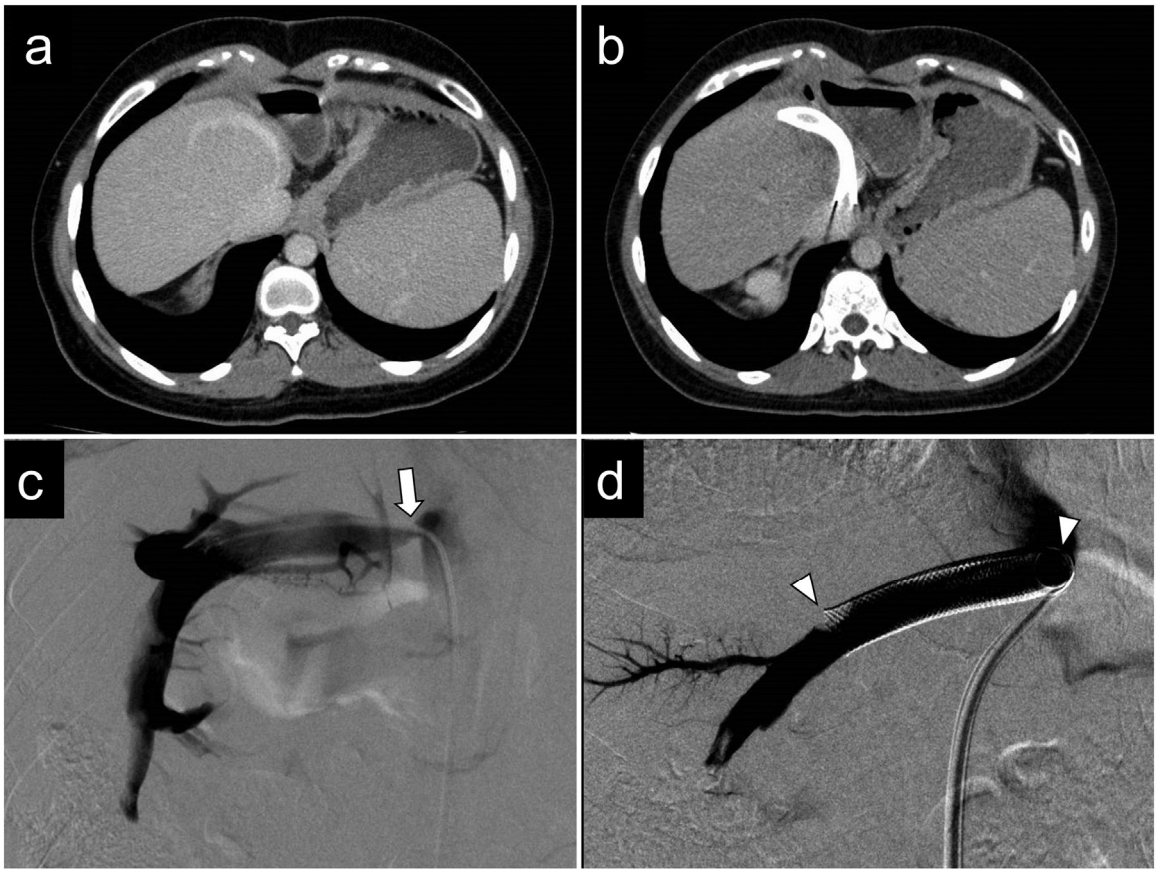

Fig 2. A representative case of stent implantation in the hepatic vein. (A) The contrast-enhanced computed tomography showed stenosis at the anastomotic site due to stretching of the right hepatic vein (RHV) and the attached venous patch in the right lateral sector graft. (B) The contrast-enhanced computed tomography obtained after the procedure shows the implanted stent in the RHV. (C) The white arrow indicates stenosis at the anastomotic site of the RHV of the right lateral sector graft. (D) Two white arrowheads indicate the implanted stent (69 mm in length and 10 mm in diameter).

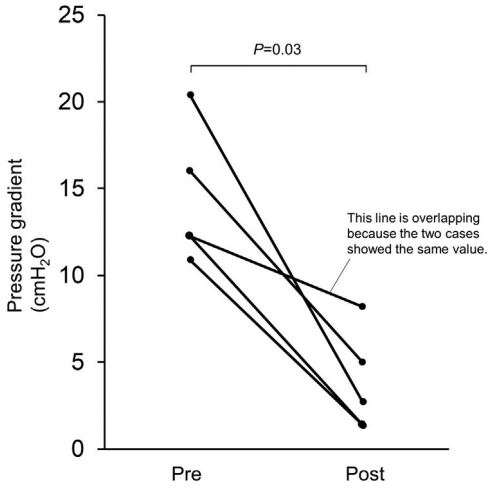

Fig 3. Change in the pressure gradient before and after the stent implantation.

the values tended to decrease after the procedure, but the differ- ence was not significant (Fig 5).

Procedure-Related Complication and Stent Patency

The technical success rate of the initial stent implantation was 100%. The median time required for the treatment was 150 minutes (120-355 minutes). Two cases (cases 9 and 15) devel- oped HVOO before being discharged after liver transplantation, and stent implantation was performed. In all other cases, HVOO occurred after discharge, and the treatment was carried out during readmission. The median hospital length of stay after stent implantation was 7 days (1-50 days). No IR-related severe complications requiring any additional treatment occurred dur- ing the procedure or during hospitalization. Three patients required additional IR after stent implantation. In case 16, tran- sient oxygen desaturation was observed during the treatment of thrombus in the right hepatic vein (RHV; Fig 6). It was sus- pected that a thrombus dislodged during catheter manipulation might have embolized into the pulmonary artery. However, no

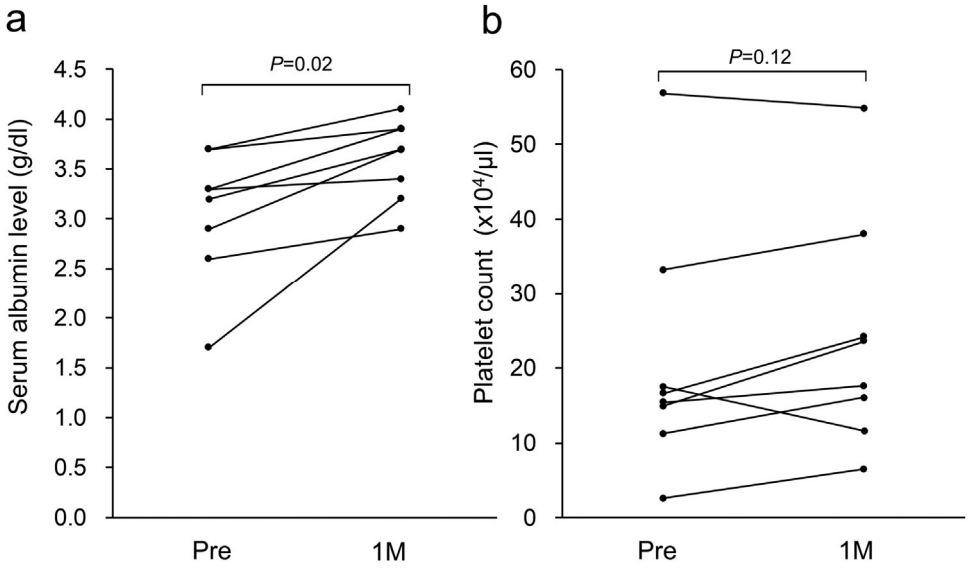

Fig 4. Change in the biochemical values before and 1 month after the stent implantation. (A) Serum albumin level. (B) Platelet count.

evidence of pulmonary embolization was provided by imaging studies such as CE-CT. The patient had fully recovered on the same day with oxygen and anticoagulation. This patient required 5 additional IR sessions with local infusion of uroki- nase before discharge. She had to undergo another IR session 5 months after the stent implantation to recanalize the occluded RHV due to a massive thrombus. In another 2 patients, balloon dilation for stent stenosis was required 18 days and 3 months after the stent implantation, respectively. All patients are cur- rently alive, and the patency of all the implanted stents has been maintained.

DISCUSSION

Here, we described our experience of HVOO after LDLT at our institute and the therapeutic effect of IR, with special reference to stent implantation. The total incidence of HVOO was 16 of
592 (2.7%). Of 16 cases, 8 underwent stent implantation. Among these, 3 required additional IR sessions for re- stenosis or thrombosis after the procedure, but all patients survived, and stent patency has been maintained. We consider that the observed decrease in graft volume indicates a releasing of graft congestion and an improvement of hemodynamics status. The

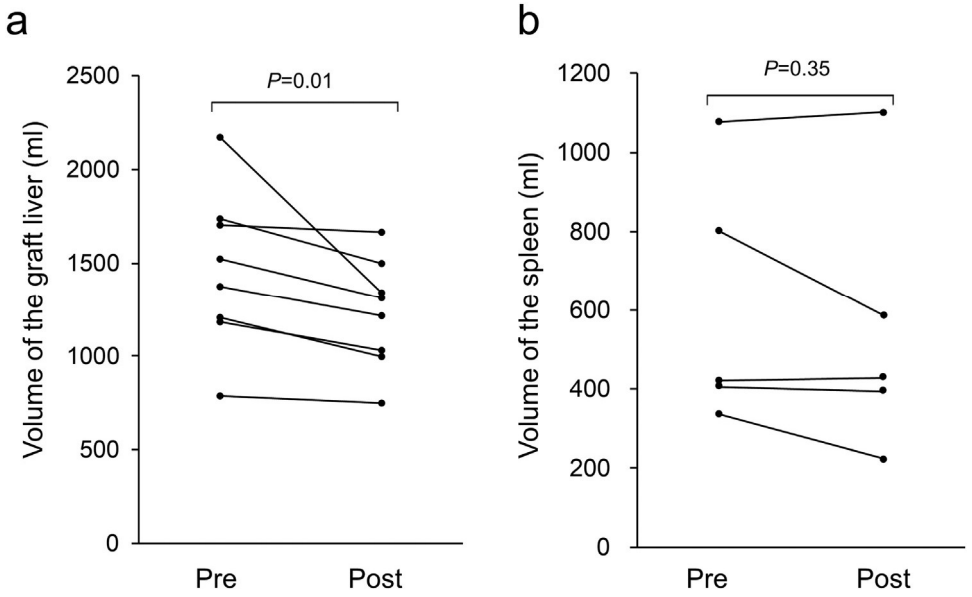

Fig 5. Volumetric analysis of the graft liver and spleen. (A) Change in the graft volume before and after the procedure. (B) Change in the splenic volume before and after the procedure.

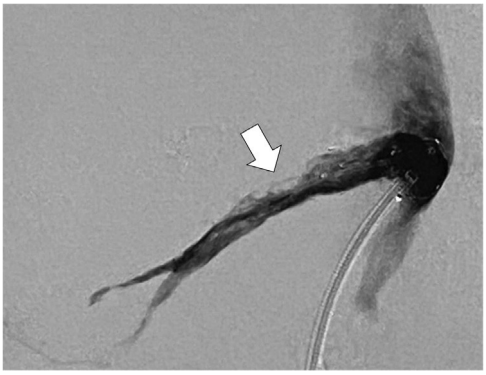

Fig 6. Thrombus in the right hepatic vein near the implanted stent. The white arrow indicates a thrombus that developed on the peripheral side of the implanted stent. During thrombolytic therapy, a transient decrease in oxygen saturation was observed, and a pulmonary embolization was suspected.

improvement in serum albumin levels also reflects the recovery of liver function by stent implantation. There were no treat- ment-related complications, with 100% long-term patency. The present results indicate that metallic stent implantation is a use- ful and promising treatment for HVOO after LDLT.

Hepatic venous outflow obstruction is a serious and demand- ing complication that may lead to graft loss and patient death [3–8,26], and transplant clinicians should be able to treat this as minimally invasively and reliably as possible. Early diagnosis and adequate treatment of HVOO are essential for good graft function and patient survival [7]. As for hepatic venous recon- struction, in DDLT, the IVC of the graft is anastomosed to the recipient IVC in a piggyback fashion [14], and thus the HVOO rarely develops. In LDLT, however, performing the anastomosis between the graft hepatic vein and recipient IVC is difficult, and thus, HVOO develops more frequently than in DDLT. Venous complications can occur over a wide range of periods, from as early as a few days after transplantation to months or years after liver transplantation [7–9,1,26,27]. In our cohort, the timing of HVOO development ranged from the earliest 7 days post-transplant to the latest cases >5 years later. The occurrence of HVOO should be kept in mind at any time after liver transplantation.

The 2.7% incidence rate of HVOO after LDLT at our institu- tion is relatively low compared with previous reports [7–11]. Our experience is that venous reconstruction with a wide orifice decreases the rate of HVOO, facilitates graft regeneration, and improves patient outcomes. Key to our hepatic vein reconstruction method is the use of a cryopreserved venous homograft to form a large reservoir between the IVC and the graft to prevent stenosis or kinking during graft enlargement. Another purpose of this method is to facilitate anastomosis with the IVC by creat- ing one large common orifice for the venous outflow in bench surgery [5,13,14]. This technique has contributed to the relatively low incidence of HVOO in our cohort, although it has not eliminated this complication. The right side of the graft is fixed to the abdominal wall in RLG or RLSG, so it can only extend to the left direction during regenerative hypertrophy. This sometimes leads to stretching or compression of the con- duit or reservoir reconstructed using the cryopreserved venous homograft (Fig 7A). In particular, the anatomic characteristics of the RLSG may lead to a long exposure of the RHV at the cut surface of the graft, which may be directly affected by inflammatory changes such as bile leakage and subsequent peritonitis, and thus becomes vulnerable to the stretching by during graft regeneration. Indeed, the HVOO rate was relatively higher among those with RLSG in our cohort, which raises the level of caution required during venous reconstruction of the RLSG.

Although a study reported that the LLG was more prone to HVOO than the RLG [9], that was not the case in our institu- tion, where the right-sided graft was dominant in HVOO cases. Five LLG cases developed HVOO in our department. In the LLG, the round ligament of the graft is fixed to the abdominal wall, and the graft is suspended. The reservoir formed by the homograft circular cuff is thought to maintain its shape, making it less likely to compress the anastomosis (Fig 7B). This may be why HVOO was relatively rare in LLG in our cohort. Indeed, there have been only 2 HVOO cases in LLG with the circular cuff method since the introduction of this method in November 2005 [5], with an incidence 2 of 112 cases (1.8% incidence rate), and both cases were relatively easy to treat by IR without stent implantation. These findings may validate the efficacy of our way of venous reconstruction in LLG in preventing HVOO. It was previously considered difficult to avoid surgical intervention for vascular complications after liver transplantation. In our early days, we experienced 3 cases requiring direct redo sur- gery for late-onset HVOO after LDLT [15]. With the accumula- tion of experience with IR, it has become a mainstay for the treatment, including pediatric patients [3,7–12,26,28,29]. Along with these previous reports, our results demonstrating no surgical direct approach for HVOO after 2005 demonstrated the safety of the stent implantation for HVOO after LDLT.

The therapeutic effects of stent implantation were discussed here from 2 perspectives. The first indicator is the volumetric change in the graft liver. The volume of the graft decreased sig- nificantly and became close to that of the recipient SLV after stent implantation. This observation suggests that congestion due to HVOO can cause abnormal swelling of the graft and that stent implantation relieves the congestion and reinstates the appropriate graft volume. This study is the first to report a change in the graft volume by stent implantation, which we believe is an important therapeutic effect of stent implantation. Kim et al. suggested that spleen size would be an indicator of the stent patency in the hepatic vein [8]. We hypothesized that the spleen volume would decrease after intervention; although we observed that spleen volume tended to decrease after treat- ment, the change was not statistically significant. However, in 3 of the 8 cases, the spleen was removed by the time of LDLT, and it is possible that the number of cases evaluated was not

sufficient.

The second indicator is the serum level of the albumin. It is widely known that albumin levels reflect the synthetic capacity of the liver, and low platelet counts reflect a portal hypertensive state [30]. Low albumin and platelet levels before

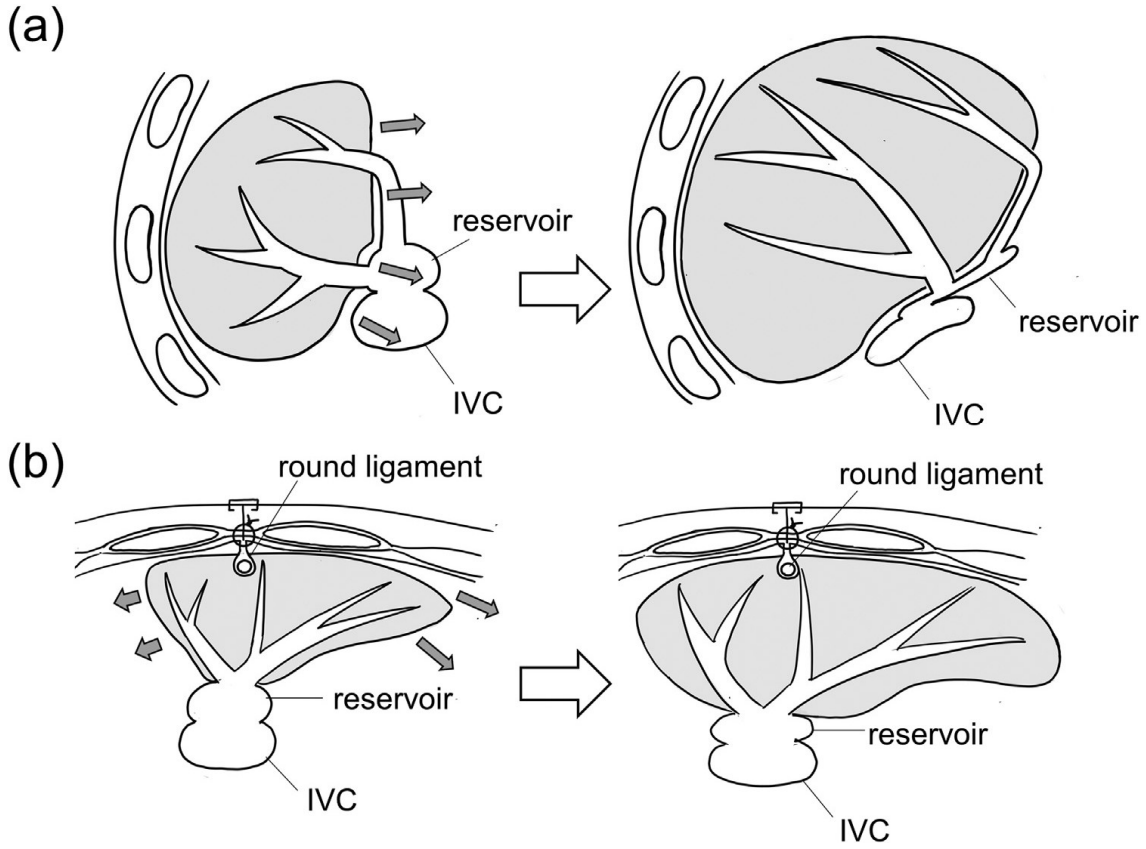

Fig7. The schematic hypothesis of the effect of graft regeneration on the anastomotic site. (A) In a right liver graft or right lateral sector graft, the right side of the graft is fixed to the thoracoabdominal wall, and the grafts are only allowed to extend in the leftward-ventral direc- tion. The graft itself may stretch the homograft vein at the anastomosis, impairing its function as a reservoir. (B) In a left liver graft, the round ligament is fixed to the abdominal wall, and the graft is suspended, thus avoiding pressure on the anastomotic site. Additionally, the graft can be extended relatively freely in both directions. Therefore, the function of a reservoir is maintained. IVC, inferior vena c

transplantation are reported to significantly recover 1 month after successful LDLT [31]. Therefore, the significant improve- ment in the serum albumin value after stent implantation indi- cates recovery of graft function impaired by HVOO. There is one previous report of improvement in albumin levels after stent implantation for HVOO among DDLT recipients [14], which was consistent with the present results among the LDLT cohort. As with the spleen volume, platelet levels tended to improve, but the change was not statistically significant. Platelet levels are thought to be strongly influenced by the spleen. There were only 5 cases with spleen remaining in the present study; thus, it is necessary to accumulate more cases.

To date, there is no consensus on established anticoagulant or antiplatelet therapy for the long-term patency of metallic stents in these low-pressure vessels. In the short term after the proce- dure, previous studies reported using heparin or LMWH [7–9,17–19] and then switching to warfarin for long-term main- tenance [9,19] or aspirin as an antiplatelet agent [7,8]. There is a recent report of the use of direct oral anticoagulants given for maintenance therapy after intravenous stenting in the iliac vein [32]. The rationale for administering anticoagulants or antiplate- lets is a report of autopsy findings showing that the implanted stent was not always covered with neointima [33]. In our series, 6 patients took warfarin, and 2 cases were given edoxaban as a direct oral anticoagulant. No adverse events were observed. On the other hand, some facilities do not use these drugs after stent implantation without any clinical problems [10,34]. Whether or not anticoagulation or antiplatelet therapy is necessary, and if so, the optimal type, are topics for future study.

Ko et al. reported that overall 1-, 3-, and 5-year patency rates for hepatic veins with stents implanted were 82%, 75%, and 72%, respectively [10]. Although our results are limited to only 8 cases and 3 cases required additional IR procedures after stent implantation, all patients survived and maintained stent patency. We believe these outcomes are not only a product of our advanced technique of stent implantation but also a result of our efforts to minimize the occurrence of HVOO at the time of LDLT.

There is an important limitation in the present study. This was a compilation of cases experienced in our 25-year history of liver transplantation; however, it is a retrospective study. Therefore, the present study could not indicate what informa- tion, such as the difference in caliber of the stenotic site and the degree of pressure gradient, obtained from IR in the actual treat- ment of HVOO should be used to determination of stent implantation. Some previous reports have established criteria, for example, a pressure gradient of ≥5 mm Hg for diagnosis of HVOO [7,8,11], but we do not yet have a clear cutoff for deci- sion-making. Based on the findings of this study, we would like to establish more specific criteria in the future.

CONCLUSION

Stent implantation for HVOO after LDLT is a safe and effective procedure. The present results demonstrated the efficacy of stent implantation for long-term patency and for correcting graft con- gestion and serum albumin values.

DECLARATION OF COMPETING INTEREST

The authors declare that they have no known competing finan- cial interests or personal relationships that could have appeared to influence the work reported in this paper.

REFERENCES

[1] Chen CL, Kabiling CS, Concejero AM. Why does living donor liver transplantation flourish in Asia? Nat Rev Gastroenterol Hepatol 2013;10:746–51.

[2] Umeshita K, Inomata Y, Furukawa H, Kasahara M, Kawasaki S, Kobayashi E, et al. Liver transplantation in Japan: registry by the Jap- anese Liver Transplantation Society. Hepatol Res 2016;46:1171–86.

[3] Akun E, Yaprak O, Killi R, Balci NC, Tokat Y, Yuzer Y. Vas- cular complications in hepatic transplantation: single-center experience in 14 years. Transplant Proc 2012;44:1368–72.

[4] Navarro F, Le Moine MC, Fabre JM, Belghiti J, Cherqui D, Adam R, et al. Specific vascular complications of orthotopic liver trans- plantation with preservation of the retrohepatic vena cava: review of 1361 cases. Transplantation 1999;68:646–50.

[5] Hashimoto T, Sugawara Y, Tamura S, Kaneko J, Motomura N, Takamoto S, et al. One orifice vein reconstruction in left liver plus cau- date lobe grafts. Transplantation 2007;83:225–7.

[6] Akamatsu N, Sugawara Y, Nagata R, Kaneko J, Aoki T, Saka- moto Y, et al. Adult right living-donor liver transplantation with special reference to reconstruction of the middle hepatic vein. Am J Transplant 2014;14:2777–87.

[7] Chu HH, Yi NJ, Kim HC, Lee KW, Suh KS, Jae HJ, et al. Longterm outcomes of stent placement for hepatic venous outflow obstruction in adult liver transplantation recipients. Liver Transpl 2016;22:1554–61.

[8] Kim KS, Lee JS, Choi GS, Kwon CHD, Cho JW, Lee SK, et al. Long-term outcomes after stent insertion in patients with early and late hepatic vein outflow obstruction after living donor liver transplantation. Ann Surg Treat Res 2018;95:333–9.

[9] Kitajima T, Kaido T, Iida T, Yagi S, Fujimoto Y, Ogawa K, et al. Left lobe graft poses a potential risk of hepatic venous outflow obstruction in adult living donor liver transplantation. Liver Transpl 2016;22:785–95.

[10] Ko GY, Sung KB, Yoon HK, Kim KR, Kim JH, Gwon DI, et al. Early posttransplant hepatic venous outflow obstruction: Long-term effi- cacy of primary stent placement. Liver Transpl 2008;14:1505–11.

[11] Fujimori M, Yamakado K, Takaki H, Nakatsuka A, Uraki J, Yamanaka T, et al. Long-term results of stent placement in patients with outflow block after living-donor- liver transplantation. Cardiovasc Intervent Radiol 2016;39:566–74.

[12] Ito K, Akamatsu N, Togashi J, Tamura S, Sakamoto Y, Hase- gawa K, et al. Outflow reconstruction using

[13] cryopreserved homologous venous grafts in living donor liver transplantation. Transplant Proc 2017;49:109–14.

[14] Sugawara Y, Makuuchi M, Akamatsu N, Kishi Y, Niiya T, Kaneko J, et al. Refinement of venous reconstruction using cryopre- served veins in right liver grafts. Liver Transpl 2004;10:541–7.

[15] Wang SL, Sze DY, Busque S, Razavi MK, Kee ST, Frisoli JK, et al. Treatment of hepatic venous outflow obstruction after piggyback liver transplantation. Radiology 2005;236:352–9.

[16] Akamatsu N, Sugawara Y, Kaneko J, Kishi Y, Niiya T, Kokudo N, et al. Surgical repair for late-onset hepatic venous outflow

block after living-donor liver transplantation. Transplantation 2004;77:1768–70.

[17] Mizuno T, Ebata T, Yokoyama Y, Igami T, Sugawara G, Mori Y, et al. Percutaneous transhepatic portal vein stenting for malignant portal vein stenosis secondary to recurrent perihilar biliary cancer. J Hepatobiliary Pancreat Sci 2015;22:740–5.

[18] Shirata C, Nishioka Y, Sato J, Watadani T, Arita J, Akamatsu N, et al. Therapeutic effect of portal vein stenting for portal vein steno- sis after upper-abdominal surgery. HPB (Oxford) 2021;23:238–44.

[19] Khan A, Kleive D, Aandahl EM, Fosby B, Line PD, Dorenberg E, et al. Portal vein stent placement after hepatobiliary and pancreatic surgery. Langenbecks Arch Surg 2020;405:657–64.

[20] Sambommatsu Y, Shimata K, Ibuki S, Narita Y, Isono K, Honda M, et al. Portal vein complications after adult living donor liver transplantation: time of onset and deformity patterns affect long-term outcomes. Liver Transpl 2021;27:854–65.

[21] Kyoden Y, Tamura S, Sugawara Y, Matsui Y, Togashi J, Kaneko J, et al. Portal vein complications after adult-to-adult living donor liver transplantation. Transpl Int 2008;21:1136–44.

[22] Urata K, Hashikura Y, Ikegami T, Terada M, Kawasaki S. Standard liver volume in adults. Transplant Proc 2000;32:2093–4.

[23] Okazaki M, Asato H, Takushima A, Nakatsuka T, Sarukawa S, Inoue K, et al. Hepatic artery reconstruction with double-needle micro- suture in living-donor liver transplantation. Liver Transpl 2006;12:46– 50.

[24] Dulundu E, Sugawara Y, Sano K, Kishi Y, Akamatsu N, Kaneko J, et al. Duct-to-duct biliary reconstruction in adult living-donor liver transplantation. Transplantation 2004;78:574–9.

[25] Egawa H, Teramukai S, Haga H, Tanabe M, Mori A, Ikegami T, et al. Impact of rituximab desensitization on blood-type-incompatible adult living donor liver transplantation: a Japanese multicenter study. Am J Transplant 2014;14:102–14.

[26] Akamatsu N, Hasegawa K, Sakamoto S, Ohdan H, Nakagawa K, Egawa H. Rituximab desensitization in liver transplant recipients with preformed donor-specific hla antibodies: a Japanese nationwide survey. Transplant Direct 2021;7:e729.

[27] Karakayali H, Boyvat F, Coskun M, Isiklar I, S€ozen H, Filik L, et al. Venous complications after orthotopic liver transplantation. Trans- plant Proc 2006;38:604–6.

[28] Buell JF, Funaki B, Cronin DC, Yoshida A, Perlman MK, Lor- enz J, et al. Long-term venous complications after full-size and segmen- tal pediatric liver transplantation. Ann Surg 2002;236:658–66.

[29] Karakaya E, Akdur A, Ayvazog˘lu Soy EH, Boyvat F, Moray G, Haberal M. Vascular complications in pediatric liver transplants and their management. Exp Clin Transplant 2022;20(suppl 3):72–5.

[30] Igus B, Boyvat F, Ozen O, Ayvazoglu Soy EH, Karakaya E, Haberal M. Role of interventional radiology in the management of early vascular complications after liver transplant. Exp Clin Transplant 2022;20:1085–93.

[31] Shindoh J, Kawamura Y, Kobayashi Y, Kiya Y, Sugawara T, Akuta N, et al. Platelet-albumin score as a sensitive measure for surgical risk prediction and survival outcomes of patients with hepatocellular carcinoma. J Gastrointest Surg 2019;23:76–83.

[32] Urano E, Yamanaka-Okumura H, Teramoto A, Sugihara K, Morine Y, Imura S, et al. Pre- and postoperative nutritional assessment and health-related quality of life in recipients of living donor liver trans- plantation. Hepatol Res 2014;44:1102–9.

[33] Hays K, Jolly M, Silver M, Phillips J, Huff C, Secic M, et al. Outcomes of endovascular venous stenting in patients on direct oral anticoagulants and antiplatelet therapy at a tertiary referral center. J Vasc Surg Venous Lymphat Disord 2021;9 753–9.e1.

[34] Yamakado K, Nakatsuka A, Tanaka N, Fujii A, Isaji S, Kawar- ada Y, et al. Portal venous stent placement in patients with pancreatic and biliary neoplasms invading portal veins and causing portal hyper- tension: initial experience. Radiology 2001;220:150–6.

[35] Jang JY, Jeon UB, Park JH, Kim TU, Lee JW, Chu CW, et al. Efficacy and patency of primary stenting for hepatic venous outflow obstruction after living donor liver transplantation. Acta Radiol 2017;58:34–40

communications medicine

Article

https://doi.org/10.1038/s43856-024-00448-4

Humoral and cellular immune responses to COVID-19 mRNA vaccines in immunosuppressed liver transplant recipients

Check for updates

Takuto Nogimori[1,8], Yuta Nagatsuka[1,2,8], Shogo Kobayashi[2] ✉, Hirotomo Murakami[1,2], Yuji Masuta[1], Koichiro Suzuki[3], Yoshito Tomimaru[2], Takehiro Noda[2], Hirofumi Akita[1,4,5], Shokichi Takahama[1], Yasuo Yoshioka[3], Yuichiro Doki[2], Hidetoshi Eguchi[2] & Takuya Yamamoto[1,5,6,7] ✉

Abstract

Background Liver transplant recipients (LTRs) are at a high risk of severe COVID-19 owing to immunosuppression and comorbidities. LTRs are less responsive to mRNA vaccines than healthy donors (HDs) or other immunosuppressed patients. However, the disruption mechanism in humoral and cellular immune memory responses is unclear.

Methods We longitudinally collected peripheral blood mononuclear cells and plasma samples from HDs ($n = 44$) and LTRs ($n = 54$) who received BNT162b2 or mRNA-1273 vaccines. We measured the levels of anti-receptor-binding domain (RBD) antibodies and spike-specific $CD4^+$ and $CD8^+$ T-cell responses.

Results Here, we show that the induction of anti-RBD IgG was weaker in LTRs than in HDs. The use of multiple immunosuppressive drugs is associated with lower antibody titers than only calcineurin inhibitor, and limits the induction of $CD4^+$ T-cell responses. However, spike-specific $CD4^+$ T-cell and antibody responses improved with a third vaccination. Furthermore, mRNA vaccine-induced spike-specific $CD8^+$ T cells are quantitatively, but not qualitatively, limited to LTRs. Both $CD4^+$ and $CD8^+$ T cells react to omicron sublineages, regardless of the presence in HDs or LTRs. However, there is no boosting effect of spike-specific memory $CD8^+$ T-cell responses after a third vaccination in HDs or LTRs.

Conclusions The third mRNA vaccination improves both humoral responses and spike-specific $CD4^+$ T-cell responses in LTRs but provides no booster effect for spike-specific memory $CD8^+$ T-cell responses. A third mRNA vaccination could be helpful in LTRs to prevent severe COVID-19, although further investigation is required to elicit $CD8^+$ T-cell responses in LTRs and HDs.

Plain language summary

People with a liver transplant don't have as strong an immune response to COVID-19 vaccines as healthy people. This study investigates how these individuals produce protective proteins, called antibodies, and CD4 and CD8 T cell immune responses. CD4 T cells are responsible for commanding the immune response and CD8 T cells for remembering and fighting the virus in future. We found that liver transplant recipients have a weaker ability to produce antibodies after vaccination, which is even more noticeable in those taking drugs to prevent transplant rejection. While a third vaccine dose improves their ability to produce antibodies, and to have a CD4 T cell response, it doesn't boost the CD8 T cell response. In summary, an extra vaccine dose can strengthen the immune response in liver transplant recipients but doesn't improve some aspects of their immune memory.

[1]Laboratory of Precision Immunology, Center for Intractable Diseases and ImmunoGenomics, National Institutes of Biomedical Innovation, Health and Nutrition, Osaka 567-0085, Japan. [2]Department of Gastroenterological Surgery, Graduate School of Medicine, Osaka University, Osaka 565-0871, Japan. [3]The Research Foundation for Microbial Diseases of Osaka University (BIKEN), Osaka 565-0871, Japan. [4]Department of Gastroenterological Surgery, Osaka International Cancer Institute, Osaka 540-0008, Japan. [5]Laboratory of Translational Cancer Immunology and Biology, Next-generation Precision Medicine Research Center, Osaka International Cancer Institute, Osaka 540-0008, Japan. [6]Department of Virology and Immunology, Graduate School of Medicine, Osaka University, Osaka 565-0871, Japan. [7]Laboratory of Aging and Immune Regulation, Graduate School of Pharmaceutical Sciences, Osaka University, Osaka 565-0871, Japan. [8]These authors contributed equally: Takuto Nogimori, Yuta Nagatsuka. ✉e-mail: skobayashi@gesurg.med.osaka-u.ac.jp; yamamotot2@nibiohn.go.jp

Severe acute respiratory syndrome coronavirus 2 (SARS-CoV-2) emerged in late 2019 and caused a respiratory disorder known as coronavirus disease 2019 (COVID-19)[1]. Although most infected patients experienced mild symptoms, older adults and immunosuppressed patients, such as transplant recipients and autoimmune disease patients, are at risk of developing severe COVID-19[2,3]. An international database study revealed that the rate of ICU admission and invasive ventilation required after SARS-CoV-2 infection was significantly higher in liver transplant recipients (LTRs) than in healthy individuals[4]. Age, serum creatinine level, and non-liver cancer status are associated with post-infection mortality in LTRs, indicating that LTRs require adequate infection prevention methods[4].

As a preventive method against COVID-19, mRNA vaccines are believed to be the most effective. Currently, two or more doses (three or four) of mRNA vaccinations are being administered worldwide[5]. Two doses of mRNA vaccines reduce the possibility of SARS-CoV-2 infection and COVID-19-related deaths by 64% and 87%, respectively, in LTRs[6]. However, the use of multiple immunosuppressive drugs, especially mycophenolate mofetil or steroids, is a risk factor for reduced antibodies in LTRs after two mRNA vaccine doses[7,8]. Although two doses of mRNA vaccines effectively prevent SARS-CoV-2 infection, their effects were weaker in LTRs than in healthy individuals or patients with other immunosuppressive conditions[9]. Additionally, three mRNA vaccine doses can improve antibody induction in LTRs[10], although they remain inadequate for LTRs to induce a strong neutralizing activity.

Clinically, immunosuppressive drugs used in LTRs include calcineurin inhibitors (CNIs), such as tacrolimus and cyclosporine, mycophenolate mofetil, everolimus, and steroids[11]. CNIs suppress immune responses by inhibiting initial T-cell activation[12,13]. Therefore, the unresponsiveness of LTRs to antibody induction after mRNA vaccination could be caused by the suppression of T-cell responses. However, studies on mRNA vaccine-induced changes in T-cell responses in LTRs are limited. Moreover, many studies have been limited to verification at specific time points, such as after the second or third vaccination, and insights into the changes in antibody titers and memory T-cell responses over time are insufficient.

A bivalent mRNA vaccine has been designed against an Omicron strain[14] and induces the production of antibodies against BA.5 more efficiently than the monovalent mRNA vaccine against the Wuhan-1 strain[15–17]. However, the neutralizing activity induced by mRNA vaccines is limited in newly emerged strains, such as BA.2.75.2, BQ.1.1, XBB, and XBB.1, as SARS-CoV-2 can evade neutralizing antibodies via mutations in the spike protein[18]. In other words, inducing T-cell responses that can react to mutant strains, rather than relying on neutralizing antibodies, is key to preventing future infections due to emerging mutant strains. Nevertheless, whether mRNA vaccine-induced T-cell responses in immunosuppressed LTRs are reactive to Omicron sublineages is unclear, although mRNA vaccine-induced antigen-specific T-cell responses in healthy individuals could be cross-reactive against the SARS-CoV-2 Omicron strain (BA.1)[19,20].

In this study, we longitudinally collect peripheral blood mononuclear cells (PBMCs) and plasma samples from healthy donors (HDs) and LTRs who received BNT162b2 or mRNA-1273 vaccines. We evaluate the mRNA vaccine-induced humoral and cellular immune memory responses over time and demonstrate that the generation of anti-RBD IgG antibodies is less effective in LTRs compared to HDs. The employment of a combination of immunosuppressive medications results in reduced antibody levels as opposed to using solely calcineurin inhibitors, and this adversely impacts the development of $CD4^+$ T-cell responses. Nevertheless, the response of spike-specific $CD4^+$ T cells and antibodies is enhanced following a third dose of the mRNA vaccine. Additionally, while the quantity of mRNA vaccine-elicited spike-specific $CD8^+$ T cells in LTRs is lower, their functionality remains unchanged. Both $CD4^+$ and $CD8^+$ T cells show reactivity to omicron subvariants, irrespective of their occurrence in HDs or LTRs. However, no enhancement in the memory responses of spike-specific $CD8^+$ T cells is observed after a third vaccine dose in either HDs or LTRs.

Methods

Study participants

A total of 98 individuals (44 healthy donors and 54 LTRs) were recruited from Osaka University, Japan. Blood samples were collected, and peripheral blood mononuclear cells (PBMCs) were isolated via density gradient centrifugation using a BD Vacutainer cell preparation tube (CPT) containing sodium heparin (Becton, Dickinson and Co., Franklin Lakes, NJ, USA) according to the manufacturer's instructions. PBMCs were immersed in fetal bovine serum containing 10% dimethyl sulfoxide and stored in liquid nitrogen until analysis. The donor information used in this study is presented in Table 1.

SARS-CoV-2 spike-specific antibody detection

Plasma levels of total IgG-targeting SARS-CoV-2 spike receptor-binding domain (RBD)-specific antibodies were determined by ELISA[20]. Recombinant spike RBD proteins (Wuhan-1, BA.1, BA.2, BA.5, BQ.1.1, XBB, BA.4.6, and BA.2.75) were obtained from SinoBiological (Beijing, China). To calculate RBD-specific antibody titers, 96-well plates were coated with RBD protein and incubated overnight at 4 °C. The plates were then washed and incubated for 1 h with blocking buffer, then washed again, and incubated with diluted plasma samples for 2 h at 25 °C. The plates were washed and incubated with biotinylated anti-human total IgG (BD Biosciences, San Jose, CA, USA) for 1 h. The plates were washed and incubated with horseradish peroxidase-conjugated streptavidin (Thermo Fisher Scientific, Waltham, MA, USA) for 1 h at 25 °C. The plates were washed and incubated with the TMB peroxidase substrate (KPL, Gaithersburg, MD, USA) for color development. After 10 min, 2 mol/L H_2SO_4 was added to each well to stop the reaction. Antibody expression was measured by determining the optical density at 450 nm using an Epoch 2 Microplate Spectrophotometer (Agilent, Santa Clara, CA, USA). The antibody endpoint titer was determined using a cut-off value of 0.3. The cutoff value of OD = 0.3 was determined based on the OD values of plasma from unvaccinated individuals used as a negative control, specifically by adding twice the standard deviation to the average OD value.

Neutralization assay of pseudotyped virus

To determine the pseudotyped virus neutralization titer (pVNT) of the vaccinated donors' plasma, HEK-293A cells expressing ACE2 and TMPRSS2 were seeded in 96-well plates. After 24 h, the human plasma was diluted 2- or 4-fold, starting at 1:2, and incubated with SARS-CoV-2 pseudotyped virus at 37 °C for 1 h. After incubation, a mixture of plasma and the pseudotyped virus was added to each well. After 24 h, luciferase activity was measured using EnSpire (PerkinElmer, Waltham, MA, USA). pVNT50 was defined as the plasma dilution that achieved 50% inhibition of pseudotyped virus infection using Prism software (GraphPad Software, Boston, MA, USA).

Flow cytometry analysis

To analyze SARS-CoV-2 spike-specific T cells, we performed surface and intracellular cytokine staining of $CD4^+$ and $CD8^+$ T cells[20,21]. Briefly, PBMCs were incubated in 1 mL RPMI 1640 medium containing 50 U/mL benzonase nuclease (Millipore, Darmstadt, Germany), 10% fetal bovine serum, and penicillin-streptomycin for 2 h. Next, cells were incubated in 200 µL of medium with or without peptides (17-mers overlapping by 11 residues) corresponding to the full-length SARS-CoV-2 spike, at a final concentration of 2 µg/mL of each peptide, for 30 min. Thereafter, 0.2 µL BD GolgiPlug and 0.14 µL BD GolgiStop (both from BD Biosciences) were added and incubated for 5.5 h. The cells were then stained using a LIVE/DEAD Fixable Blue Dead Cell Stain Kit (Thermo Fisher Scientific) and anti-CD3 (SP34-2, 1:100 dilution), anti-CD8 (RPA-T8, 1:400 dilution), anti-CD4 (L200, 1:100 dilution), anti-CD45RO (UCHL1, 1:200 dilution), anti-CD27 (O323, 1:100 dilution), and anti-CD57 (NK-1, 1:2000 dilution) antibodies. After fixation and permeabilization using a Cytofix/Cytoperm kit (BD Biosciences), the cells were stained with anti-CD154 (TRAP1, 1:14 dilution), anti-4-1BB

Table 1 | Donor characteristics enrolled in this study

Caracteristics	Liver transplant recipients (*n* = 54)	Healthy donors (*n* = 44)
Demographic		
Age, median years (interquartile range)	65 (56.3–70.8)	36 (34–44.3)
Male (%)	28 (51.9)	35 (79.5)
Female (%)	26 (48.1)	9 (20.5)
Vaccine		
2nd		
Pfizer/BNT162b2	42 (77.8)	25 (56.8)
Moderna/mRNA-1273	12 (22.2)	19 (43.1)
3rd		
Pfizer/BNT162b2	29 (53.7)	25 (56.8)
Moderna/mRNA-1273	25 (46.3)	19 (43.1)
Laboratory values (Median, Interquartile range)		
WBC (×10^3/L)	5.2 (4.5–6.8)	NA
Lymphocytes (×10^3/L)	1.5 (1.0–1.9)	NA
Neutrophils (×10^3/L)	3.2 (2.7–4.0)	NA
Monocytes (×10^3/L)	0.32 (0.27–0.45)	NA
CRP (mg/dL)	0.08 (0.043–0.13)	NA
eGFR (mL/min)	51.6 (41.6–65.0)	NA
HbA1c (%)	5.9 (5.3–6.6)	NA
Immunotherapy (*n*, %)		
Monotherapy	23 (42.6)	NA
Tacrolimus	19 (35.2)	NA
Cyclosporine	4 (7.4)	NA
CNI + MMF	12 (22.2)	NA
CNI + mTORi	2 (3.7)	NA
CNI + steroid	11 (20.4)	NA
CNI + MMF + steroid	5 (9.3)	NA
CNI + mTORi + steroid	1 (1.9)	NA
Entecavir	7 (13.0)	NA

(4B4-1, 1:400), anti-CD69 (FN50, 1:67), anti-IFN-γ (4 S. B3, 1:100), anti-TNF (MAb11, 1:50 dilution), anti-IL-2 (MQ-17H12, 1:400 dilution), anti-IL-4 (8D4-8, 1:40 dilution), anti-IL-13 (JES10-5A2, 1:40 dilution), anti-granzyme A (CB9, 1:400 dilution), anti-granzyme B (GB11, 1:2000), and anti-perforin (B-D45, 1:67 dilution) antibodies. The cells were then analyzed using a BD FACSymphony A5 flow cytometer (BD Biosciences) and FlowJo v. 10.8.1. After gating live single T cells based on the forward scatter area and height (FSC-A and -H), side scatter area (SSC-A), live/dead cell exclusion, and CD3 staining, PBMCs were separated into $CD4^+$ and $CD8^+$ T cells. Subsequently, $CD4^+$ and $CD8^+$ T cells were further divided into memory phenotypes based on their CD27 and CD45RO expression. For spike-specific $CD4^+$ and $CD8^+$ T cells, memory cells were gated based on the expression of CD154 and 4-1BB and CD69 expression, respectively. We defined $CD154^+CD4^+$ T cells expressing IFN-γ, TNF, or IL-2 as Th1 cells and those expressing IL4 or IL-13 as Th2 cells. Frequencies of $CD154^+CD4$ T cells, Th1, Th2 and $CD69^+4\text{-}1BB^+CD8$ T cells were calculated by subtracting background of unstimulated samples (DMSO). Positive responses were defined if there was a reactivity of 0.01% or more after background subtraction from the unstimulated condition.

Statistics

Indivisual endpoint titers, $pVNT_{50}$ and FACS data are shown as median with interquartile range. Statistical analyses were performed with GraphPad Prism 9, Spice 6.1, and R programming language. Mann–Whitney *U* test and Wilcoxon matched-pairs signed-rank test were used for comparisons of groups. Correlations were calculated using a nonparametric Spearman's rank test. Multivariable logistic regression model was used for prediction of the relationships between dependent and independent variables. In all figures, *P* values are indicated by $^*P < 0.05$; $^{**}P < 0.01$; $^{***}P < 0.001$; $^{****}P < 0.0001$.

Study approval

The study protocol and procedures were reviewed and approved by the Institutional Ethics Committees of the National Institutes of Biomedical Innovation, Health, and Nutrition (approval nos. 137, 505, and 117-4), Osaka, Japan, and Osaka University (approval no. 21195), Osaka, Japan, and complied with the 1975 Declaration of Helsinki. All the participants provided written informed consent to participate in the study.

Reporting summary

Further information on research design is available in the Nature Portfolio Reporting Summary linked to this article.

Results

Anti-RBD IgG titers and plasma neutralizing activity induced by COVID-19 mRNA vaccination in HDs and LTRs

We enrolled 44 HDs and 54 LTRs to comprehensively evaluate mRNA vaccine-induced antibodies and cellular immune responses (Table 1). The mRNA vaccines, Pfizer BNT162b2 or Moderna mRNA-1273 were investigated. Blood samples were obtained at five-time points: before vaccination, 1, 3, and 6 months after the second vaccination, and 1 month after the third vaccination (Fig. 1a).

All LTRs were administered CNIs, such as tacrolimus or cyclosporine. Some LTRs took additional medications, such as the metabolic antagonist MMF, a steroid, or the mTOR inhibitor everolimus. Specifically, 23, 12, 2, 11, 5, and 1 LTRs had taken only a CNI; CNI and MMF; CNI and everolimus; CNI and a steroid; CNI, MMF, and a steroid; and CNI, everolimus, and a steroid, respectively. Seven LTRs received entecavir, a drug used to treat hepatitis B, and immunosuppressive therapy.

Anti-RBD antibody titers in LTRs were significantly lower than those in HDs at all time points (Fig. 1b) ($p < 0.0001$ at 1 and 3 months, $p = 0.0005$ at 6 months after the second vaccination, $p = 0.0002$ after the third vaccination). Anti-RBD antibody titers in all HDs exceeded the WHO standard (dashed line, 1000 U/mL); however, 53.2% of LTRs had anti-RBD antibody titers below the WHO standard at 1 month after the second vaccination. However, anti-RBD antibody titers in 92.2% of the LTRs after the third vaccination exceeded the WHO standard, suggesting that effective immune responses can be achieved in immunosuppressed LTRs by the third vaccination.

Interestingly, the variability in antibody levels among LTRs was wide compared with that in HDs. Therefore, we aimed to identify the factors that affect the variability in antibody production in LTRs. LTRs that obtained anti-RBD antibody levels higher and lower than the median value of antibody titers in HDs after the third vaccination were categorized as strong and weak responders, respectively. We conducted a multiple logistic regression analysis with clinical parameters (Fig. 1c), suggesting that taking multiple drugs decreased antibody levels ($p = 0.0048$, OR = 0.0285).

We regrouped LTRs for comparison between LTRs taking only a CNI and taking a CNI and more drugs (CNI+other drug(s)) (Fig. 1d). There was no difference in the antibody titers between the CNI group and HDs after the third vaccination. Contrarily, antibody titers were significantly lower in the CNI+other drug(s) group than in the HDs and the CNI group ($p < 0.0001$ among HDs vs. CNI+other drug(s), $p < 0.0001$ among CNI vs. CNI+other drug(s)). However, the anti-RBD antibody titers after the third vaccination in the CNI+other drug(s) group were the same as those in HDs 1 month after the second vaccination (Fig. 1e; $p = 0.3255$). After the second vaccination, anti-RBD antibodies in plasma were induced in 49 of 54 LTRs. The 5 LTRs in whom anti-RBD antibodies were not induced after the second vaccination all showed induction of the antibodies after the third vaccination. However, there was one individual who, despite having a positive

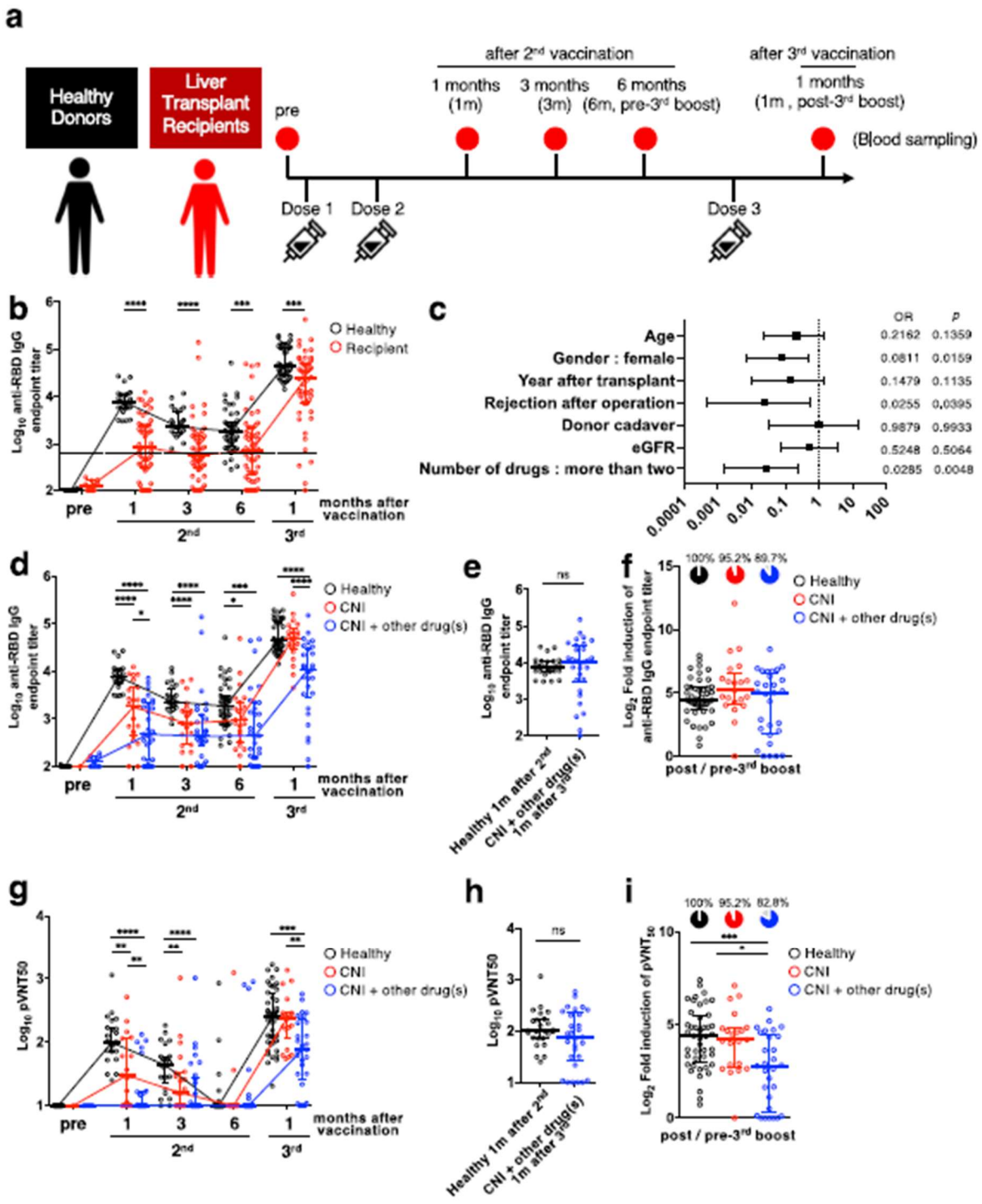

plasma anti-RBD antibody titer after the second dose, did not benefit from the third booster dose and tested negative. This individual was taking three medications, namely CNI, MMF, and steroids (5 mg/day), and had a low anti-RBD antibody titer even after the second vaccination.

Additionally, LTRs were regrouped based on clinical information apart from medication (Supplementary Fig. 1). Antibody titers were considerably lower in deceased donor liver transplant (DDLT) than in living-donor liver transplant (LDLT) (Supplementary Fig. 1a). Furthermore, antibody titers in LTRs less than 12 years after transplantation were lower (Supplementary Fig. 1b). LTRs who experienced rejection reactions after transplantation also exhibited lower antibody titers than those who did not (Supplementary Fig. 1c). LTRs who have taken MMF also exhibited lower antibody titers

Fig. 1 | Changes in anti-RBD IgG titers and plasma neutralizing activity in HDs and LTRs immunized by COVID-19 mRNA vaccine. **a** Schematic overview of the cohort. **b** Anti-RBD IgG endpoint titers in HDs (black) and LTRs (red) (sample size, pre: 25 vs 12, 1 m after 2nd: 25 vs 54, 3 m after 2nd: 24 vs 53, 6 m after 2nd: 44 vs 54, 1 m after 3rd: 44 vs 51). **c** Multivariable logistic regression model (OR and 95% CI) for predictors of weak and strong responders (lower and higher than median antibody titer in HDs at 1 month after third vaccination, respectively). **d** Anti-RBD antibody titers in HDs (black), LTRs taking only a calcineurin inhibitor (CNI group, red) and LTRs taking CNI and other medications (CNI+other drug(s) group, blue) (sample size, pre: 25 vs 1 vs 11, 1 m after 2nd: 25 vs 20 vs 27, 3 m after 2nd: 25 vs 23 vs 30, 6 m after 2nd: 44 vs 23 vs 31, 1 m after 3rd: 44 vs 21 vs 29). **e** Anti-RBD IgG endpoint titers in HDs 1 month after 2nd vaccination (black) and in CNI+other drug(s) group 1 month after 3rd vaccination (blue) (sample size, 25 vs 29). **f** Fold-induction in anti-RBD IgG endpoint titers after third vaccination (HDs: black, CNI: red, CNI+other drug(s): blue). Pie charts represent the proportion of individuals with fold-induction > 1, and gray slice shows frequency of negative responders. (sample size, 44 vs 21 vs 29). **g** $pVNT_{50}$ against SARS-CoV-2 Wuhan-1 (HDs: black, CNI: red, CNI+other drug(s): blue). **h** $pVNT_{50}$ in HDs 1 month after 2nd vaccination (black) and in CNI+other drug(s) group 1 month after 3rd vaccination (blue) (sample size, 25 vs 29). **i** Fold-induction in $pVNT_{50}$ after third vaccination. Pie charts represent the proportion of individuals with fold-induction > 1, and gray slice shows frequency of negative responders (HDs: black, CNI: red, CNI+other drug(s): blue) (sample size, 44 vs 21 vs 29). *P* values (two-sided) were calculated using the Mann–Whitney *U*-test. All experiments were performed once. Error bars indicate the interquartile range.

than those who have not (Supplementary Fig. 1d). These factors are related to the regimen of immunosuppressive drugs, and the multivariate analysis suggested that the number of drugs has the most significant impact. Noteworthily, antibody titers of 89.7% in the CNI+other drug(s) group were increased by the third vaccination, and the fold induction of antibody titers in the CNI+other drug(s) group was similar to that in HDs (Fig. 1f; $p = 0.7666$).

Next, we measured the changes in the neutralizing activity of plasma from HDs and LTRs (Fig. 1g). Neutralizing activity in most of the CNI +other drug(s) was below the detection limit after the second vaccination, and was significantly lower than that in HDs after the third vaccination ($p = 0.0001$). Contrarily, the neutralizing activity in the CNI+other drug(s) group after the third vaccination was similar to that in HDs one month after the second vaccination (Fig. 1h; $p = 0.2985$). Furthermore, although the fold-induction of neutralizing activity in CNI+other drug(s) by the third vaccination was significantly lower than that of HDs, 82.8% of the CNI +other drug(s) group got a booster effect (Fig. 1i) ($p = 0.0006$ among HDs vs. CNI+other drug(s)). These results suggest that the third doses of mRNA vaccine are worthwhile for the induction of neutralizing activity in LTRs, but may not be sufficient compared to HDs.

$CD4^+$ T-cell responses correlate with anti-RBD IgG titers in HDs and LTRs

Generally, immunosuppressive drugs, including CNIs, contribute to the suppression of T-cell responses. To investigate whether the reduction in antibody titers in LTRs is affected by changes in CD4 helper T-cell function, we performed flow cytometry analysis to evaluate the $CD4^+$ T-cell responses. The frequency of total SARS-CoV-2 spike-specific $CD4^+$ T cells was measured using CD154 as an activation marker (Supplementary Fig. 2a). The frequency of spike-specific $CD4^+$ T cells in CNI+other drug(s) at 1, 3, and 6 months after the second vaccination was significantly lower compared to HDs (Fig. 2a; $p = 0.0117$, $p = 0.0208$, and $p = 0.0047$ at 1, 3, and 6 months after the second vaccination, respectively). There was no significant difference between HDs and the CNI group at 1 month ($p > 0.9999$), 3 months ($p = 0.6506$), and 6 months ($p = 0.1379$) after the second vaccination. Moreover, there were significant differences between the CNI and CNI+other drug(s) groups 3 months ($p = 0.024$), and 6 months ($p = 0.0051$) after the second vaccination (Fig. 2a). However, there is no significant difference among HDs, the CNI group, and the CNI+other drug(s) group after the third vaccination. Regardless of HDs or LTRs, spike-specific $CD4^+$ T cells decreased over time after the second mRNA vaccination (Supplementary Fig. 2b).

Next, we measured the cytokine profiles of the total spike-specific $CD4^+$ T cells (Fig. 2b, c, Supplementary Fig. 2a). The frequency of Th1 cells in CNI+other drug(s) after the second vaccination was significantly lower compared to HDs (Fig. 2b). On the contrary, the frequency of Th2 cells was higher in the CNI group than in HDs (Fig. 2c). The frequency of total $CD154^+$ spike-specific $CD4^+$ T cells and Th1 cells increased by the third mRNA vaccination in HDs and LTRs, and there was no significant difference between HDs and LTRs after the third vaccination (Fig. 2a, b).

We next examined the effect of the third booster on memory $CD4^+$ T cell responses by calculating the fold-induction of $CD154^+$, Th1, and Th2 cell frequencies. We observed a boost effect in ~75% of individuals for $CD154^+$ and Th1 cells in all groups, and in ~50% of individuals for Th2 cells (Fig. 2d–f). Furthermore, Th1/Th2 ratio in LTRs was significantly lower compared to HDs (Fig. 2g), suggesting that LTRs are more susceptible to the induction of Th2-biased $CD4^+$ T-cell responses.

We next evaluated the correlation between $CD4^+$ T-cell and antibody responses. One month after the second vaccination, the frequency of $CD154^+CD4^+$ T and Th1 cells was positively correlated with anti-RBD antibody titers in HDs and LTRs (Fig. 2h). Moreover, $CD4^+$ T-cell frequency before the third vaccination positively correlated with antibody titers after the third vaccination (HDs: $r = 0.299$, $p = 0.049$ for $CD154^+CD4^+$ T cells vs. anti-RBD IgG; LTRs: $r = 0.483$, $p = 0.0004$ for $CD154^+CD4^+$ T cells vs. anti-RBD IgG; $r = 0.433$, $p = 0.0019$ for Th1 CD4 T cells vs. anti-RBD IgG). These results suggest that long-term $CD4^+$ T-cell responses after the second vaccination contribute to the booster effect on antibody levels after the third vaccination.

Characterization of spike-specific $CD8^+$ T-cell responses in HDs and LTRs

In addition to antibodies and $CD4^+$ T cells, $CD8^+$ T-cell responses also contribute to defense against SARS-CoV-2 infection[22,23]. However, COVID-19 mRNA vaccines reportedly have a lower ability to induce $CD8^+$ T cells than $CD4^+$ T cells[24]. Moreover, few reports demonstrate $CD8^+$ T-cell responses to mRNA vaccines in LTRs. Therefore, we investigated whether spike-specific $CD8^+$ T cells were induced in LTRs and compared their frequency with HDs. We defined 4-1BB$^+$CD69$^+$CD8$^+$ T cells as spike-specific $CD8^+$ T cells in the PBMCs stimulated with spike peptides (Supplementary Fig. 3a). Spike-specific $CD8^+$ T cells were detected in 100% of HDs and 93% of LTRs 1 month after the second vaccination (Fig. 3a). However, the frequency of spike-specific $CD8^+$ T cells by the third vaccination did not increase in most HDs and LTRs (Fig. 3b, HDs 55.8%, CNI 55%, and CNI+other drug(s) 42.9%). Compared to HDs, the frequency of LTRs was significantly lower at all time points, regardless of taking single or multiple drugs (Fig. 3a). Furthermore, in contrast to antibody responses, there was no correlation between spike-specific $CD8^+$ and $CD4^+$ T cell responses (Fig. 3c). These results suggest that the third boost effect on memory T-cell responses differs between $CD4^+$ and $CD8^+$ T cells. We then checked the differentiation status of the spike-specific $CD8^+$ T cells induced by vaccination using CD27, CD45RO, and CD57 markers to define central memory (CM; $CD27^+CD45RO^+$), effector memory (EM; $CD27^-CD57^-$), and effector ($CD27^-CD57^+$) subsets. As a result, the phenotypes of spike-specific $CD8^+$ T cells were changed from CM to EM at 6 months after 2nd vaccination in both the HDs and LTRs who showed positive effects of boosting spike-specific $CD8^+$ T-cell responses (Healthy boost+ and LTR boost +), although the phenotypes of total memory $CD8^+$ T cells were not changed over time (Fig. 3d, e). After 3rd mRNA vaccination, HDs and LTRs showed different phenotypes of spike-specific $CD8^+$ T cells, with decreased CM and increased EM and Effector in HDs, but a trend toward increased CM in LTRs.

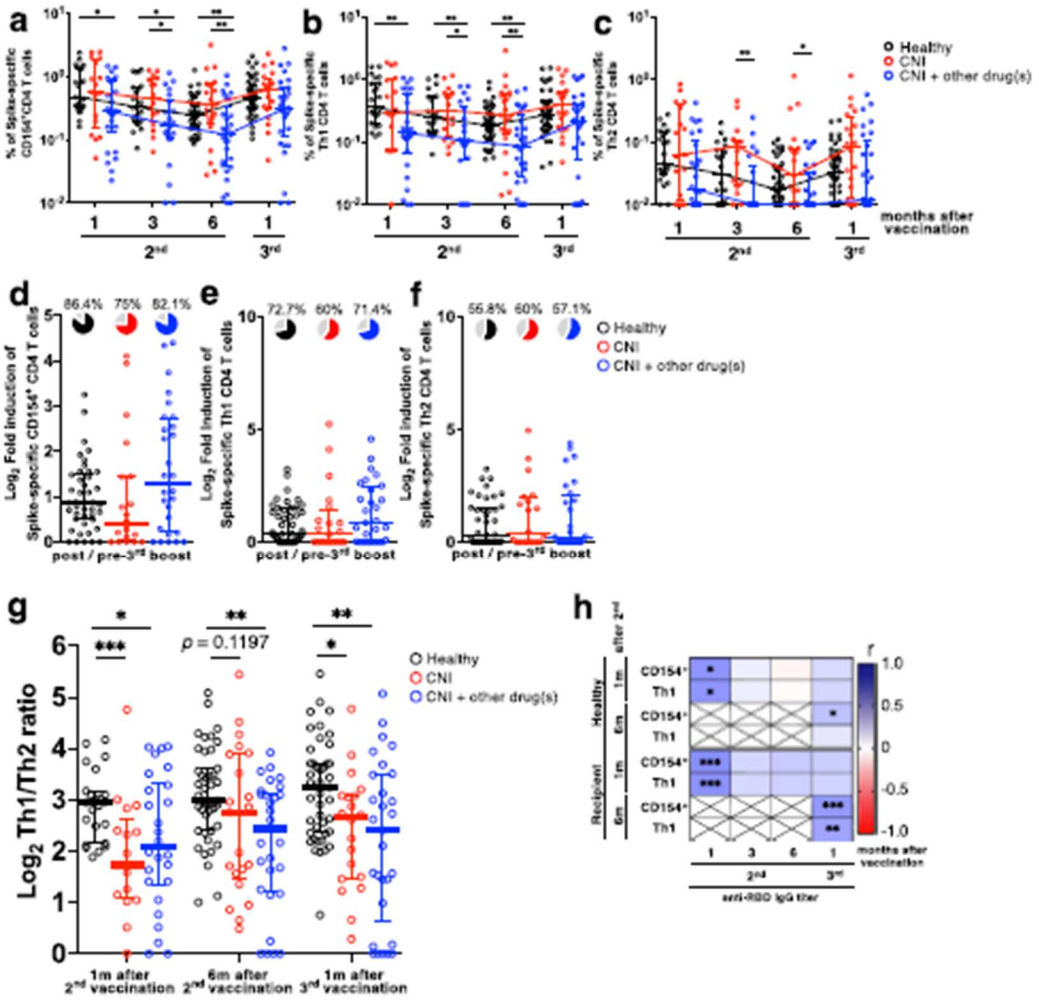

Fig. 2 | CD4⁺ T-cell responses correlate with anti-RBD IgG titers in HDs and LTRs. Frequency of spike-specific CD154⁺ (**a**), Th1 (**b**), and Th2 (**c**) CD4⁺ T cells in total memory T cells from HDs (black), CNI group (red), and CNI+other drug(s) group (blue). **d**–**f** Fold-induction of spike-specific CD154⁺, Th1, and Th2 CD4⁺ T cells by the third vaccination. Pie charts represent the proportion of individuals with fold-induction higher than 1, and gray slice shows frequency of negative responders. (HDs: black, CNI: red, CNI+other drug(s): blue). **g** The ratio of spike-specific Th1 to Th2 CD4⁺ T cells (HDs: black, CNI: red, CNI+other drug(s): blue). *P* values (two-sided) in (**a**) to (**g**) were calculated using the Mann-Whitney U-test. **h** Correlation matrix of antibody and CD4⁺ T-cell responses in HDs and LTRs. Shades of blue represent positive correlations approaching 1, while shades of red denote negative correlations nearing -1. *P* values (two-sided) were calculated using the Spearman's rank test. Sample size, 1 m after 2nd: 23 vs 17 vs 26, 3 m after 2nd: 22 vs 16 vs 22, 6 m after 2nd: 43 vs 21 vs 29, 1 m after 3rd: 43 vs 20 vs 29. All experiments were performed once. Error bars indicate the interquartile range.

Furthermore, we previously reported that differences in the expression patterns of cytotoxic molecules could observe qualitative differences in mRNA vaccine-induced spike-specific CD8⁺ T cells[20]. Therefore, we compared the expression of cytotoxic molecules in spike-specific CD8⁺ T cells between HDs and LTRs. Supplementary Fig. 3b shows the expression patterns of GZMA, GZMB, and Perforin, and gating. Regardless of HDs or LTRs, most spike-specific CD8⁺ T cells expressed GZMA before and after the third vaccination (Fig. 3f). The proportion of cells expressing GZMA in CNI+other drug(s) was significantly, but slightly, lower than that in HDs before the third vaccination ($p = 0.0237$). However, the proportion of cells expressing GZMB and Perforin was not different between HDs and LTRs before and after the third boost (Fig. 3g, h). Furthermore, the expression profiles of GZMA, GZMB, and Perforin were not significantly different between the groups (Supplementary Fig. 4a, b). The proportion of subpopulations expressing GZMA, GZMB, and Perforin was approximately 20% in the spike-specific CD8⁺ T cells of each group, and the proportion of subpopulations expressing only GZMA was over 50% (Fig. 3i). However, we did not observe any qualitative differences in spike-specific CD8⁺ T cells induced by the third boost.

Antibody against SARS-CoV-2 variants of concern induced by mRNA vaccine

HDs and LTRs were vaccinated with an mRNA vaccine based on the Wuhan-1 strain, and the induced antibodies potentially reduced the effectiveness against the recently emerged Omicron sublineages. Therefore, we measured the antibody titers before and after the third boost against RBD corresponding to the Omicron sublineages, and found that anti-RBD antibody titers before the third boost against all sublineages were significantly reduced compared to those against the Wuhan-1 (Fig. 4a, b). Among sublineages, the anti-RBD antibody titers against BQ.1.1 and XBB were particularly reduced (HDs, 8.43-fold reduction; CNI, 5.23-fold reduction; CNI+other drug(s), 4.41-fold reduction against BQ.1.1, HDs, 11.9-fold reduction; CNI, 6.35-fold reduction; CNI+other drug(s), 4.41-fold reduction against XBB). Furthermore, the neutralizing activity before the

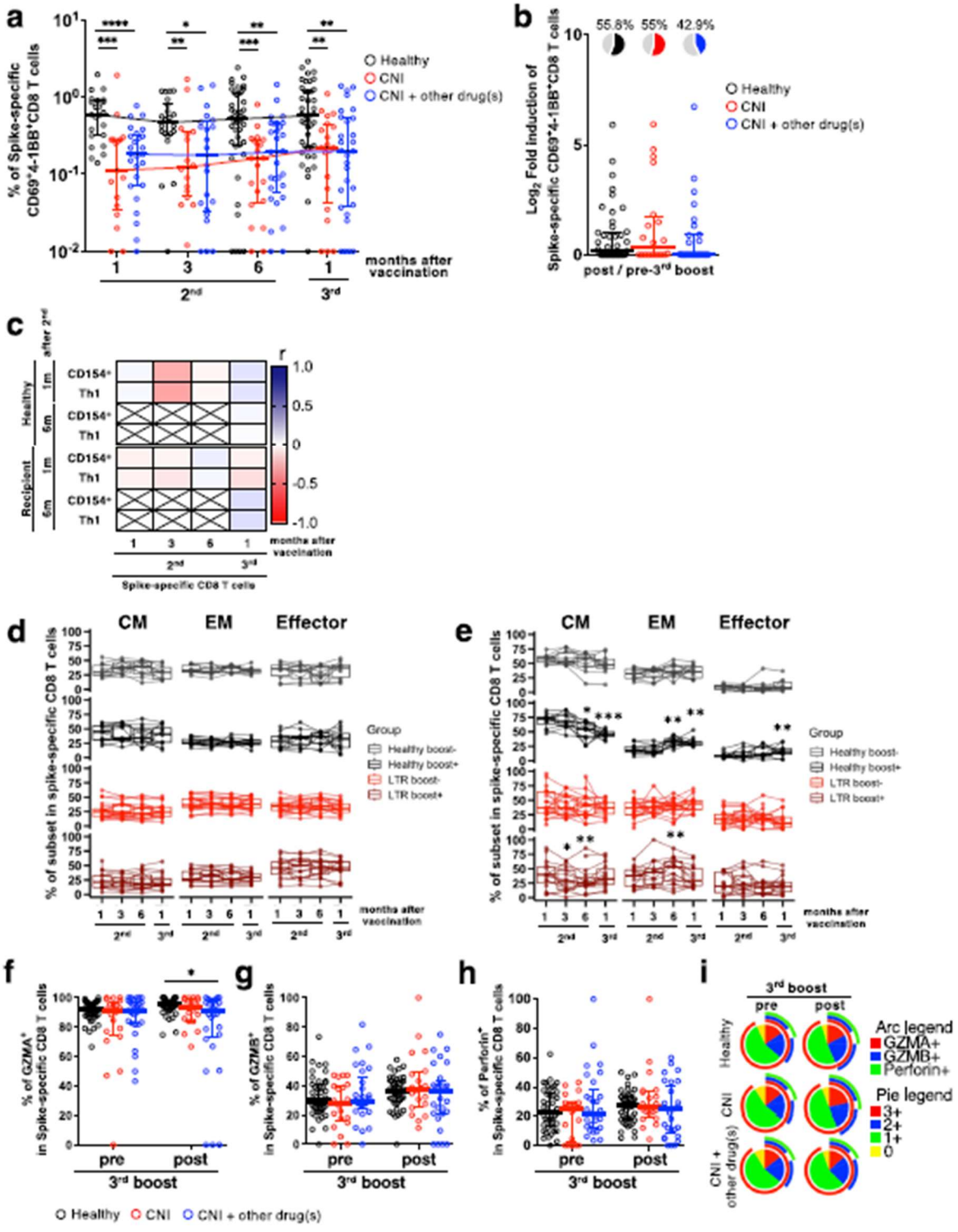

third boost was below the detection limit for BA.5, BQ.1.1, and XBB in most individuals (Fig. 4c). Furthermore, there was no change in the trend toward lower antibody titers for each Omicron sublineage (Fig. 4d, e). In particular, the CNI+other drug(s) group showed significantly lower anti-RBD antibody levels against all sublineages than the HDs and CNI groups. Additionally, there was a slight improvement in neutralizing activity against the BA.5 strain, but not BQ.1.1 and XBB strains, by the third vaccination (Fig. 4f).

Collectively, these results suggest that the third vaccination with the Wuhan-1 mRNA vaccine may not be sufficient to induce antibody

Fig. 3 | CD8⁺ T-cell responses were reduced in LTRs but there no significant difference in the expression of cytotoxic molecules. **a** Frequencies of spike-specific CD69⁺4-1BB⁺CD8⁺ T cells in total memory T cells from HDs (black), CNI group (red), and CNI+other drug(s) group (blue). **b** Fold-induction of spike-specific CD69⁺4-1BB⁺CD8⁺ T cells after third vaccination. Pie charts represent the proportion of individuals with fold-induction > 1, and gray slice shows frequency of negative responders (HDs: black, CNI: red, CNI+other drug(s): blue). **c** Correlation matrix of CD4⁺ and CD8⁺ T-cell responses. Shades of blue represent positive correlations approaching 1, while shades of red denote negative correlations nearing -1. *P* values were calculated using the Spearman's rank test. Frequencies of CM, EM and effector within CD8⁺ total memory T cells (**d**) and spike-specific CD69⁺4-1BB⁺ CD8⁺ T cells (**e**) in individuals who did (boost +) or did not (boost-) receive boost effect from 3 doses of mRNA vaccine (HDs boost-: gray, HDs boost +: black, LTRs boost-: red, LTRs boost + : dark red). *P* values (two-sided) were calculated using the Wilcoxon matched-pairs signed rank test compared to 1 month after 2ⁿᵈ vaccination. Frequency of spike-specific CD69⁺4-1BB⁺CD8⁺ T cells expressing GZMA (**f**), GZMB (**g**), and Perforin (**h**) (HDs: black, CNI: red, CNI+other drug(s): blue). **i** Expression of multiple cytotoxic molecules in spike-specific CD69⁺4-1BB⁺CD8⁺ T cells. Each color's arc length and pie chart's area represent the expression of each cytotoxic molecule (GZMA: red, GZMB: blue, Perforin: green) and cells expressing the indicated number of cytotoxic molecules (0: yellow, 1: green, 2: blue, 3: red), respectively. *P* values (two-sided) in (**a**), (**b**), (**f**), (**g**), and (**h**) were calculated using the Mann–Whitney *U*-test. Sample size, 1 m after 2nd: 23 vs 17 vs 26, 3 m after 2nd: 22 vs 16 vs 22, 6 m after 2nd: 43 vs 21 vs 29, 1 m after 3rd: 43 vs 20 vs 29. All experiments were performed once. Error bars indicate the interquartile range.

responses against Omicron sublineages, particularly BQ.1.1 and XBB, in HDs and LTRs.

Cellular immune responses against SARS-CoV-2 variants of concern induced by mRNA vaccine

Finally, we investigated the differences in cellular immunity against Omicron sublineages between HDs and LTRs. The frequency of spike-specific CD154⁺CD4⁺ T cells was evaluated in PBMCs before the third boost. There was no difference in response to the Wuhan-1 and mutant strains in all groups (Supplementary Fig. 5a, b). The same trend was observed for spike-specific Th1 CD4⁺ T cells (Fig. 5a, b). However, the frequency of CD154⁺CD4⁺ T cells and Th1 cells responding to mutant strains in HDs after the third boost was significantly and slightly lower than that of cells responding to Wuhan-1(Supplementary Fig. 5c, d, Fig. 5c, d). The same trend was observed in spike-specific Th2 CD4⁺ T cells (Supplementary Fig. 4e–h). These results indicate that, unlike antibody responses, CD4⁺ T-cell responses induced by mRNA vaccines can react to Omicron sublineages. Moreover, LTRs resulted in CD4⁺ T-cell responses to Omicron sublineages with comparable reactivity to those in HDs.

Next, we investigated CD8⁺ T cell responses to Omicron sublineages. Interestingly, the frequency of spike-specific CD8⁺ T-cell responses to mutant strains was not significantly decreased, regardless of the pre- and post-third boost (Fig. 6a, b). The fold-changes in the frequency of CD8⁺ T-cell responses to mutant strains relative to Wuhan-1 are shown (Fig. 6c, d). Collectively, these results demonstrate that mRNA vaccines induce CD8⁺T-cell responses reactive to BA.5, BQ.1.1, and XBB mutant strains and that these responses are maintained in LTRs.

Discussion

In this study, the anti-RBD IgG titers in LTRs induced by the mRNA vaccines were lower than those in HDs after the second and third vaccination. Multivariate analysis based on LTRs' background information revealed that the use of multiple immunosuppressive drugs was a key factor in the lack of antibody induction, which is consistent with recent studies[7,8]. Even in LTRs receiving multiple medications, the third mRNA vaccination induced antibody responses similar to those observed in HDs after the second vaccination. However, neutralizing antibodies obtained with only three doses of the Wuhan-1-type mRNA vaccine are insufficient against Omicron sublineages. It could be necessary to receive a fourth dose of a vaccine or a bivalent vaccine[15,25], especially for LTRs.

Furthermore, in this cohort, eight patients had a history of rituximab treatment, which targets B cells. A study in patients with multiple sclerosis receiving anti-CD20 therapy within 20 weeks before mRNA vaccination showed that antibody production following mRNA vaccination was drastically reduced, while T-cell responses were induced[26]. However, in our cohort, no LTRs received anti-CD20 therapy within 1 year before vaccination, and rituximab treatment did not affect antibody induction. Another critical point is that, unlike in Western countries, LDLT is the primary method in our cohort. Our study could uniquely compare LDLT with DDLT (LDLT; $n = 46$, DDLT; $n = 8$) and evaluate the changes in immune responses over time in vaccine efficacy in LTRs from LDLT. Furthermore, passive immunotherapy such as HBIG is mainly used in LTR because HBV vaccine is less effective in LTRs[27]. While the HBV vaccine is a recombinant protein vaccine, the mRNA vaccine developed as a new modality during the SARS-CoV-2 pandemic is a potentially effective platform for inducing neutralizing antibodies even in immunosuppressed LTR.

CNIs are the most commonly used immunosuppressive drugs targeting T cells in LTRs. CNIs inhibit calcineurin, resulting in the inactivation of the nuclear factor of activated T-lymphocytes (NFAT) and suppression of IL-2 production[28]. In other words, CNIs specifically target T cells, but for the evaluation of mRNA vaccine effects in LTR, the focus is on humoral immunity due to technical limitations. Notably, the early induction of CD4⁺ T-cell responses by mRNA vaccines is reportedly necessary for antibody production[29]. Therefore, it is crucial to investigate the effectiveness of mRNA vaccine-induced T-cell responses in LTRs. Our findings demonstrate that CD4⁺ T-cell responses before the third mRNA vaccination significantly correlated with anti-RBD IgG titers after the third vaccination. These results suggest that the long-term maintenance of CD4⁺ T cell responses is an important factor for the acquisition of high antibody titers in LTRs.

Furthermore, taking multiple drugs reduced spike-specific CD4⁺ T-cell responses after the second vaccination, similar to antibody titers; however, the third vaccination significantly improved CD4⁺ T-cell responses. Therefore, a third mRNA vaccination is considered effective for acquiring immune responses in LTRs regarding both antibody and CD4⁺ T-cell responses. Additionally, CNI alone did not affect the induction of spike-specific CD154⁺CD4⁺ T cells. However, CD4⁺ T cells were biased toward the Th2 phenotype in the LTRs. The induced Th2-biased CD4⁺ T cells in mice and hamsters reportedly lead to vaccine-associated enhanced respiratory disease (VAERD) upon SARS-CoV-2 infection[30,31]. Although the occurrence of VAERD caused by COVID-19 mRNA vaccines in humans has not been verified, it is necessary to consider the possibility of VAERD in LTRs. Moreover, although COVID-19 mRNA vaccines have a strong Th1 induction ability[32,33], it is possible that the environment in which CD4 naive T cells are more prone to differentiate into Th2 phenotype is created due to the effect of CNI. It has been shown that CD4 naive T cells polarize into Th1 phenotype upon receiving strong TCR signals and into Th2 phenotype upon receiving weak TCR signals in mice[34]. Furthermore, previous studies have demonstrated a clear shift from Th1 to a Th2 cytokine-secreting profile as an additional mechanism of immunosuppression by cyclosporin A[35] and steroids[36]. However, Th1/Th2 ratio in LTRs was not different after the second and third mRNA vaccination, suggesting that the possibility of Th2-biased reactions becoming predominant after multiple mRNA vaccinations is low.

The cytolytic activity of spike-specific CD8⁺ T-cell responses is a key factor for reducing the risks of severity against SARS-CoV-2 infection in HDs[37]. Recent studies suggest that mRNA vaccines induce weaker CD8⁺ T-cell responses in healthy donors compared to CD4⁺ T-cell responses[38,39]. In solid organ transplant recipients, including liver and kidney transplantation, the frequency of spike-specific CD8⁺ T cells was found to be significantly lower after 2nd mRNA vaccination compared to healthy donors[9]. This finding also indicates that solid organ transplant recipients have weaker CD4⁺ and CD8⁺ T-cell responses compared to other groups of

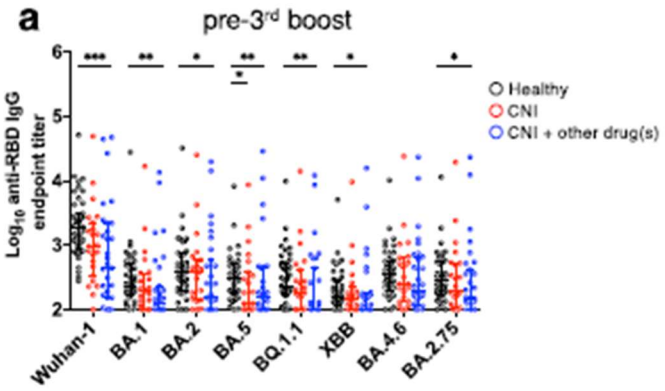

b

Fold-change (relative to Wuhan-1)

pre-3rd boost	Wuhan-1	BA.1	BA.2	BA.5	BQ.1.1	XBB	BA.4.6	BA.2.75
Healthy	1.00	-8.00	-4.80	-6.09	-8.43	-11.90	-5.35	-6.46
CNI	1.00	-4.83	-2.54	-7.66	-5.23	-6.35	-3.83	-4.90
CNI + other drug(s)	1.00	-3.48	-2.90	-2.81	-4.41	-4.41	-2.32	-2.95

Significant difference (compared to Wuhan-1)

pre-3rd boost	Wuhan-1	BA.1	BA.2	BA.5	BQ.1.1	XBB	BA.4.6	BA.2.75
Healthy		****	****	****	****	****	****	****
CNI		****	****	****	****	****	****	****
CNI + other drug(s)		****	****	***	****	****	****	****

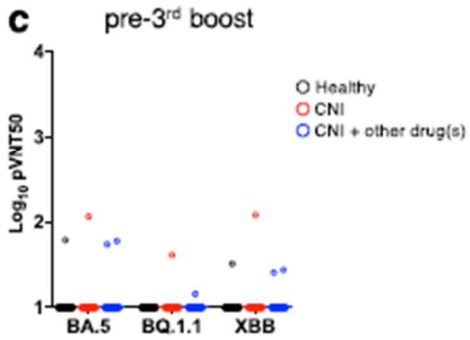

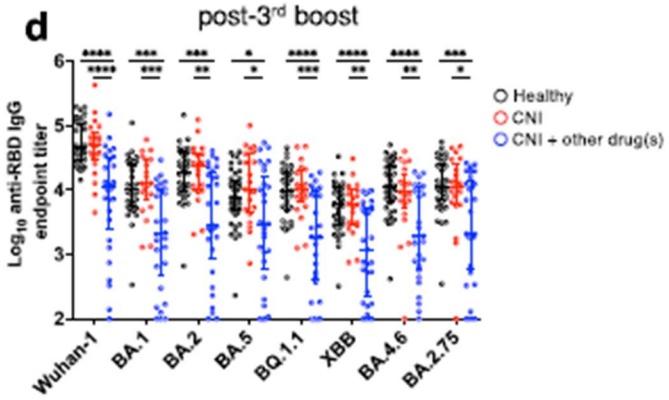

e

Fold-change (relative to Wuhan-1)

post-3rd boost	Wuhan-1	BA.1	BA.2	BA.5	BQ.1.1	XBB	BA.4.6	BA.2.75
Healthy	1.00	-4.49	-2.32	-6.06	-4.66	-7.53	-4.10	-4.10
CNI	1.00	-3.87	-2.02	-4.77	-4.73	-8.26	-5.20	-4.34
CNI + other drug(s)	1.00	-5.02	-3.82	-3.64	-5.78	-9.09	-5.62	-5.16

Significant difference (compared to Wuhan-1)

post-3rd boost	Wuhan-1	BA.1	BA.2	BA.5	BQ.1.1	XBB	BA.4.6	BA.2.75
Healthy		****	****	****	****	****	****	****
CNI		***	***	***	****	****	****	****
CNI + other drug(s)		****	***	****	****	****	****	****

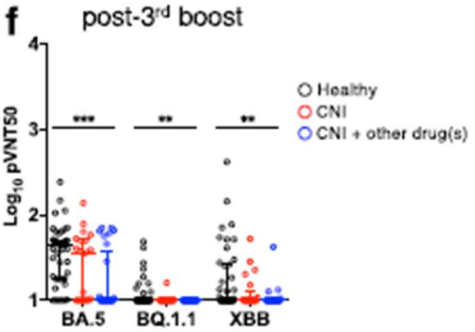

Fig. 4 | Antibody against SARS-CoV-2 variants of concern induced by mRNA vaccine. a, **d** Anti-RBD antibody endpoint titers against indicated strains at (**a**) pre- and (**d**) post-third boost (HDs: black, CNI: red, CNI+other drug(s): blue). Fold-change of anti-RBD IgG against variants of concern endpoint titers at (**b**) pre- and (**e**) post-third boost relative to Wuhan-1. The minus symbol denotes increased resistance. Shades of red indicate a decrease in antibody titers, with darker shades signifying a larger negative fold change. $pVNT_{50}$ against strains at (**c**) pre- and (**f**) post-third boost (HDs: black, CNI: red, CNI+other drug(s): blue). *P* values (two-sided) in (**a**), (**c**), (**d**), and (**f**) were calculated using the Mann–Whitney *U*-test. *P* values (two-sided) in (**b**) and (**e**) were calculated using the Wilcoxon matched-pairs signed rank test. Sample size, pre-3rd boost: 44 vs 23 vs 31, post-3rd boost: 44 vs 21 vs 30). All experiments were performed once. Error bars indicate the interquartile range.

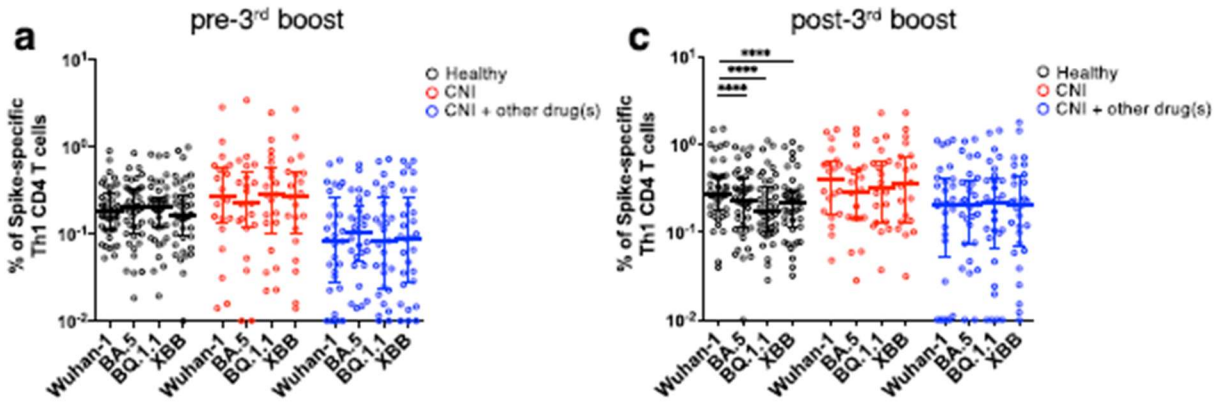

b Fold-change (relative to Wuhan-1)

pre-3rd boost	Wuhan-1	BA.5	BQ.1.1	XBB
Healthy	1.00	1.10	1.13	-1.10
CNI	1.00	-1.20	1.05	1.00
CNI + other drug(s)	1.00	1.22	-1.02	1.05

Significant difference (compared to Wuhan-1)

pre-3rd boost	Wuhan-1	BA.5	BQ.1.1	XBB
Healthy		ns	ns	ns
CNI		ns	ns	ns
CNI + other drug(s)		ns	ns	ns

d Fold-change (relative to Wuhan-1)

post-3rd boost	Wuhan-1	BA.5	BQ.1.1	XBB
Healthy	1.00	-1.19	-1.58	-1.25
CNI	1.00	-1.35	-1.21	-1.12
CNI + other drug(s)	1.00	1.00	1.05	-1.03

Significant difference (compared to Wuhan-1)

post-3rd boost	Wuhan-1	BA.5	BQ.1.1	XBB
Healthy		****	****	****
CNI		ns	ns	ns
CNI + other drug(s)		ns	ns	ns

Fig. 5 | CD4⁺ T-cell responses against SARS-CoV-2 variants of concern induced by mRNA vaccine. a Comparison of spike-specific Th1 CD4⁺ T-cell frequency against spike peptides in CD4⁺ total memory T cells at pre-third boost (HDs: black, CNI: red, CNI+other drug(s): blue). **b** Fold-change of spike-specific Th1 CD4⁺ T-cell frequency against variants of concern at pre-third boost relative to Wuhan-1. The minus symbol denotes increased resistance. Shades of blue represent an increase in fold change, with darker shades indicating a larger positive fold change. Conversely, shades of red denote a decrease, with darker shades signifying a larger negative fold change. **c** Comparison of spike-specific Th1 CD4⁺ T-cell frequency against spike peptides in CD4⁺ total memory T cells at post-third boost (HDs: black, CNI: red, CNI+other drug(s): blue). **d** Fold-change of spike-specific Th1 CD4⁺ T-cell frequency against variants of concern at post-third boost relative to Wuhan-1. The minus symbol denotes increased resistance. Shades of blue represent an increase in fold change, with darker shades indicating a larger positive fold change. Conversely, shades of red denote a decrease, with darker shades signifying a larger negative fold change. *P* values (two-sided) were calculated using the Wilcoxon matched-pairs signed rank test. Sample size, 1 m after 2nd: 23 vs 17 vs 26, 3 m after 2nd: 22 vs 16 vs 22, 6 m after 2nd: 43 vs 21 vs 29, 1 m after 3rd: 43 vs 20 vs 29. All experiments were performed once. Error bars indicate the interquartile range.

immunocompromised patients, such as primary immunodeficiency syndromes, AIDS, hematopoietic stem cell transplant recipients, and chronic lymphocytic leukemia patients. In our study, the frequency of spike-specific CD8⁺ T cells was significantly lower than that of healthy donors at all time points. Although spike-specific CD8⁺ T-cell responses decreased quantitatively in CNI group and CNI+other drug(s) group compared to healthy donors, there is no significant difference between healthy donors and LTR in terms of the booster effect of mRNA vaccines (Fig. 3b).

In recent years, it has been reported that the expression of GZMB and perforin in bulk CD8⁺ T cells, not antigen-specific CD8⁺ T cells, in SARS-CoV-2 infected patients is higher than that in healthy donors[40]. This suggests that the induction of CD8⁺ T cells expressing high levels of cytotoxic molecules contributes potentially to the suppression of COVID-19 severity. However, a recent study using MHC multimers has demonstrated that the expression levels of GZMB and perforin in SARS-CoV-2 spike epitope-specific CD8⁺ T cells decrease over time after 2nd mRNA vaccination, and do not increase after 3rd vaccination[41]. Therefore, the ability of mRNA vaccines to induce CD8⁺ T cells with high cytotoxic activity is limited. In our study, the subpopulations expressing GZMA, GZMB, and perforin were not different between HDs and LTRs, indicating that mRNA vaccine-induced spike-specific CD8⁺ T cells are quantitatively, but not qualitatively, limited to LTRs. In summary, no improvement was observed in both the quantitative or qualitative aspects of spike-specific CD8⁺ T cells even after 3rd vaccination in both healthy donors and LTR in our study. Moreover, both CD4⁺ and CD8⁺ T-cell responses induced by Wuhan-1 mRNA vaccines were reactive to Omicron sublineages BA.5, BQ.1.1, and XBB in HDs and LTRs, suggesting that inducing T-cell responses is crucial for dealing with new mutant strains.

We also examined the relationship between LTRs' background information and the induction of spike-specific CD8⁺ T cells (Fig. 1c). Although taking multiple drugs did not affect the responsiveness of spike-specific CD8⁺ T cells to the third boost, unlike the antibody responses, a decline in eGFR affected CD8⁺ T-cell responses (Supplementary Fig. 6A). This result suggests that LTRs with decreased kidney function may be a potential risk factor for weaker CD8⁺ T-cell responses, as shown by an epidemiological study demonstrating high serum creatinine levels in severe COVID-19 patients[4]. Since CD8⁺ T-cell responses during SARS-CoV-2 infection in LTRs with decreased kidney function have not been evaluated, further investigation is needed to address this. Furthermore, the median steroid dose administered to the liver transplant recipients in this study was 5 mg/day (range: 0.5–10 mg/day). Within this range, an effect was observed on the antibody titer, but no effect on the T-cell response was noted (Supplementary Fig. 7a).

Finally, the booster effect of the third vaccination was found in terms of spike-specific CD4⁺ T-cell and antibody responses but not CD8⁺ T-cell responses in HDs and LTRs. Regarding the quantitative changes in CD8⁺ T-cell responses, only ~50% of HDs and LTRs obtained a boosting effect by the third vaccination (Fig. 3b). This cannot be explained simply by HDs vs. LTRs. In our phenotypic analysis of spike-specific CD8 T cells, we found that the differentiation/maturation of the spike-specific CD8⁺ T cells after two doses of mRNA vaccine could be a key factor for boosting spike-specific CD8⁺ T cells by the third vaccination. Further investigation is still required

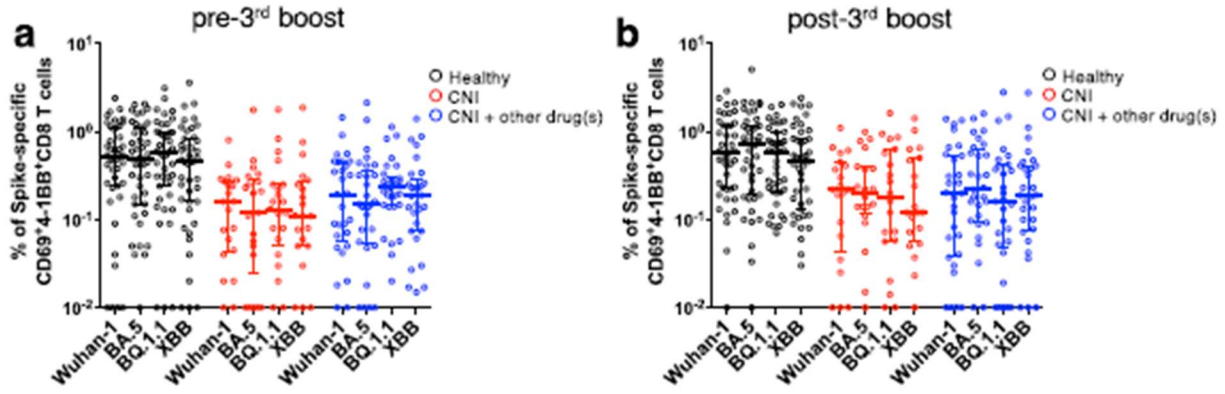

c Fold-change (relative to Wuhan-1)

pre-3rd boost	Wuhan-1	BA.5	BQ.1.1	XBB
Healthy	1.00	-1.06	1.10	-1.16
CNI	1.00	-1.33	-1.22	-1.45
CNI + other drug(s)	1.00	-1.29	1.19	-1.04

Significant difference (compared to Wuhan-1)

pre-3rd boost	Wuhan-1	BA.5	BQ.1.1	XBB
Healthy		ns	ns	ns
CNI		ns	ns	ns
CNI + other drug(s)		ns	ns	ns

d Fold-change (relative to Wuhan-1)

post-3rd boost	Wuhan-1	BA.5	BQ.1.1	XBB
Healthy	1.00	1.34	1.08	-1.20
CNI	1.00	-1.10	-1.22	-1.83
CNI + other drug(s)	1.00	1.11	-1.24	-1.05

Significant difference (compared to Wuhan-1)

post-3rd boost	Wuhan-1	BA.5	BQ.1.1	XBB
Healthy		ns	ns	ns
CNI		ns	ns	ns
CNI + other drug(s)		ns	ns	ns

Fig. 6 | CD8⁺ T-cell responses against SARS-CoV-2 variants of concern induced by mRNA vaccine. Comparison of spike-specific CD69⁺4-1BB⁺ CD8⁺ T-cell frequency against spike peptides in CD8⁺ total memory T cells at (a) pre- and (b) post-third boost (HDs: black, CNI: red, CNI+other drug(s): blue). Fold-change of spike-specific CD8⁺ T-cell frequency against variants of concern at (c) pre- and (d) post-third boost relative to Wuhan-1. The minus symbol denotes increased resistance. Shades of blue represent an increase in fold change, with darker shades indicating a larger positive fold change. Conversely, shades of red denote a decrease, with darker shades signifying a larger negative fold change. *P* values (two-sided) were calculated using the Wilcoxon matched-pairs signed rank test. Sample size, 1 m after 2nd: 23 vs 17 vs 26, 3 m after 2nd: 22 vs 16 vs 22, 6 m after 2nd: 43 vs 21 vs 29, 1 m after 3rd: 43 vs 20 vs 29. All experiments were performed once. Error bars indicate the inter-quartile range.

to address the moleculer mechanism of this observation. While mRNA vaccines are expected to be effective platforms for various pathogens that may emerge, low CD8⁺ T-cell induction ability could be an issue for future mRNA vaccine development.

In summary, the third mRNA vaccination improves humoral responses and spike-specific CD4⁺ T-cell responses in LTRs but exhibited no booster effect for spike-specific memory CD8⁺ T-cell responses. Spike-specific CD4⁺ and CD8⁺ T cells can react to Omicron sublineages in HDs and LTRs, which suggests that a third mRNA vaccination could be helpful in LTRs to prevent SARS-CoV-2 infection, although the further investigation will be needed to elicit CD8 T-cell responses in not only LTRs but also HDs.

Data availability

Source data, datasets generated and/or analyzed during the current study, are available in the paper or are appended as Supplementary Data 1. The data supporting the findings of this study are available from the corresponding author upon request.

Received: 23 May 2023; Accepted: 1 February 2024;
Published online: 26 February 2024

References

1. Dong, E., Du, H. & Gardner, L. An interactive web-based dashboard to track COVID-19 in real time. *Lancet Infect. Dis.* **20**, 533–534 (2020).
2. Pereira, M. R. et al. COVID-19 in solid organ transplant recipients: Initial report from the US epicenter. *Am. J. Transplant.* **20**, 1800–1808 (2020).
3. Zhou, F. et al. Clinical course and risk factors for mortality of adult inpatients with COVID-19 in Wuhan, China: a retrospective cohort study. *Lancet* **395**, 1054–1062 (2020).
4. Webb, G. J. et al. Outcomes following SARS-CoV-2 infection in liver transplant recipients: an international registry study. *Lancet Gastroenterol. Hepatol.* **5**, 1008–1016 (2020).
5. Bar-On, Y. M. et al. Protection of BNT162b2 vaccine booster against Covid-19 in Israel. *N. Engl. J. Med.* **385**, 1393–1400 (2021).
6. John, B. V. et al. Coronavirus Disease 2019 vaccination is associated with reduced severe acute respiratory syndrome coronavirus 2 infection and death in liver transplant recipients. *Gastroenterology* **162**, 645–647.e642 (2022).
7. Rabinowich, L. et al. Low immunogenicity to SARS-CoV-2 vaccination among liver transplant recipients. *J. Hepatol.* **75**, 435–438 (2021).
8. Thuluvath, P. J., Robarts, P. & Chauhan, M. Analysis of antibody responses after COVID-19 vaccination in liver transplant recipients and those with chronic liver diseases. *J. Hepatol.* **75**, 1434–1439 (2021).
9. Gao, Y. et al. Immunodeficiency syndromes differentially impact the functional profile of SARS-CoV-2-specific T cells elicited by mRNA vaccination. *Immunity* **55**, 1732–1746.e1735 (2022).
10. Davidov, Y. et al. A third dose of the BNT162b2 mRNA vaccine significantly improves immune responses among liver transplant recipients. *J. Hepatol.* **77**, 702–709 (2022).
11. Tasdogan, B. E., Ma, M., Simsek, C., Saberi, B. & Gurakar, A. Update on Immunosuppression in Liver Transplantation. *Eurasian J. Hepatogastroenterol.* **9**, 96–101 (2019).

12. Flanagan, W. M., Corthesy, B., Bram, R. J. & Crabtree, G. R. Nuclear association of a T-cell transcription factor blocked by FK-506 and cyclosporin A. *Nature* **352**, 803–807 (1991).
13. Sigal, N. H. & Dumont, F. J. Cyclosporin A, FK-506, and rapamycin: pharmacologic probes of lymphocyte signal transduction. *Annu. Rev. Immunol.* **10**, 519–560 (1992).
14. Collier, A. Y. et al. Immunogenicity of BA.5 bivalent mRNA vaccine boosters. *N. Engl. J. Med.* **388**, 565–567 (2023).
15. Scheaffer, S. M. et al. Bivalent SARS-CoV-2 mRNA vaccines increase breadth of neutralization and protect against the BA.5 Omicron variant in mice. *Nat. Med.* **29**, 247–257 (2023).
16. Fang, Z. et al. Bivalent mRNA vaccine booster induces robust antibody immunity against Omicron lineages BA.2, BA.2.12.1, BA.2.75 and BA.5. *Cell Discov.* **8**, 108 (2022).
17. Davis-Gardner, M. E. et al. Neutralization against BA.2.75.2, BQ.1.1, and XBB from mRNA Bivalent Booster. *N. Engl. J. Med.* **388**, 183–185 (2023).
18. Kurhade, C. et al. Low neutralization of SARS-CoV-2 Omicron BA.2.75.2, BQ.1.1 and XBB.1 by parental mRNA vaccine or a BA.5 bivalent booster. *Nat. Med.* **29**, 344–347 (2023).
19. Tarke, A. et al. SARS-CoV-2 vaccination induces immunological T cell memory able to cross-recognize variants from Alpha to Omicron. *Cell* **185**, 847–859.e811 (2022).
20. Nogimori, T. et al. Functional changes in cytotoxic CD8+ T-cell cross-reactivity against the SARS-CoV-2 Omicron variant after mRNA vaccination. *Front. Immunol.* **13**, 1081047 (2022).
21. Nogimori, T., Moriishi, E., Ikeda, M., Takahama, S. & Yamamoto, T. OMIP 075: A 22-color panel for the measurement of antigen-specific T-cell responses in human and nonhuman primates. *Cytometry A* **99**, 884–887 (2021).
22. Bergamaschi, L. et al. Longitudinal analysis reveals that delayed bystander CD8+ T cell activation and early immune pathology distinguish severe COVID-19 from mild disease. *Immunity* **54**, 1257–1275.e1258 (2021).
23. Tan, A. T. et al. Early induction of functional SARS-CoV-2-specific T cells associates with rapid viral clearance and mild disease in COVID-19 patients. *Cell Rep.* **34**, 108728 (2021).
24. Goel, R. R. et al. mRNA vaccines induce durable immune memory to SARS-CoV-2 and variants of concern. *Science* **374**, abm0829 (2021).
25. Wang, Q. et al. Antibody response to omicron BA.4-BA.5 bivalent booster. *N. Engl. J. Med.* **388**, 567–569 (2023).
26. Apostolidis, S. A. et al. Cellular and humoral immune responses following SARS-CoV-2 mRNA vaccination in patients with multiple sclerosis on anti-CD20 therapy. *Nat. Med.* **27**, 1990–2001 (2021).
27. Iketani, S. et al. Antibody evasion properties of SARS-CoV-2 Omicron sublineages. *Nature* **604**, 553–556 (2022).
28. Kung, L. & Halloran, P. F. Immunophilins may limit calcineurin inhibition by cyclosporine and tacrolimus at high drug concentrations. *Transplantation* **70**, 327–335 (2000).
29. Painter, M. M. et al. Rapid induction of antigen-specific CD4(+) T cells is associated with coordinated humoral and cellular immunity to SARS-CoV-2 mRNA vaccination. *Immunity* **54**, 2133–2142.e2133 (2021).
30. DiPiazza, A. T. et al. COVID-19 vaccine mRNA-1273 elicits a protective immune profile in mice that is not associated with vaccine-enhanced disease upon SARS-CoV-2 challenge. *Immunity* **54**, 1869–1882.e1866 (2021).
31. Ebenig, A. et al. Vaccine-associated enhanced respiratory pathology in COVID-19 hamsters after T(H)2-biased immunization. *Cell Rep.* **40**, 111214 (2022).
32. Jackson, L. A. et al. An mRNA Vaccine against SARS-CoV-2 - Preliminary Report. *N. Engl. J. Med.* **383**, 1920–1931 (2020).
33. Sahin, U. et al. BNT162b2 vaccine induces neutralizing antibodies and poly-specific T cells in humans. *Nature* **595**, 572–577 (2021).
34. van Panhuys, N., Klauschen, F. & Germain, R. N. T-cell-receptor-dependent signal intensity dominantly controls CD4(+) T cell polarization In Vivo. *Immunity* **41**, 63–74 (2014).
35. Tian, L. et al. Cytokine mRNA expression in tolerant heart allografts after immunosuppression with cyclosporine, sirolimus or brequinar. *Transpl. Immunol.* **5**, 189–198 (1997).
36. Blotta, M. H., DeKruyff, R. H. & Umetsu, D. T. Corticosteroids inhibit IL-12 production in human monocytes and enhance their capacity to induce IL-4 synthesis in CD4+ lymphocytes. *J. Immunol.* **158**, 5589–5595 (1997).
37. Habel, J. R. et al. Suboptimal SARS-CoV-2-specific CD8(+) T cell response associated with the prominent HLA-A*02:01 phenotype. *Proc. Natl. Acad. Sci. USA* **117**, 24384–24391 (2020).
38. Guerrera, G. et al. BNT162b2 vaccination induces durable SARS-CoV-2-specific T cells with a stem cell memory phenotype. *Sci. Immunol.* **6**, eabl5344 (2021).
39. Mateus, J. et al. Low-dose mRNA-1273 COVID-19 vaccine generates durable memory enhanced by cross-reactive T cells. *Science* **374**, eabj9853 (2021).
40. Ahmadi, P. et al. Defining the CD39/CD73 Axis in SARS-CoV-2 infection: The CD73(-) phenotype identifies polyfunctional cytotoxic lymphocytes. *Cells* **9**, 1750 (2020).
41. Reinscheid, M. et al. COVID-19 mRNA booster vaccine induces transient CD8+ T effector cell responses while conserving the memory pool for subsequent reactivation. *Nat. Commun.* **13**, 4631 (2022).

Acknowledgements

We thank all the members of the Laboratory of Precision Immunology, Center for Intractable Diseases and ImmunoGenomics, National Institutes of Biomedical Innovation, Health and Nutrition, Osaka, Japan, especially MSes. Yuki Katayama and Mami Ikeda for their excellent technical support. This study was supported by the Japan Agency for Medical Research and Development (grant numbers JP21nf0101627 and JP21fk0108493).

Author contributions

Conceptualization, T.Nogimori, Y.N., S.K., and T.Y.; investigation, T.Nogimori, Y.N., H.M., and Y.M.; data analysis, T.Nogimori, Y.N, H.A., S.T., S.K., and T.Y.; resources, Y.N., H.M., K.S., Y.Y., Y.T., T.Noda, Y.D., H.E., and S.K.; writing - original draft, T.Nogimori and T.Y.; Writing - review and editing, all authors; funding acquisition, T.Y.; supervision, T.Y.

Competing interests

K.S. and Y.Y. declare the following competing interests: the Research Foundation for Microbial Diseases of Osaka University. The other authors declare no competing interests.

Additional information

Supplementary information The online version contains supplementary material available at https://doi.org/10.1038/s43856-024-00448-4.

Correspondence and requests for materials should be addressed to Shogo Kobayashi or Takuya Yamamoto.

Peer review information *Communications Medicine* thanks Natalia Egri and Anand Kulkarni for their contribution to the peer review of this work. A peer review file is available.

Reprints and permissions information is available at http://www.nature.com/reprints

Publisher's note Springer Nature remains neutral with regard to jurisdictional claims in published maps and institutional affiliations.

Open Access This article is licensed under a Creative Commons Attribution 4.0 International License, which permits use, sharing, adaptation, distribution and reproduction in any medium or format, as long as you give appropriate credit to the original author(s) and the source, provide a link to the Creative Commons licence, and indicate if changes were made. The images or other third party material in this article are included in the article's Creative Commons licence, unless indicated otherwise in a credit line to the material. If material is not included in the article's Creative Commons licence and your intended use is not permitted by statutory regulation or exceeds the permitted use, you will need to obtain permission directly from the copyright holder. To view a copy of this licence, visit http://creativecommons.org/licenses/by/4.0/.

© The Author(s) 2024

MINIMALLY INVASIVE THERAPY & ALLIED TECHNOLOGIES
2024, VOL. 33, NO. 4, 245–251
https://doi.org/10.1080/13645706.2024.2328610

Taylor & Francis
Taylor & Francis Group

ORIGINAL ARTICLE

Check for updates

Application of a laparoscopic device for cell-derived sheet transplantation on the liver in a porcine model

Keisuke Toya[a], Yoshito Tomimaru[a], Shogo Kobayashi[a], Kiyokazu Nakajima[a,b], Akima Harada[c], Kazuki Sasaki[a], Yoshifumi Iwagami[a], Daisaku Yamada[a], Takehiro Noda[a], Hidenori Takahashi[a], Koichi Hayakawa[d], Isamu Matsuda[d], Takahiro Naka[d], Shigeru Miyagawa[c], Yuichiro Doki[a] and Hidetoshi Eguchi[a]

[a]Department of Gastroenterological Surgery, Graduate School of Medicine, Osaka University, Osaka, Japan; [b]Department of Next Generation Endoscopic Intervention (Project ENGINE), Graduate School of Medicine, Osaka University, Osaka, Japan; [c]Department of Cardiovascular Surgery, Graduate School of Medicine, Osaka University, Osaka, Japan; [d]Terumo Kabushiki Kaisha, Terumo Corporation, Tokyo, Japan

ABSTRACT

Background: Cell-derived sheets are of global interest for regenerative therapy. Transplanting a sheet for abdominal organs requires a device for laparoscopic delivery to minimize invasiveness. Here, using a porcine model, we aimed to confirm the feasibility of a device developed to deliver sheets to the thoracic cavity in a laparoscopic transplantation procedure.

Material and methods: We used the device to transplant human skeletal myoblast cell sheets onto the liver and measured extra-corporeal, intra-abdominal, and total procedure times for sheet transplantation. Tissues, including the liver and the sheet, were collected two days after transplantation and analyzed histologically.

Results: In all experiments ($n = 27$), all sheets were successfully placed at target locations. The mean (± standard deviation) extra-corporeal, intra-abdominal, and total procedure times were 44 ± 29, 33 ± 12, and 77 ± 36 s, respectively. We found no difference between the two surgeons in procedure times. Histological analyses showed no liver damage with the transplantation and that sheets were transplanted closely onto the liver tissue without gaps.

Conclusion: We confirmed the feasibility of a simple universal device to transplant cell-derived sheets *via* laparoscopic surgery. This device could support a minimally invasive procedure for sheet transplantation.

ARTICLE HISTORY
Received 18 December 2023
Accepted 13 February 2024

KEYWORDS
Sheet transplantation; device; laparoscopic surgery

Introduction

Regenerative therapy using cells derived from various sources is of global interest. Intravenous injection and local injection are among several methods of cell delivery [1–4]. Compared with these methods, the so-called 'sheet technology' has some advantages linked to improved therapeutic effects, such as the large number of deliverable cells and their persistence at the therapeutic target [5]. For example, sheet technology has been used to treat heart failure and to prevent perforation after duodenal endoscopic submucosal dissection [6–9].

Laparoscopic or endoscopic approaches have been considered preferable to minimize the invasiveness of sheet delivery. This preference has led to the development of endoscopic esophageal and epicardial devices [10,11]. Although a device for laparoscopic procedures in the abdominal cavity has been described [12], the carrier, made of medical-grade silicon and nylon mesh, must be pinched and rolled up using conventional laparoscopic forceps. This requirement means that sheet size and surgeon skill may be factors affecting the difficulty of the procedure. To simplify delivery and make it more reproducible, new devices are needed that can be integrated with laparoscopic forceps.

We previously reported the efficacy of skeletal myoblast cell sheet transplantation for liver regeneration in cases of liver failure [13]. However, no easy, suitable device is available for achieving a transplant on the liver using a laparoscopic approach. Thus, we sought to determine whether a novel device developed

CONTACT Shogo Kobayashi s-kobayashi@umin.ac.jp Department of Gastroenterological Surgery, Graduate School of Medicine, Osaka University, 2-2-E2, Yamadaoka, Suita, Osaka 565-0871, Japan

Supplemental data for this article can be accessed online at https://doi.org/10.1080/13645706.2024.2328610.

© 2024 Society of Medical Innovation and Technology

for cell sheet transplantation in the thoracic cavity for heart failure could be applied for laparoscopic intra-abdominal sheet transplantation onto the liver. Here, we investigated the feasibility of this device for laparoscopic transplantation of the cell sheet on the liver in a porcine model.

Material and methods

Device for laparoscopic transplantation

The design of the new device is shown in Figure 1. The device consisted of an outer frame, an inner frame, and a carrier for sheet delivery. The diameter of the outer frame (Figure 1A) ranged from 10.3 to 10.7 mm to ensure passage through a 12-mm trocar, and the inner frame diameter was 6.5 mm. The carrier (Figure 1B) consisted of two parts: a large carrier made of polyethylene terephthalate and designed to deliver sheets up to 45 mm in diameter, and a small brown carrier, consisting of a plastic film 50 µm thick for placing the sheet on the liver surface atraumatically. Figure 1C demonstrates the movement of the carriers when the device stores the sheet, and Figure 2 illustrates how to use the device. In the extracorporeal procedure (Figure 2A), the sheet was placed onto both the small and large carriers and introduced into the outer frame by pulling of the inner frame. In the intra-abdominal procedure (Figure 2B), the sheet was transplanted onto the target organ by pushing of the inner frame and the small carrier.

Preparation of skeletal myoblast cell sheets

Human skeletal myoblast cells were used in this study. Cells were surplus specimens from other clinical trials, harvested from the vastus medialis muscle of patients with heart failure. The cell sheets were prepared as described previously [14]. Cells were collected and cultured at 37°C for one day on temperature-responsive culture dishes (UpCell; CellSeed, Tokyo, Japan) at a density of 1.0×10^6 cells/cm^2, and the cell sheets were detached from the dishes at room

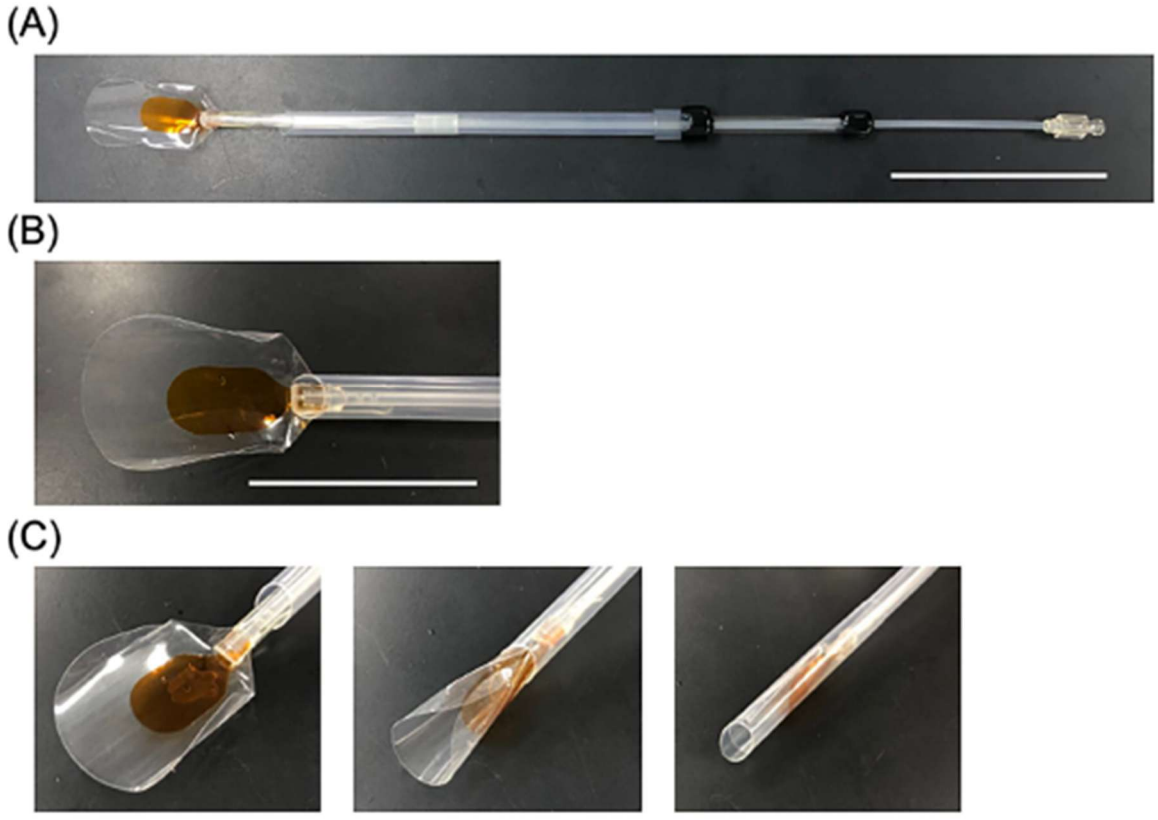

Figure 1. Design of the novel device used in transplanting the cell-derived sheet in a laparoscopic procedure. (A) Overall view of the device. Scale bar = 10 cm. (B) The distinctive tip of the device. The device comprises a small brown carrier and a large colorless carrier. Scale bar = 5 cm. (C) The movement of both the small and large carriers to store the sheet. Left, the condition with the sheet placed onto the carrier. Middle, both carriers have been gradually pulled into the inner frame and curled up. Right, the sheet fully encapsulated in the inner frame.

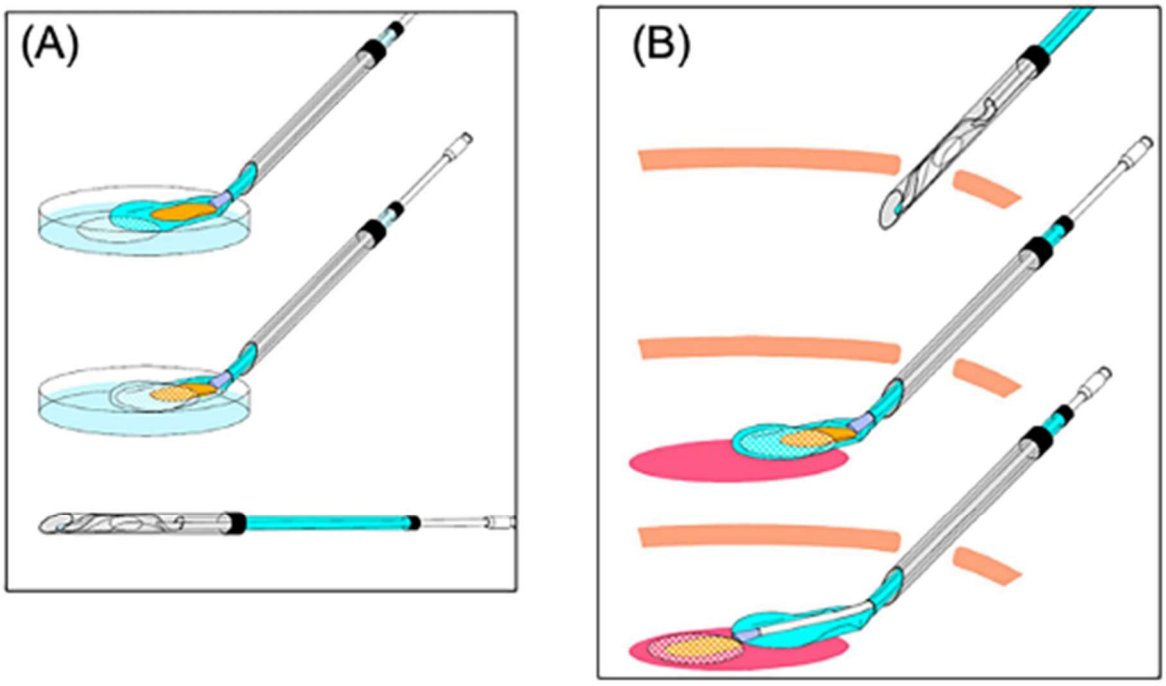

Figure 2. Illustration of the procedure using the new device for sheet transplantation. (A) The procedure outside the body. A sheet is placed on the carrier in a dish and retracted by pulling the inner frame. (B) The procedure inside the body. The device is passed through a 12-mm trocar. First, the inner frame is pressed to unfold the sheet, and then the small brown carrier is pressed to transplant the sheet onto the liver surface.

temperature (20–25°C). For animal experiments, cell sheets were produced at a density of 6.0×10^7 cells/sheet. The sheets were round, with a diameter of approximately 4 cm.

Animal experiments

All procedures were conducted in three-month-old female pigs (average weight = 35 kg) in a standard manner, with animals under general anesthesia and intubation. A 12-mm periumbilical trocar was placed for the laparoscope, and another 12-mm trocar was placed in the left upper quadrant for sheet transplantation. A 5-mm trocar was placed in the right lower quadrant for support.

Surgical procedure for sheet transplantation

Before sheet transplantation into the abdominal cavity, fibrin glue (Beriplast, CSL Behring, Tokyo, Japan) was sprayed onto the surface of the cell sheet using a dedicated spraying kit (Beriplast P Combi kit, CSL Behring, Tokyo, Japan) to strengthen the sheet. The sheet was then placed on the device and advanced into the abdominal cavity through a 12-mm trocar. Next, the sheet was transplanted at the target location on the liver surface using the device and conventional laparoscopic forceps through the other trocar. No liver mobilization was needed for the sheet transplantation. After transplantation, the liver surface, including the sheet, was covered by Beriplast to prevent exfoliation of the sheets from the liver. After confirmation that the sheets were fixed, the laparoscopic ports were sutured and the surgical procedure finished. Two surgeons performed 27 sheet transplantations in a total of four pigs, with the time frame measured from placing the sheet on the carrier to transplantation onto the liver surface.

Histological analysis

The pigs were sacrificed by injection of pentobarbital sodium (50 mg/kg) and potassium chloride (20 milliequivalent) two days after sheet transplantation. Tissues were collected and fixed with 4% paraformaldehyde–phosphate-buffered saline for paraffin embedding before being cut into 5-μm sections using a microtome. The paraffin-embedded sections were stained with hematoxylin and eosin (H&E) and visualized under standard light microscopy. To confirm the presence of the myoblast cell sheet immunohistochemically, sections were labeled with

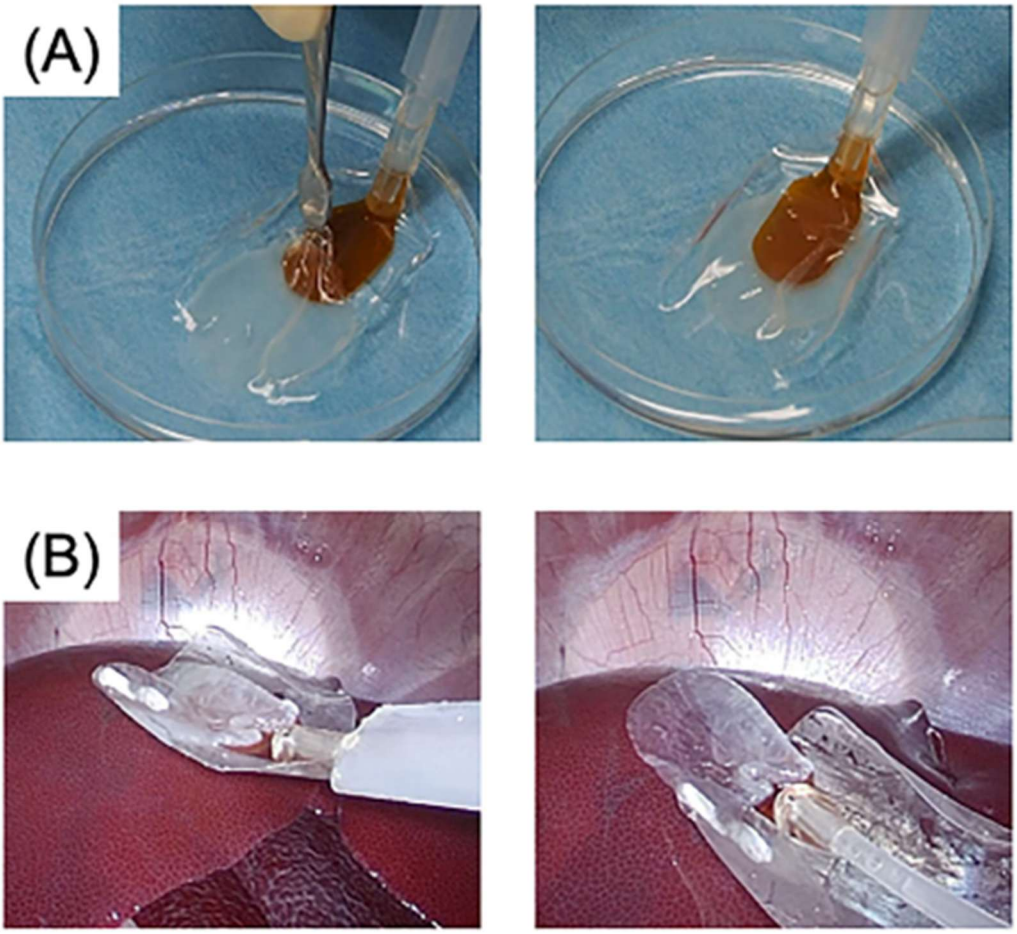

Figure 3. Surgical procedure using the new device in pigs. (A) A sheet was placed on the small brown carrier and retracted by pulling the inner frame. (B) The device was passed through a 12-mm laparoscopic trocar and the sheet transplanted onto the target by pushing the inner frame and the small carrier.

monoclonal antibodies against desmin (Abcam, Cambridge, UK) and visualized using the LSAB™ kit (DAKO, Glostrup, Denmark) and an automated immune-staining system based on the labeled streptavidin/biotinylated antibody method.

Ethical statement

The use of human skeletal myoblast cells was approved by the Human Ethics Review Committee of the Graduate School of Medicine, Osaka University (approval number 21389). The entire protocol of the animal experiment was approved by the Institutional Animal Care and Use Committee Guidelines of Osaka University (approval number 03-030-001).

Results

The overall procedure is shown in Figure 3, and a video of the procedure is included as Supplemental File 1. The myoblast cell sheet was successfully placed on the carrier of the device without any damage. Passage of the device through the laparoscopic port and exit of the carrier from the device proceeded smoothly. As noted, the procedure was performed 27 times, and all sheets were transplanted successfully while retaining their original shape without damage. The mean times (± standard deviation) of the extracorporeal, intra-abdominal, and total procedures were 44 ± 29, 33 ± 12, and 77 ± 36 s, respectively. The times each surgeon took for each of these procedure periods were 54 ± 37, 36 ± 12, and 90 ± 44 s, respectively, and 39 ± 24, 31 ± 12, and 70 ± 30 s, respectively. These durations did not differ between surgeons (extra-corporeal procedure, $p = 0.2260$; intra-abdominal procedure, $p = 0.3061$; and total procedure, $p = 0.1841$).

The H&E staining and immunohistochemical staining for desmin are shown in Figure 4. These images demonstrate that the sheet remained viable on the

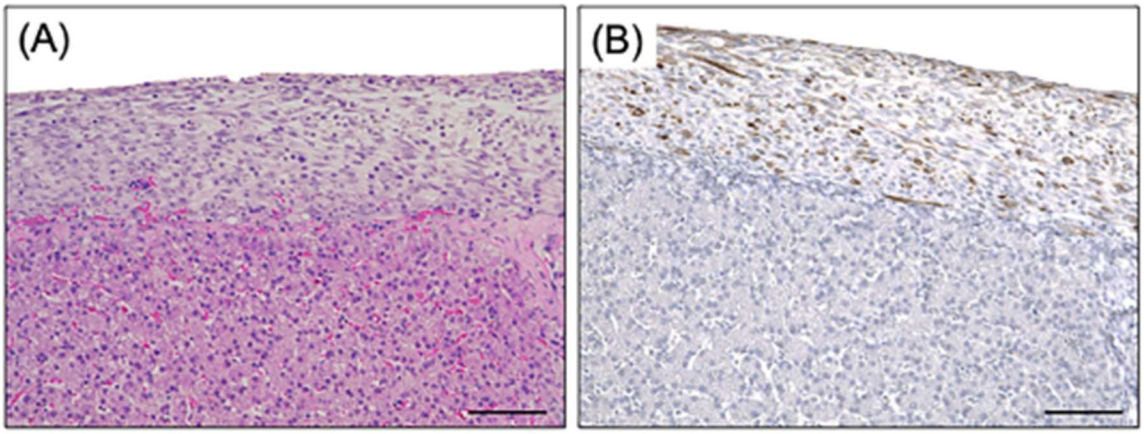

Figure 4. Histopathology of the transplanted cell sheet in the liver. (A) H&E staining and (B) immunohistochemical staining of desmin two days after sheet transplantation, confirming that the sheet was transplanted onto the liver without any gaps or tissue damage. Scale bar = 100 μm.

surface of the liver tissue. No liver damage from sheet transplantation was observed, and the sheet was transplanted closely onto the liver tissue without gaps.

Discussion

We show that a new device developed to deliver a cell-derived sheet to the thoracic cavity for heart failure is feasible for laparoscopic transplantation of a cell-derived sheet onto the liver. In the past decade, regenerative therapies using sheet technology have been developed in various fields. Many benign and malignant diseases have been treated by minimally invasive surgery, so it is clinically worthwhile to develop devices to transplant cell sheets as non-invasively as possible [15–18]. Based on this concept, several devices for minimally invasive transplantation have been reported. Osada et al. described a novel device for endoscopic cell sheet transplantation using a three-dimensional printed simulator [11]. Their device was developed for cardiovascular surgery but could be applied for other procedures. There were some issues to resolve, such as difficulty distinguishing the side attached on the nylon mesh and no validation of utility *in vivo*. The device also needed a trocar >12 mm because it consisted of an outer steel frame that was 18 mm in diameter. Yamaguchi et al. demonstrated a highly feasible procedure for laparoscopic transplantation [12]. Their study illustrated application of the method for several sites in the abdominal cavity, including liver, stomach, colon, and small intestine. The procedure required several steps for sheet transplantation, implying complexity in the use of the device.

In contrast, our device was designed to be simple and easily handled. The integrated design could allow the same procedure to be repeated by anybody without any special tips and could make the sheet transplantation as targeted as possible. Furthermore, improving the structure and material of the small carrier could avoid damage to and deformation of the sheet. Maintaining the sheet structure is important, as its compromise could weaken its effectiveness. The data collected using the device in this study suggest simplicity and certainty in transplanting the sheet *via* laparoscopic surgery. Although we did not compare the data to results with previously reported devices, the advantages suggested by the data seem to be important when considering the clinical applications of the device.

Some issues remain to be resolved. First, we used the device to transplant the sheet only onto the liver surface. We did not have trouble transplanting any section of the liver, such as the cranial and caudal portions, and although we assume it could be applicable to other abdominal organs, we did not validate this assumption. This point should be kept in mind when considering use of the device for transplantation of cell sheets onto other organs. Second, because of the difficulty in preparing a porcine model with liver cirrhosis, we could not examine transplantation onto the cirrhotic liver, which has a rough surface. There may be some difference between transplantation onto rough versus smooth liver. Third, this device required a 12-mm periumbilical trocar to move the sheet into the abdominal cavity. The incision site for a 12-mm trocar should be sutured by fascia to avoid an incisional hernia. If we make the device smaller so that it fits a 5-mm trocar, which is possible, the size of the

sheet would be limited to ensure the original shape. Although there is not much difference to surgeons between suturing the incision site for a 12-mm trocar versus a 5-mm trocar, the structure of this device would need to be radically changed to fit a 5-mm trocar without changes to the sheet. In terms of size, further assessment is warranted. Finally, a limitation of the study was the short observation period after sheet transplantation (two days). Because we used a xenogeneic cell–derived sheet that would likely activate the immune response, our observation period had to be short. Longer observation would be possible without immune rejection by using a syngeneic model, and a pig cell–derived sheet may be suitable for longer observation. However, our priority was to confirm the usefulness of the device with human cell–derived sheets with a view to clinical application, requiring us to use a xenogeneic cell–derived sheet in this study. In this regard, the finding of no device-inducing complications after the transplantation should be viewed with caution given the short-term observation period. More studies are needed to monitor for complications in the long term and to confirm proof of function for sheet transplantation by the device.

In conclusion, we confirmed the feasibility and usefulness of a simple universal device to laparoscopically transplant cell sheets onto the liver. Therapy with cell sheet technology is expected to be further developed, and this device could be useful in minimally invasive procedures for sheet transplantation.

Acknowledgments

The authors thank all of the doctors and participants in the study.

Disclosure statement

Shogo Kobayashi received honoraria and speaker fees from AstraZeneca, Ethicon Inc., Intuitive, Olympus, and Taiho Pharmaceutical.

Funding

Keisuke Toya, Yoshito Yomimaru, Shogo Kobayashi, Kazuki Sasaki, Yoshifumi Iwagami, Daisaku Yamada, Takehiro Noda, Hidenori Takahashi, Yuichiro Doki, and Hidetoshi Eguchi received funding support for cooperative research from Terumo Corporation. Koichi Hayakawa, Isamu Matsuda, and Takahiro Naka are employees of Terumo Corporation.

ORCID

Kiyokazu Nakajima http://orcid.org/0000-0001-8635-7585

Data availability statement

The data used in this study are available from the corresponding authors on reasonable request.

References

[1] Tsuchiya A, Takeuchi S, Watanabe T, et al. Mesenchymal stem cell therapies for liver cirrhosis: MSCs as "conducting cells" for improvement of liver fibrosis and regeneration. Inflamm Regen. 2019;39:18.

[2] Kinney SM, Ortaleza K, Vlahos AE, et al. Degradable methacrylic acid-based synthetic hydrogel for subcutaneous islet transplantation. Biomaterials. 2022;281:121342. doi:10.1016/j.biomaterials.2021.121342.

[3] Miyake K, Miyagawa S, Harada A, et al. Engineered clustered myoblast cell injection augments angiogenesis and muscle regeneration in peripheral artery disease. Mol Ther. 2022;30(3):1239–1251. doi:10.1016/j.ymthe.2022.01.008.

[4] Terai S, Ishikawa T, Omori K, et al. Improved liver function in patients with liver cirrhosis after autologous bone marrow cell infusion therapy. Stem Cells. 2006;24(10):2292–2298. doi:10.1634/stemcells.2005-0542.

[5] Matsuura K, Utoh R, Nagase K, et al. Cell sheet approach for tissue engineering and regenerative medicine. J Control Release. 2014;190:228–239. doi:10.1016/j.jconrel.2014.05.024.

[6] Kainuma S, Miyagawa S, Toda K, et al. Long-term outcomes of autologous skeletal myoblast cell-sheet transplantation for end-stage ischemic cardiomyopathy. Mol Ther. 2021;29(4):1425–1438. doi:10.1016/j.ymthe.2021.01.004.

[7] Matsumoto R, Kanetaka K, Maruya Y, et al. The efficacy of autologous myoblast sheet transplantation to prevent perforation after duodenal endoscopic submucosal dissection in porcine model. Cell Transplant. 2020;29:963689720963882. doi:10.1177/0963689720963882.

[8] Amemiya T, Nakamura T, Yamamoto T, et al. Autologous transplantation of oral mucosal epithelial cell sheets cultured on an amniotic membrane substrate for intraoral mucosal defects. PLoS One. 2015;10(4):e0125391. doi:10.1371/journal.pone.0125391.

[9] Tanaka S, Kanetaka K, Fujii M, et al. Cell sheet technology for the regeneration of gastrointestinal tissue using a novel gastric perforation rat model. Surg Today. 2017;47(1):114–121. doi:10.1007/s00595-016-1360-2.

[10] Maeda M, Kanai N, Kobayashi S, et al. Endoscopic cell sheet transplantation device developed by using a 3-dimensional printer and its feasibility evaluation in a porcine model. Gastrointest Endosc. 2015;82(1):147–152. doi:10.1016/j.gie.2015.01.062.

[11] Osada H, Ho WJ, Yamashita H, et al. Novel device prototyping for endoscopic cell sheet transplantation using a three-dimensional printed simulator. Regen Ther. 2020;15:258–264. doi:10.1016/j.reth.2020.10.007.

[12] Yamaguchi S, Kanetaka K, Maruya Y, et al. Highly feasible procedure for laparoscopic transplantation of cell sheets under pneumoperitoneum in porcine

model. Surg Endosc. 2022;36(6):3911–3919. doi:10.1007/s00464-021-08708-3.

[13] Toya K, Tomimaru Y, Kobayashi S, et al. Efficacy of autologous skeletal myoblast cell sheet transplantation for liver regeneration in liver failure. Transplantation. 2023;107(8):e190–e200. doi:10.1097/TP.0000000000004567.

[14] Miyagawa S, Domae K, Kainuma S, et al. Long-term outcome of a dilated cardiomyopathy patient after mitral valve surgery combined with tissue-engineered myoblast sheets-report of a case. Surg Case Rep. 2018;4(1):142. doi:10.1186/s40792-018-0549-6.

[15] Jusoh AC, Ammori BJ. Laparoscopic versus open distal pancreatectomy: a systematic review of comparative studies. Surg Endosc. 2012;26(4):904–913. doi:10.1007/s00464-011-2016-3.

[16] Cai XJ, Yang J, Yu H, et al. Clinical study of laparoscopic versus open hepatectomy for malignant liver tumors. Surg Endosc. 2008;22(11):2350–2356. doi:10.1007/s00464-008-9789-z.

[17] Fretland ÅA, Dagenborg VJ, Bjørnelv GMW, et al. Laparoscopic versus open resection for colorectal liver metastases: the Oslo-COMET randomized controlled trial. Ann Surg. 2018;267(2):199–207. doi:10.1097/SLA.0000000000002353.

[18] Kabir T, Tan ZZ, Syn NL, et al. Laparoscopic versus open resection of hepatocellular carcinoma in patients with cirrhosis: meta-analysis. Br J Surg. 2021;109(1):21–29. doi:10.1093/bjs/znab376.

Caser Report: A Rare Case of Pulmonary Nocardiosis Caused by *Nocardia pseudobrasiliensis* After Liver Transplantation

Daiki Hokkoku, Kazuki Sasaki, Shogo Kobayashi*, Yoshifumi Iwagami, Daisaku Yamada, Yoshito Tomimaru, Takehiro Noda, Hidenori Takahashi, Yuichiro Doki, and Hidetoshi Eguchi

Department of Gastroenterological Surgery, Graduate School of Medicine, Osaka University, Osaka, Japan

ABSTRACT

Nocardia is a gram-positive bacillus with the microscopic appearance of branching hyphae and is mainly distributed in the soil. Nocardiosis more frequently occurs in immunosuppressed patients. Since nocardiosis has a high mortality rate, immediate diagnosis and treatment are needed. We report the first case of pulmonary nocardiosis caused by *Nocardia pseudobrasiliensis* after liver transplantation. A 58-year-old woman underwent living-donor transplantation for primary biliary cholangitis. Seven months after transplantation, she came to our hospital complaining of fever and anorexia. Computed tomography of the lungs showed a 45 mm large nodule affecting the upper lobe of the left lung. We started administering empiric antibiotics and tapering immunosuppression, but the patient's condition gradually worsened, and lung lesions increased. On the fifth day after hospitalization, bacteria developed from sputum cultures were identified as *N. pseudobrasiliensis* by matrix-assisted laser desorption ionization time of flight mass spectrometry. We started treatment with trimethoprim-sulfamethoxazole. The patient's clinical symptoms and laboratory data improved quickly. After one month of hospitalization, this patient was discharged. Then, the lung lesion almost vanished. Ten years after her transplant, the patient is alive with a well-functioning graft.

PNEUMONIA, one of the most frequent diseases after organ transplantation, occurs in 35% to 50% of recipients after liver transplantation (LT) [1]. Pneumonia caused by bacterial infections is the most common, but because LT recipients take immunosuppressive drugs, cases of pneumonia caused by relatively rare bacteria, such as *Nocardia*, can occur.

Nocardia is a gram-positive bacillus. On microscopy, it is characterized by branching hyphae and is mainly distributed in the soil. The species of the family Nocardiaceae form a homogeneous cluster within the Corynebacteriaceae of the Actinomycetes. Currently, the generally accepted definition of *Nocardia* is based primarily on molecular phylogenetic information, especially derived from 16S rRNA gene sequences [2]. More than 50 species of the genus *Nocardia* have been segregated, and approximately half have been recognized as human and animal pathogens [3]. *Nocardia* can disseminate hematogenously and cause abscesses in the lungs, liver, and central nervous system. Moreover, it was reported that the immune response mediated by T lymphocytes plays an essential role in preventing *Nocardia* infection [4]. Thus, patients with cancer-bearing tumors or those taking immunosuppressive drugs after organ transplantation are prone to developing infections with this *Nocardia* spp. In addition, LT recipients have been noted to have a higher rate of disseminated disease [5].

We report a case of pulmonary nocardiosis caused by a rare species, *Nocardia pseudobrasiliensis*, and summarize the case reports in the relevant literature.

Present address: Department of Gastroenterological Surgery, Graduate School of Medicine, Osaka University, 2-2-E2, Yamadaoka, Suita, Osaka, 565-0871, Japan, Telephone number: +81-6-6879-3251, Fax number: +81-6-6879-3259.

This research did not receive any specific grant from funding agencies in the public, commercial, or not-for-profit sectors.

*Address correspondence to Shogo Kobayashi, FACS, Department of Gastroenterological Surgery, Graduate School of Medicine, Osaka University, 2-2 Yamadaoka E-2, Suita, Osaka, 565-0871, Japan. E-mail: s-kobayashi@umin.ac.jp

0041-1345/20
https://doi.org/10.1016/j.transproceed.2024.05.006

© 2024 Elsevier Inc. All rights are reserved, including those for text and data mining, AI training, and similar technologies.
230 Park Avenue, New York, NY 10169

CASE PRESENTATION

A 58-year-old woman underwent living-donor LT for primary biliary cholangitis in our hospital. During hospitalization, the patient experienced an episode of acute cellular rejection on the seventh day after LT. After steroid pulse therapy, she was discharged with maintenance immunosuppression, consisting of prednisolone (7.5 mg), mycophenolate mofetil (500 mg), and tacrolimus (2.0 mg) on the 98th day after LT.

Seven months later, she presented to our hospital with complaints of fever and anorexia. On admission, the patient was breathing efficiently, with a pulse of 115 beats/min, blood pressure of 105/77 mmHg, body temperature of 38.4°C, a respiratory rate of 12 breaths/minute, and an oxygen saturation level of >95%. Laboratory results showed leukocytosis ($18.6 \times 10^3/\mu L$), an elevated C-reactive protein (CRP) of 4.82 mg/dL. She also showed an extremely high tacrolimus concentration (25.7 ng/mL) and HbA1c value (11.6%). Chest radiography and computed tomography (CT) of the lung showed a large nodule of 45 mm in size in the upper lobe of her left lung (Fig 1A). At this point, bacterial pneumonia was raised from these examinations, and she was treated with a carbapenem antibiotic (500 mg, 3 times a day, IV) together with the tapering of prednisolone (5.0 mg), mycophenolate mofetil (250 mg), and tacrolimus (1.0 mg).

Figure 2 shows the clinical course after hospitalization. Despite these treatments, the patient required oxygen administration, her body temperature increased to 38.7°C, and her CRP level was elevated at 5.50 mg/dL. The same lung lesion grew progressively by 75 mm on the fifth day after hospitalization (Fig 1B). At this time, sputum culture revealed *N. pseudobrasiliensis*, a gram-positive bacillus with branching hyphae (Fig 1C). CT ruled out disseminated disease, since *Nocardia* may cause these diseases in the liver and brain.

After this result, we started treatment with trimethoprim-sulfamethoxazole (TMP-SMX) (960 mg, twice daily, IV) according to the drug sensitivity test of *N. pseudobrasiliensis*. Thereafter, the patient's clinical symptoms and laboratory data improved quickly, and we could switch to oral TMP-SMX (4 g, twice a day). After one month of hospitalization, the patient was discharged. She continued to take oral medicine 6 months after discharge. Finally, the lung lesion almost vanished (Fig 1D). At 10 years after her transplant, she is alive with a good graft function.

DISCUSSION

Pneumonia after LT occurs in 8% to 23% of patients and contributes greatly to the prognosis when it occurs. The organisms that

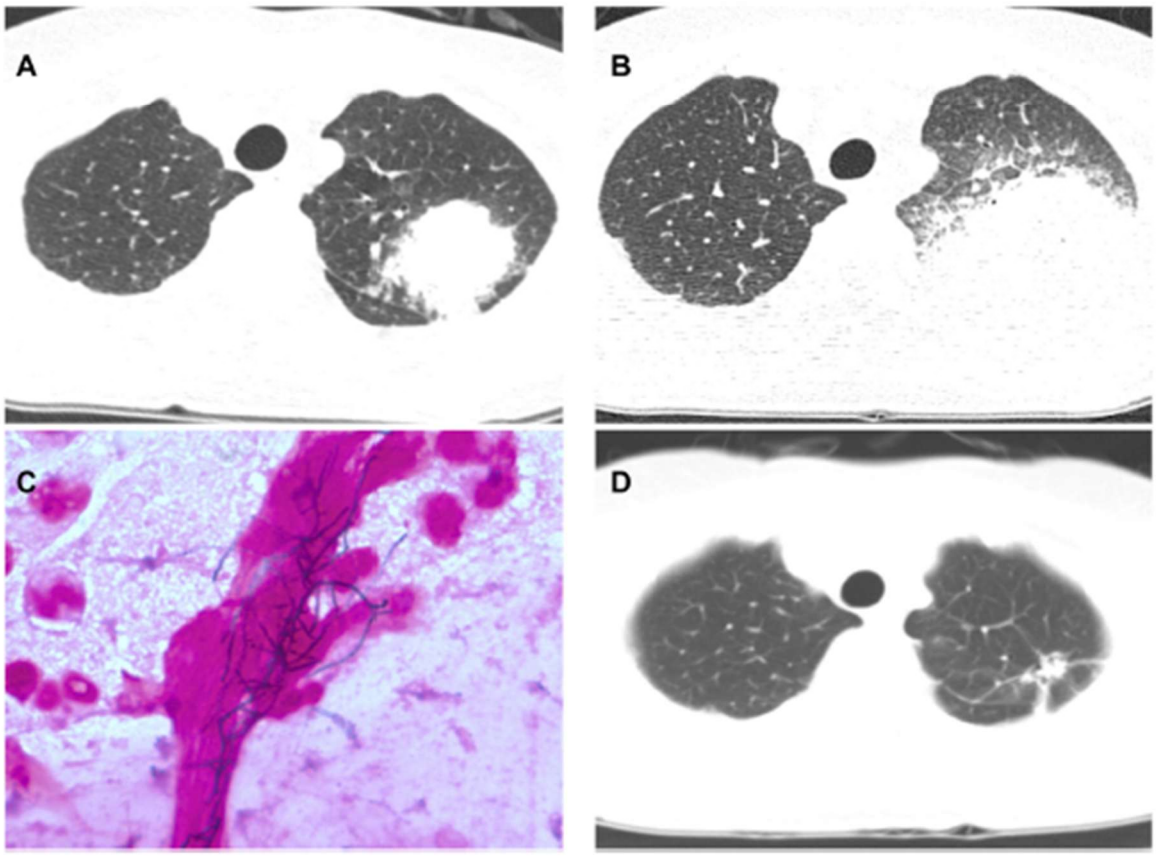

Fig 1. CT findings and microbiological examination. (A) Chest CT demonstrated a 45 mm nodule in the left upper lobe on admission. (B) The lung lesion worsened on the fifth day after hospitalization. (C) The sputum culture test revealed *N. pseudobrasiliensis*, a gram-positive rod with a branching filament. (D) The pulmonary lesion disappeared in the 6 months after admission. CT, computed tomography.

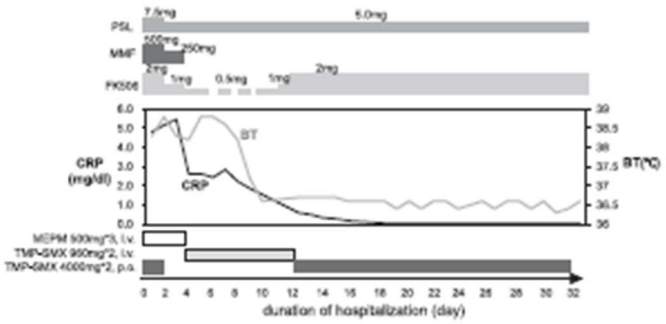

Fig 2. Clinical course after hospitalization. BT, body temperature; CRP, C-reactive protein; FK506, tacrolimus; MEPM, meropenem; MMF, mycophenolate mofetil; PSL, prednisolone; TMP-SMX, trimethoprim-sulfamethoxazole.

most commonly cause pneumonia are bacteria; among them, gram-negative bacteria account for more cases than gram-positive bacteria. This is followed by fungi, viruses, and protozoa. *Nocardia* spp. is a gram-positive bacterium that grows aerobically and more frequently in patients with malignant tumors, diabetes mellitus, and healthy people undergoing immunosuppressor treatment. Pulmonary nocardiosis is the most common clinical presentation of infection because inhalation is the primary route of bacterial exposure. Extrapulmonary nocardiosis is relatively common and can occur through hematogenous dissemination or a contiguous spread of necrotizing pneumonitis into the pleura, pericardium, mediastinum, and vena cava. Among these sites, the central nervous system (CNS) is the most common extrapulmonary location for nocardiosis. Nocardiosis is reported to occur in 3.7% of patients 3 to 5 years after LT, and the risk of developing this infection is considered relatively high [5].

Pulmonary nocardiosis may cause shortness of breath, dry cough, hemoptysis, fever, weight loss, and asthenia. A definitive diagnosis of this disease is made when *Nocardia* is detected on culture, but frequent culture tests are necessary because it may not be detected on the first culture [5]. TMP/SMX has functioned as first-line therapy for more than 60 years. Mortality is as high as 50% with TMP-SMX monotherapy. Drug resistance to some species, including *N. farcinica*, is the main cause, especially in disseminated infections and CNS invasion [6]. In recent years, linezolid has gained increased attention as a primary therapy for *Nocardia* infection because of the emergence of drug-resistant species [7].

Twenty-four cases of pulmonary nocardiosis that developed after LT were summarized, including our case [5,7–22]. The median age was 56.6 years (30-84) and 66.7% were male. The most common organisms were *N. asteroides* and *N. farcinia* (5 cases each). The most common sites of involvement were the lung (15 cases), skin (11 cases), central nervous system (6 cases), thyroid gland (2 cases), liver, testes, teeth, and liver (1 case each). Of these patients, 45.8% had disseminated lesions in multiple organs. The mortality rate was 20.8%. These included cases in which it took time to detect *Nocardia* from culture studies. Interestingly, 83.3% of patients developed nocardiosis within only one year after LT. This may be due to poorly controlled blood levels of immunosuppressive drugs immediately after surgery.

To our knowledge, this is the first case of *N. pseudobrasiliensis* causing pulmonary nocardiosis after LT. *N. pseudobrasiliensis* is a newly described species previously thought to belong to the species *N. brasiliensis*. *N. pseudobrasiliensis* was identified in 1996 because it differs from *N. brasiliensis* in mycolic acid pattern, adenine degradation, nitrate reduction, and antimicrobial susceptibility [23]. Only 2 strains have been isolated in Japan thus far. In this case, we identified *N. pseudobrasiliensis* by bacterial identification using matrix-assisted laser desorption ionization time of flight mass spectrometry (MALDI-TOF MS). MALDI-TOF MS is a method of analyzing bacterial proteins by applying a laser beam to the ionized sample and applying a voltage to the ionized sample. The sample is ionized by irradiating the bacterial protein with a laser beam and then passed through a vacuum tube with a voltage applied to measure the mass of the target by the difference in time of flight. Bacteria can be identified by matching the mass spectrum obtained from the time and detection intensity with a database [24].

We summarized the cases of nocardiosis caused by this species in the relevant literature (Table 1) [25–30]. Most patients

Table 1. Clinical Characteristics of Patients with Nocardiosis Caused by *N. pseudobrasiliensis*

Case Number	Author	Age (years)	Sex	Co-morbid Condition	Location of Infection	Treatment	Outcome
1	Brown BA. et al.	33	M	AIDS	Lung	TMP-SMX+AMK	Death
2	Kageyama A. et al.	71	M	Esophageal and stomach cancer	Lung	No data	No data
3	Lebeaux D. et al.	55	M	Multiple myeloma	Lung	TMP-SMX	Death
4	Seol CA. et al.	57	F	MPA	Disseminated mycetoma	SBT/ABPC	Survived
5	Veerappan Kandasamy V. et al.	79	M	Myasthenia gravis	Multiple leg abscess	LZD	Survived
6	Makadia S. et al.	67	F	None	Skin	TMP-SMX	Survived
7	Our case	58	F	LDLT for PBC	Lung	TMP-SMX	Survived

AIDS, acquired immunodeficiency syndrome; AMK, amikacin sulfate; LDLT, living donor liver transplantation; LZD, linezolid; MPA, microscopic polyangiitis; PBC, primary biliary cholangitis; SBT/ABPC, sulbactam/ampicillin; TMP-SMX, trimethoprim-sulfamethoxazole.

Table 2. Drug Sensitivity Test of *N. pseudobrasiliensis*

Antibiotics	Our Case	Case 1	Case 3	Case 4	Case 5
Ceftriaxone	<8 (S)	<32 (S)		8 (S)	>64 (R)
Cefotaxime		<32 (S)			
Ciprofloxacin		<0.5 (S)	0.125 (S)	<0.12 (S)	0.5 (S)
Moxifloxacin				<0.25 (S)	<0.25 (S)
Cefepime	<8 (S)			16 (S)	>32 (R)
Imipenem	>8 (R)		>32 (R)	64 (R)	64 (R)
Amoxicillin-clavulanate	<8 (S)	>8/2 (R)	2 (S)	32/16 (R)	32/16 (R)
Gentamicin	4 (S)				
Amikacin	<4 (S)	4-16 (S)		4 (S)	16 (R)
Doxycycline				16 (R)	16 (R)
Clarithromycin	<16 (S)	<0.5 (S)	0.125 (S)	0.25 (S)	0.5 (S)
Minocycline	>8 (R)	>8 (MS-R)		>8 (R)	8 (R)
TMP-SMX	<2 (S)	<32 (S)		8/152 (R)	4/76 (R)
Linezolid	<2 (S)			<1.0 (S)	<1.0 (S)

MIC, minimum inhibitory concentration; MS, moderately susceptible; R, resistant; S, susceptible; TMP-SMX, trimethoprim-sulfamethoxazole.

were immunosuppressed and 6/7 (85.7%) had pulmonary involvement, and mortality was high at 33.3%. The results of drug sensitivity testing in these cases were summarized (Table 2). Although TMP-SMX is considered the standard treatment for nocardiosis, resistant strains have been observed in *N. pseudobrasiliensis* and early antimicrobial switching based on susceptibility testing is recommended in cases that do not respond to treatment [27,29]. In our patient's case, unstable blood levels of immunosuppressive drugs in the early postoperative period and poorly controlled diabetes may have contributed to his susceptibility to infection. Furthermore, the patient's gardening hobby may have facilitated exposure to *Nocardia* spp. Fortunately, in this patient's case, the organism could be identified from the initial sputum culture, and appropriate treatment could be given. In the case of a patient in an immunosuppressed state after transplantation therapy, it may be difficult to identify the causative organism with a single culture test, and multiple surveillance should be performed while monitoring the patient's general condition. Pulmonary nocardiosis is most likely to occur within the first year after LT. Due to the high mortality rate, it is important to include it in the differential diagnosis.

DECLARATION OF COMPETING INTEREST

The authors declare that they have no known competing financial interests or personal relationships that could have appeared to influence the work reported in this paper.

AUTHOR CONTRIBUTIONS

D.H. and S.K. substantially contributed to the study conceptualization. D.H. substantially contributed to the manuscript drafting. All authors critically reviewed and revised the manuscript draft and approved the final version for submission.

DATA AVAILABILITY

The datasets generated and/or analyzed during the current study are available from the corresponding author on reasonable request.

INFORMED CONSENT

Informed consent was obtained from the patient.

ACKNOWLEDGMENTS

All listed authors have made a significant scientific contribution to the research in the manuscript approved its claims and agreed to be an author. We would like to thank Japan Medical Communication (www.japan-mc.co.jp/editing/) for English language editing.

REFERENCES

[1] Levesque E, Hoti E, Azoulay D, Honore I, Guignard B, Vibert E, et al. Pulmonary complications after elective liver transplantation-incidence, risk factors, and outcome. Transplantation 2012;94(5):532–8.

[2] Stackebrandt E, Rainey FA, Ward-Rainey NL. Proposal for a new hierarchic classification system, Actinobacteria classis nov. Int J Syst Evol Microbiol 1997;47(2):479–91.

[3] Brown-Elliott BA, Brown JM, Conville PS, Wallace Jr. RJ. Clinical and laboratory features of the Nocardia spp. based on current molecular taxonomy. Clin Microbiol Rev 2006;19(2):259–82.

[4] Deem RL, Doughty FA, Beaman BL. Immunologically specific direct T lymphocyte-mediated killing of Nocardia asteroides. J Immunol 1983;130(5):2401–6.

[5] Forbes GM, Harvey FA, Philpott-Howard JN, O'Grady JG, Jensen RD, Sahathevan M, et al. Nocardiosis in liver transplantation: variation in presentation, diagnosis and therapy. J Infect 1990;20(1):11–9.

[6] Moylett EH, Pacheco SE, Brown-Elliott BA, Perry TR, Buescher ES, Birmingham MC, et al. Clinical experience with linezolid for the treatment of Nocardia infection. Clin Infect Dis 2003;36(3):313–8.

[7] Shen T, Wu L, Geng L, Wei Z, Zheng S. Successful treatment of pulmonary *Nocardia farcinica* infection with linezolid: case report and literature review. Braz J Infect Dis 2011;15(5):486–9.

[8] López E, Ferrero M, Lumbreras C, Gimeno C, González-Pinto I, Palengue E. A case of testicular nocardiosis and literature review. Eur J Clin Microbiol Infect Dis 1994;13(4):310–3.

[9] Weinberger M, Eid A, Schreiber L, Shapiro M, Ilan Y, Libson E, et al. Disseminated *Nocardia transvalensis* infection resembling pulmonary infarction in a liver transplant recipient. Eur J Clin Microbiol Infect Dis 1995;14(4):337–41.

[10] Kontoyiannis DP, Ruoff K, Hooper DC, bacteremia Nocardia. Report of 4 cases and review of the literature. Medicine (Baltimore) 1998;77(4):255–67.

[11] Carriere C, Marchandin H, Andrieu JM, Vandome A, Perez C. Nocardia thyroiditis: unusual location of infection. J Clin Microbiol 1999;37(7):2323–5.

[12] Wiesmayr S, Stelzmueller I, Tabarelli W, Bargehr D, Graziadei I, Freund M, et al. Nocardiosis following solid organ transplantation: a single-centre experience. Transpl Int 2005;18(9):1048–53.

[13] Shin N, Sugawara Y, Tsukada K, Tamura S, Akamatsu N, Okugawa S, et al. Successful treatment of disseminated *Nocardia farcinica* infection in a living-donor liver transplantation recipient. Transpl Infect Dis 2006;8(4):222–5.

[14] Parra IH, Galimberti R, Galimberti G, Guanella B, Kowalczuk A. Lymphocutaneous nocardiosis and cutaneous pheohyphomycosis in a liver transplant recipient. Int J Dermatol 2008;47(6):571–4.

[15] del Pozo JL, Herrero JI, Manubens A, Garcia-Quetglas E, Yuste JR, Alfonso M, et al. Disseminated Nocardia asteroides infection presenting as an atraumatic leg fracture in a liver transplant recipient. Liver Transpl 2008;14(2):257–8.

[16] Jimenez-Galanes Marchan S, Meneu Diaz JC, Caso Maestro O, Perez Saborido B, Moreno Elola-Olaso A, Abradelo Usera M, et al. Disseminated nocardiosis: a rare infectious complication following non-heart-beating donor liver transplantation. Transplant Proc 2009;41(6):2495–7.

[17] Reechaipichitkul W, Thanasatirakul P. Nocardiosis revealed by thyroid abscess and pneumonia in a liver transplant recipient. Southeast Asian J Trop Med Public Health 2015;46(6):1055–62.

[18] Hanchanale P, Jain M, Varghese J. Nocardia liver abscess post liver transplantation—a rare presentation. Transpl Infect Dis 2017;19:e12670.

[19] Cheronis N, Carr D, Bhanot N. Cutaneous Nocardia arthritidis infection in an orthotopic liver transplant recipient. IDCases 2019;18:e00623.

[20] Iyer RN, Rao JR, Rudramurthy SM, Kapoor D. Two cases of *Nocardia bacteraemia* in solid organ transplant recipients. Indian J Med Microbiol 2020;38(1):124–7.

[21] Kober P, Gozdowska J, Sawicka M, Ślubowska K, Pacholczyk M, Durlik M. Cutaneous nocardiosis in a liver transplant recipient - case report. Pol Merkur Lekarski 2020;48(284):108–11.

[22] Campoli C, Ferraro S, Salfi N, Coladonato S, Morelli MC, Giannella M, et al. Diffuse primary cutaneous infection by Alternaria alternata in a liver transplant recipient with pulmonary nocardiosis: importance of prompt identification for clinical resolution. Med Mycol Case Rep 2020;28:42–5.

[23] Ruimy R, Riegel P, Carlotti A, Boiron P, Bernardin G, Monteil H, et al. *Nocardia pseudobrasiliensis* sp. nov., a new species of Nocardia which groups bacterial strains previously identified as *Nocardia brasiliensis* and associated with invasive diseases. Int J Syst Bacteriol 1996;46(1):259–64.

[24] Wieser A, Schneider L, Jung J, Schubert S. MALDI-TOF MS in microbiological diagnostics-identification of microorganisms and beyond (mini review). Appl Microbiol Biotechnol 2012;93(3):965–74.

[25] Brown BA, Lopes JO, Wilson RW, Costa JM, de Vargas AC, Alves SH, et al. Disseminated *Nocardia pseudobrasiliensis* infection in a patient with AIDS in Brazil. Clin Infect Dis 1999;28(1):144–5.

[26] Kageyama A, Sato H, Nagata M, Yazawa K, Katsu M, Mikami Y, et al. First human case of nocardiosis caused by *Nocardia pseudobrasiliensis* in Japan. Mycopathologia 2002;156(3):187–92.

[27] Seol CA, Sung H, Kim DH, Ji M, Chong YP, Kim MN. The first Korean case of disseminated mycetoma caused by *Nocardia pseudobrasiliensis* in a patient on long-term corticosteroid therapy for the treatment of microscopic polyangiitis. Ann Lab Med 2013;33(3):203–7.

[28] Lebeaux D, Lantermier F, Degand N, Catherinot E, Podglajen I, Rubio MT, et al. *Nocardia pseudobrasiliensis* as an emerging cause of opportunistic infection after allogeneic hematopoietic stem cell transplantation. J Clin Microbiol 2010;48(2):656–9.

[29] Veerappan Kandasamy V, Nagabandi A, Horowitz EA, Vivekanandan R. Multidrug-resistant *Nocardia pseudobrasiliensis* presenting as multiple muscle abscesses. BMJ Case Rep 2015.

[30] Makadia S, Patel I, Soosaipillai I, Tarasiuk-Rusek A. First case of *Nocardia pseudobrasiliensis* causing primary cutaneous nocardiosis in an immunocompetent patient. J Investig Med High Impact Case Rep 2020;8:2324709620938228.